Application and Development of Mass Spectrometry-based Approaches to Investigate the Regulation of Lysosomal-associated Proteins by Phosphorylation

Dissertation

zur

Erlangung des Doktorgrades (Dr. rer. nat.)

der

Mathematisch-Naturwissenschaftlichen Fakultät

der

Rheinischen Friedrich-Wilhelms-Universität Bonn

vorgelegt von

Alireza Dehghani

aus

Shiraz, Iran

Bonn, 2019

Angefertigt mit Genehmigung der Mathematisch-Naturwissenschaftlichen Fakultät der Rheinischen Friedrich-Wilhelms-Universität Bonn

1. Gutachter: Prof. Dr. Volkmar Gieselmann

2. Gutachter: Prof. Dr. Walter Witke

Tag der Promotion: 30.04.2019

Erscheinungsjahr: 2019

Table of contents

1. Summary

Phosphorylation is one of the most abundant and best studied posttranslational modifications in mammalian cells and refers to the addition of a phosphate group to an amino acid residue of a protein. Phosphorylation can alter protein stability, interaction with other molecules, activities, and sub-cellular location. Therefore, it has a significant role in numerous cellular functions such as signal transduction, cell differentiation, growth, and apoptosis. In order to better understand the role of phosphorylation in biological systems, different techniques and workflows have been developed in recent years to conduct phosphoproteomic analyses. In this thesis project, by using a novel workflow, regulation of lysosomal-associated proteins by phosphorylation was examined. In the first chapter of the thesis, a phosphoproteomics workflow was developed and optimized, which was applied for the phosphoproteomic investigation of cholesterol metabolism with emphasis on lysosomal proteins described in the second chapter.

In chapter one, the aim was to establish a robust, easy, and time-efficient method for large-scale phosphoproteomic studies. A common strategy in such studies is the fractionation of large amounts of peptides followed by enrichment for phosphopeptides from the resulting fractions. Fractionation followed by enrichment is a time-consuming and expensive process and requires specialized equipment and operators. In this chapter, a method was developed which addresses these problems by optimizing the workflow to batch-enrichment of phosphopeptides followed by their fractionation using in-house manufactured tip columns. This allows for cost- and time-efficient identification of large quantities of phosphopeptides without specialized equipment.

In the second chapter, the newly established phosphoproteomics workflow was employed to investigate phosphoproteome alterations in cells with perturbed cholesterol metabolism system. Using the stable isotope labeling with amino acids in cell culture (SILAC) method, mouse embryonic fibroblasts (MEFs) were labeled and treated with either U18666A (cholesterol transporter inhibitor) or DMSO (control). A large-scale phosphoproteomic experiment was performed using the labeled cells, and in total, 12881 phosphosites were identified and quantified. Six lysosomal or lysosomal-associated phosphoproteins containing differentially expresse d phosphosites (LAMTOR1, RagC, OSTM1, STARD3 STARD3NL, BNIP3, and VAMP8) were selected for further investigations. The follow-up experiments suggested that LAMTOR1 phosphorylation abolishes its interaction with other proteins such as Rag GTPase complex members and SLC38A9. Moreover, it was shown that OSTM1 phosphorylation promotes its cleavage.

2. General introduction

2.1. Mass spectrometry-based proteomics

For decades the primary approach to study the proteome and its alterations was to isolate a specific protein and then study the protein with respect of its structure and function using the established tools and methods of biochemistry and biophysics. In the last 20 years, mass spectrometry (MS) has fundamentally changed the course of proteomic studies (Aebersold and Mann 2016). Several types of mass spectrometers have been developed and used for proteomic analysis. However, independent of the type of mass spectrometer, every instrument consists of an ion source, a mass analyzer, and a detector (Awad et al. 2015). Mass spectrometers are capable of detecting only ionized molecules in the gas-phase (Awad et al. 2015). Ion source generates gas-phase ions using techniques such as electrospray ionization (ESI) or matrix-assisted laser desorption/ionization (MALDI) that are the most common methods for ionizing peptides and proteins (Aebersold and Mann 2003). The mass analyzer measures mass (m) to charge (z) ratio (m/z) of the generated ions (also called precursor ions) and the detector records m/z and the intensity of each precursor ion (Figure 2.1) (Barillot 2013). Using methods such as collisional-induced dissociation (CID), the precursor ions are fragmented to product ions to obtain more information about the parent ion (Awad et al. 2015). In the CID fragmentation, the accelerated molecular ions collide with a neutral gas such as helium or nitrogen which results in the fragmentation of the precursor ion into smaller ion fragments (Figure 2.1) (Awad et al. 2015). Mass spectrometers generate (raw-) data based on the (m/z) information obtained from precursor ions (MS) and their fragmented ions (MS/MS). Molecules (such as peptides) can be detected either by interrogating raw data manually or by comparing and matching the acquired raw data with the existing datasets using various software which have been developed in the recent years for this purpose (Schmidt et al. 2014). By identifying peptides and their intensities in a sample, software is able to quantitatively reveal the corresponding proteins in the sample (Schmidt et al. 2014).

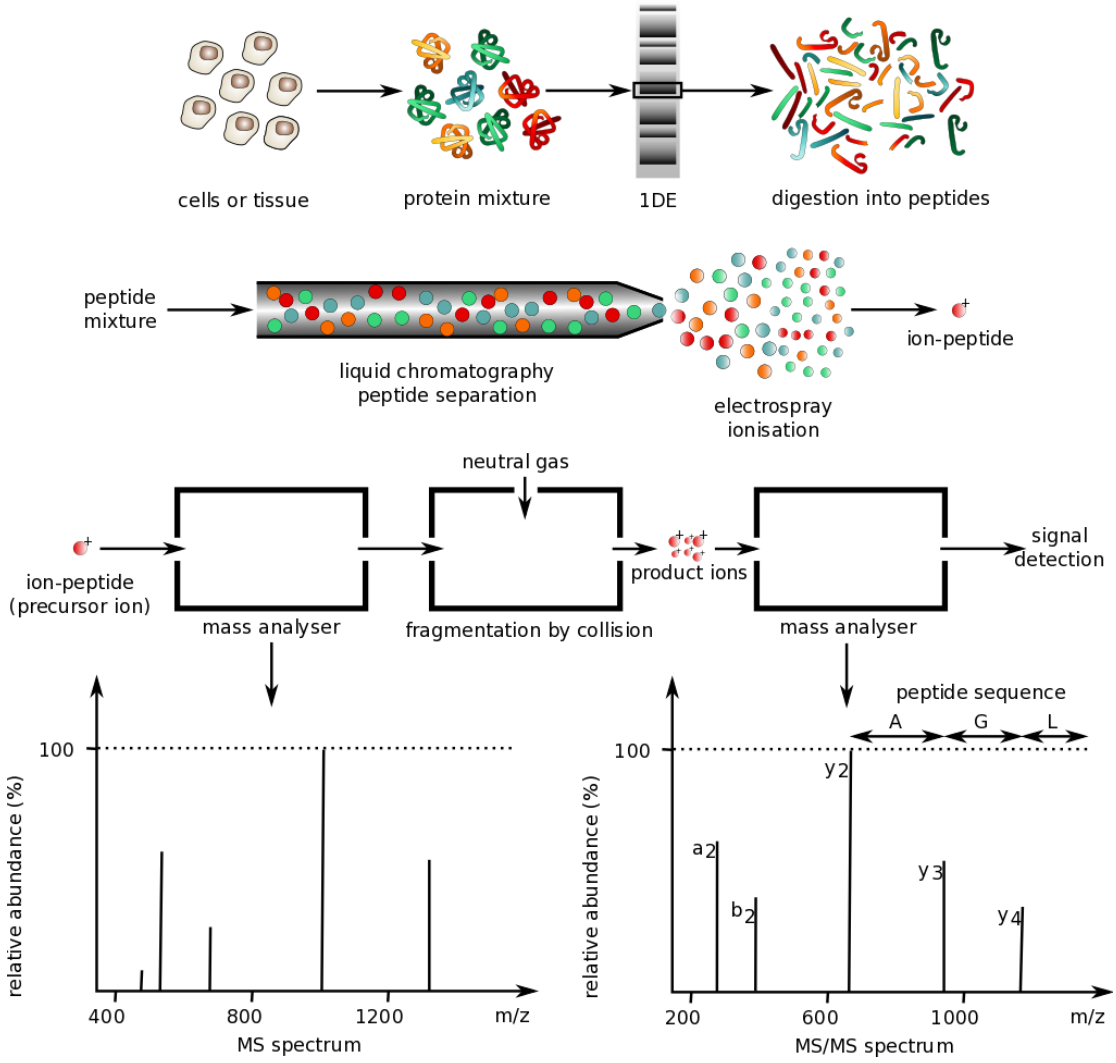

Figure 2.1 Schematic view of a bottom-up mass spectrometry-based proteomics workflow
Extracted proteins from cells or tissue are digested to peptides using sequence-specific enzymes. Peptides are subjected to an on-line liquid chromatography (LC) connected to the mass spectrometer. Electrospray ionization (ESI) technique is used to produce ions using an electrospray. The strong electric field causes the dispersion of the sample solution into an aerosol of highly charged macromolecules such as peptides. m/z ratio and relative abundance of each ionized peptide are recorded using a mass analyzer and a detector (Aebersold and Mann 2003). To obtain more information about the peptide sequence and post-translational modification (PTM), precursor ions are fragmented by colliding the accelerated ionized peptides with neutral gas molecules (CID) followed by recording the m/z ratio of each fragment (MS/MS or MS2). Different algorithms and software are available which use the obtained data from precursor ions and their corresponding fragment ions to determine the peptide sequence and PTMs (Aebersold and Mann 2003). Adapted from Barillot, 2013 (Barillot 2013).

MS has been employed for a wide range of applications in the proteome field, from large-scale proteomic studies to targeted studies of specific proteins or peptides (Aebersold and Mann 2016).

The so-called bottom-up proteomics approach allows scientists to perform large-scale proteomic studies as well as targeted investigation of a protein or peptide (Zhang et al. 2013). In this approach, proteins are extracted from different sources and digested using a sequence-specific enzyme such as trypsin. The resulting peptides are resolved using a reversed-phase chromatography column which is coupled online to a mass spectrometer (Figure 2.1) (Zhang et al. 2013). The peptides are ionized by electrospray ionization before transferring them to the vacuum of a mass spectrometer, where they are fragmented to produce MS/MS spectra, which are used to identify specific peptides and their modifications (Figure 2.1) (Aebersold and Mann 2016). In contrast to bottom-up, the top-down approach is used for whole-protein analysis. The top-down approach has some advantages for studying protein structure and interactions and also for investigating PTMs (Zhang et al. 2013).

2.2. Quantitative mass spectrometry

Although initially mass spectrometry was mainly considered to be a qualitative method, however, in recent years by developing new instruments, methods, and software, MS established itself as a precise tool for quantitative studies. MS quantitative methods can be categorized into two main groups: label-free and label-based quantification. In label-free quantification methods, the intensity of two peptides is compared relatively by assessing the intensities of the MS (precursor ions) peaks or by counting the number of peptides or MS/MS spectra (Cox et al. 2014) (Figure 2.2). However, the drawback of these methods is that the variation of different MS runs affects the results and ratios. Therefore, different label-based methods have been developed that enable scientists to combine different samples before MS analysis to minimize the technical variations caused by sample preparation and instrument performance (Ong and Mann 2005). Labeled amino acids can be incorporated into proteins by feeding cells(Ong et al. 2002) (or animals (Krüger et al. 2008)) with stable isotope-labeled amino acids (e.g., stable isotope labeling by/with amino acids in cell culture (SILAC)) for several passages (in vivo labeling). Later cells or lysates from different conditions can be combined with each other and analyzed and compared in a single MS run (Ong et al. 2002). SILAC method is based on introducing stable isotopes such as ^{13}C, ^{15}N into the peptides or protein sequences (Ong and Mann 2005). Since the ionization efficiency of the labeled and non-labeled peptides (or proteins) are the same, the mass spectrometer produces the same mass response signal with the only difference of the mass shift introduced by the stable isotope (Ong and Mann 2005).

Proteins and peptides can also be labeled in vitro before or after protein digestion using stable-isotope-labeled compounds that covalently attach to functional groups of amino acids. Dimethyl-labeling (Boersema et al. 2009), tandem mass tags (TMTs) (Thompson et al. 2003), and isobaric tags for relative and absolute quantitation (iTRAQ) (Ross et al. 2004) are the three most common techniques which have been employed for labeling the amino acids. In another method, the absolute amount of a peptide is measured quantitatively by spiking synthetic peptides with incorporated stable isotopes into the sample. By comparing the intensity of the synthetic peptide and endogenous peptide, the absolute amount of the peptide of interest and the corresponding protein can be determined (Figure 2.2) (Gerber et al. 2003).

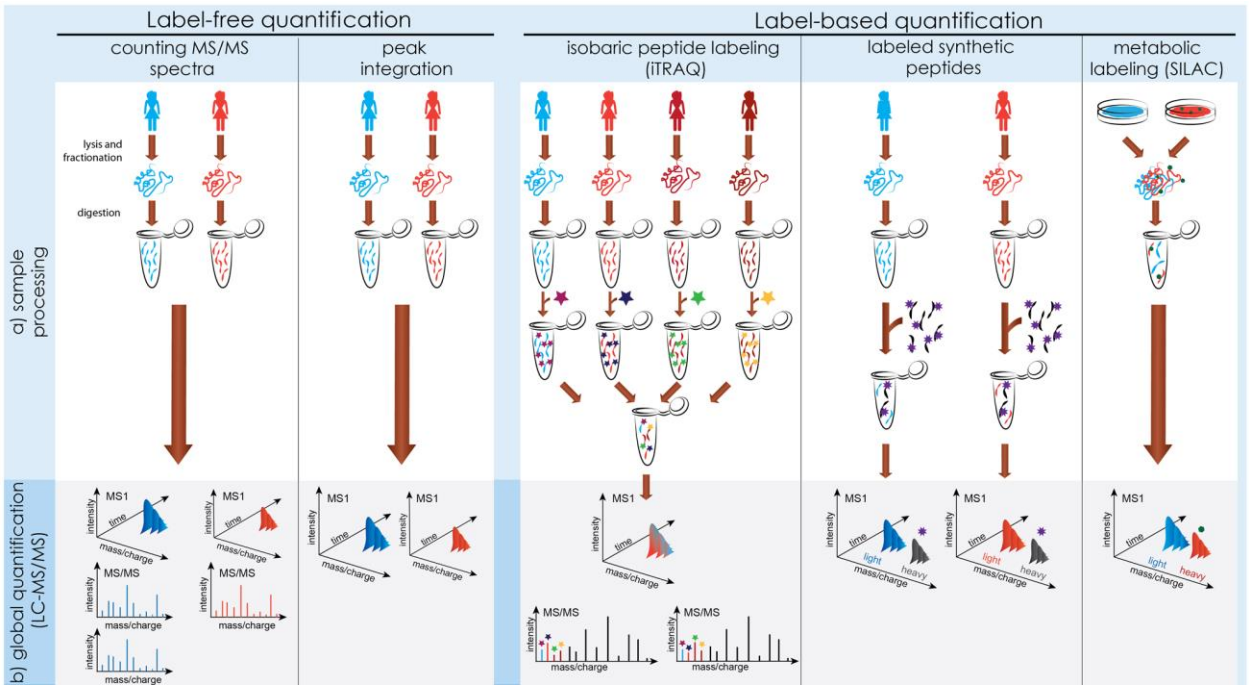

Figure 2.2 Quantitative mass spectrometry strategies.
A. Sample processing. Preparing samples for the label-based quantification is more laborious, and time-consuming in comparison to the label-free quantification methods. In contrast to label-based quantification, for the label-free quantification, samples are not combined prior to mass spectrometry analysis. **B.** Global quantification. In label-free quantification methods, relative intensity is based on either spectral counting of identified proteins or comparison of peptide peak areas or peak heights. However, label-based quantification is based on the comparison of MS peaks of synthetic (labeled synthetic) or metabolic labeled (SILAC) peptides or comparison of reporter ion intensities in MS/MS spectra of isobaric labeled peptides (iTRAQ). Adapted from Käll and Vitek, 2011 (Käll and Vitek 2011).

In the label-based workflows, samples can be quantitatively compared at the MS level (e.g., SILAC, dimethyl-labeling) or at MS/MS level (e.g., TMT and iTRAQ) (Figure 2.2) (Hsu and

Chen 2016). Using these quantitative methods, thousands of studies have been performed in the last two decades to investigate the various aspects of the proteome of different organisms in different conditions.

2.3. Identification of post-translational modifications by mass spectrometry

MS-based methods are well-suited for characterizing and localizing PTMs in proteins in an unbiased manner because PTMs cause a mass shift in peptides (Olsen and Mann 2013). Using MS and MS/MS data, a specific modification can be annotated to a specific amino acid with high probability (Witze et al. 2007). The most well-studied PTMs are phosphorylation, glycosylation, ubiquitination, methylation, and acetylation. In order to detect and study PTMs, usually, an enrichment step for the intended modification has to be added to the normal sample preparation workflow (Olsen and Mann 2013). Identification of the PTMs manually from the MS data is laborious and time-consuming. The software such as MaxQuant and Proteome Discoverer that have been developed for interpreting protein MS data are also able to identify protein modifications (Schmidt et al. 2014).

2.4. Phosphorylation and signal transduction

Extracellular and intracellular stimuli can trigger and control cell signaling cascades by PTMs. The most abundant and best-studied PTM is phosphorylation, which is a reversible attachment of an inorganic phosphate group to amino acid residues by a covalent bond. This process can be regulated by the balanced activity of phosphatases and kinases (Jin and Pawson 2012). To date, approximately 500 kinases and 100 phosphatases have been identified in human cells ((Manning et al. 2002), (Alonso et al. 2004)); therefore ~3% of the human genome is dedicated to the phosphorylation regulation. Although residues such as histidine and lysine can be phosphorylated, the most abundant phosphosites in eukaryotic cells are phospho-serine, phospho-threonine, and phospho-tyrosine residues with 81:17:2 ratio, respectively (Huttlin et al. 2010). It also has been shown that ~50% of all proteins harbor at least 1 phosphorylation site (Huttlin et al. 2010). Altogether, these numbers highlight the evolutionary importance of phosphorylation and its regulation in eukaryotic cells. Phosphorylation causes changes in protein structure and conformation; therefore it affects their cellular functions such as enzymatic activity, stability, and interaction with other proteins. Phosphorylation-induced alterations in the proteins involved in crucial cell networks and pathways regulate and govern fundamental eukaryotic processes such as cell proliferation, differentiation, division, and death (Paradela and Albar 2008). Numerous

methods and workflows have been developed in the last decade to enrich and fractionate phosphopeptides (Kanshin et al. 2012), some of which are reviewed briefly in the introduction of chapter 1 of this manuscript.

3. Materials

3.1. Chemicals / Solutions / Buffers

All mass spectrometry-related chemicals were HPLC or MS grade.

Chemicals / Solutions / Buffers	**Provider**
1-Bromo-3-chloropropane	Sigma-Aldrich (St. Louis, MO, USA)
2-Mercaptoethanol	Sigma-Aldrich (St. Louis, MO, USA)
Acetic acid, glacial	Biosolve (Valkenswaard, Netherlands)
Acetonitrile	Biosolve (Valkenswaard, Netherlands)
Acrylamide	Sigma-Aldrich (St. Louis, MO, USA)
Ammonium bicarbonate	AppliChem GmbH (Darmstadt, Germany)
Ammonium formate	Sigma-Aldrich (St. Louis, MO, USA)
Ammonium hydroxide	Sigma-Aldrich (St. Louis, MO, USA)
Ammonium persulfate (APS)	Sigma-Aldrich (St. Louis, MO, USA)
Boric acid	Fluka Chemie Ag (Buchs, Switzerland)
Bovine serum albumin	Sigma-Aldrich (St. Louis, MO, USA)
Bromophenol blue	Sigma-Aldrich (St. Louis, MO, USA)
Calcium chloride	AppliChem GmbH (Darmstadt, Germany)
Citric acid monohydrate	Sigma-Aldrich (St. Louis, MO, USA)
Clarity™ western ecl substrate	Bio-Rad Laboratories, Inc. (Hercules, CA, USA)
Cycloheximide	Sigma-Aldrich (St. Louis, MO, USA)
Dimethyl sulfoxide (DMSO)	Sigma-Aldrich (St. Louis, MO, USA)
Dipotassium phosphate	AppliChem GmbH (Darmstadt, Germany)
Dithiothreithol	Sigma-Aldrich (St. Louis, MO, USA)
DMEM for SILAC	Thermo Fisher Scientific (Waltham, MA, USA)
Dulbecco's modified eagle's medium –glutamine –pyruvate	Invitrogen Gibco (Paisley, United Kingdom)
Dulbecco's phosphate-buffered saline (DPBS)	Invitrogen Gibco (Paisley, United Kingdom)
Ethanol	AppliChem GmbH (Darmstadt, Germany)
Ethylenediaminetetraacetic acid (EDTA)	Sigma-Aldrich (St. Louis, MO, USA)
Fetal calf serum	Invitrogen Gibco (Paisley, United Kingdom)
Filipin	Sigma-Aldrich (St. Louis, MO, USA)
Fluoromount-G™, with DAPI	Thermo Fisher Scientific (Waltham, MA, USA)
Formic acid	Biosolve (Valkenswaard, Netherlands)
G-418 solution	Sigma-Aldrich (St. Louis, MO, USA)
Glucose	Merck KGaA (Darmstadt, Germany)
Glycerol	Merck KGaA (Darmstadt, Germany)
Glycolic acid	Sigma-Aldrich (St. Louis, MO, USA)

Materials

Chemicals / Solutions / Buffers	**Provider**
Hank's Balanced Salt Solution (HBSS)	Invitrogen Gibco (Paisley, United Kingdom)
HEPES (2,4 Hydroxyethyl piperazineethanesulfonic acid)	Merck KGaA(Darmstadt, Germany)
Iodoacetamide	Thermo Fisher Scientific (Waltham, MA, USA)
L-arginine	Sigma-Aldrich (St. Louis, MO, USA)
L-ARGININE:HCL ($^{13}C_6$, 99%; $^{15}N_4$, 99%)	Cambridge Isotope Laboratories, Inc. (Tewksbury, MA, USA)
L-glutamine	Sigma-Aldrich (St. Louis, MO, USA)
L-Lysine	Sigma-Aldrich (St. Louis, MO, USA)
L-LYSINE : 2HCL ($^{13}C_6$, 99%; $^{15}N_2$, 99%)	Cambridge Isotope Laboratories, Inc. (Tewksbury, MA, USA)
Magnesium chloride	Sigma-Aldrich (St. Louis, MO, USA)
Methanol	Merck KGaA (Darmstadt, Germany)
Mineral oil	GE Healthcare BioSciences (Uppsala, Sweden)
Monopotassium phosphate	AppliChem GmbH (Darmstadt, Germany)
Nonidet P-40	Fluka Chemie Ag (Buchs, Switzerland)
PageBlue™ protein staining solution	Thermo Fisher Scientific (Waltham, MA, USA)
Paraformaldehyde	Sigma-Aldrich (St. Louis, MO, USA)
Penicillin	Invitrogen Gibco (Paisley, United Kingdom)
Phenylmethanesulfonyl fluoride (PMSF)	AppliChem GmbH (Darmstadt, Germany)
Phosphoric acid	Sigma-Aldrich (St. Louis, MO, USA)
PhosSTOP™ inhibitor tablets for phosphatase	F. Hoffmann-La Roche AG (Basel, Switzerland)
Potassium chloride	AppliChem GmbH (Darmstadt, Germany)
Roche cOmplete protease inhibitor cocktail	F. Hoffmann-La Roche AG (Basel, Switzerland)
Sodium dodecyl sulfate (SDS)	Bio-Rad Laboratories, Inc. (Hercules, CA, USA)
Sodium chloride	Sigma-Aldrich (St. Louis, MO, USA)
Sodium fluoride	AppliChem GmbH (Darmstadt, Germany)
Sodium hydrogen phosphate	Merck KGaA (Darmstadt, Germany)
Sodium hydroxide	Carl Roth GmbH (Karlsruhe, Germany)
Sodium orthovanadate	AppliChem GmbH (Darmstadt, Germany)
Sodium pyrophosphate	Sigma-Aldrich (St. Louis, MO, USA)
Sodium selenite	Sigma-Aldrich (St. Louis, MO, USA)
Streptomycin	Invitrogen Gibco (Paisley, United Kingdom)
Tetramethylethylenediamine (TEMED)	Carl Roth GmbH (Karlsruhe, Germany)
Triethylamine	AppliChem GmbH (Darmstadt, Germany)
Trifluoroacetic acid	Biosolve (Valkenswaard, Netherlands)
Tris	AppliChem GmbH (Darmstadt, Germany)
Triton X-100	Fluka Chemie Ag (Buchs, Switzerland)
Trypan blue solution 0.04%	Sigma-Aldrich (St. Louis, MO, USA)
TurboFect transfection reagent	Thermo Fisher Scientific (Waltham, MA, USA)
U18666A	Merck KGaA (Darmstadt, Germany)
Urea	Sigma-Aldrich (St. Louis, MO, USA)
Water	Biosolve (Valkenswaard, Netherlands)
β-Glycerophosphate disodium salt hydrate	Sigma-Aldrich (St. Louis, MO, USA)

3.2. Equipment and consumables

Equipment and consumables	Provider
37°C Heraeus incubator	Thermo Fisher Scientific (Waltham, MA, USA)
Analytical balance CP 124-OCE	Sartorius AG (Göttingen, Germany)
Axiovert.A1 microscope	Carl Zeiss AG (Oberkochen, Germany)
Axiovert 200M microscope	Carl Zeiss AG (Oberkochen, Germany)
Axygen pipette tips maximum recovery	Corning Inc. (Corning, NY, USA)
Axygen reaction tubes maximum recovery (1.5 mL)	Corning GmbH (Kaiserslautern, Germany)
Biometra T3 thermal cycler	Analytik Jena AG (Jena, Germany)
Cell culture dishes	Sarstedt AG & Co. (Nümbrecht, Germany)
Cell culture well-plates	Corning Inc. (Corning, NY, USA)
Cell scraper	Sarstedt AG & Co. (Nümbrecht, Germany)
Centrifuge 5415D	Eppendorf AG (Hamburg, Germany)
Centrifuge 5424R	Eppendorf AG (Hamburg, Germany)
Centrifuge 5810R	Eppendorf AG (Hamburg, Germany)
Centrifuge Labofuge 400	Thermo Fisher Scientific (Waltham, MA, USA)
Centrifuge MIKRO 200	Andreas Hettich GmbH & Co. (Tuttlingen, Germany)
CO_2 water jacketed incubator	Thermo Fisher Scientific (Waltham, MA, USA)
Conical tubes (15 and 50 mL)	Sarstedt AG & Co. (Nümbrecht, Germany)
Corning 40 µm Cell Strainer	Corning Inc. (Corning, NY, USA)
Cover slides, 12 mm	VWR (Leicestershire, UK)
Cryogenic vials	Thermo Fisher Scientific (Waltham, MA, USA)
Dry block heater	STAR LAB (Hamburg, Germany)
Empore anion-SR disks	3M Corporation (St. Paul, MN, USA)
Empore C18 disks	3M Corporation (St. Paul, MN, USA)
Empore cation-SR disks	3M Corporation (St. Paul, MN, USA)
Freezer -20°C	AEG AG (Berlin, Germany)
Freezer -80°C ultra low	Sanyo Scientific (Osaka, Japan)
FUSION SOLO 4M system	VilberLourmat (Eberhardzell, Germany)
Galaxy MiniStar microcentrifuge	VWR (Darmstadt, Germany)
Glassware (beakers, bottles, measurement cylinders)	Carl Roth GmbH and Co. KG (Karlsruhe, Germany)
Heating and magnetic stirrer ARE	Velp Scientifica (Usmate, Italy)
Heating block	Gebr. Liebisch GmbH & Co. KG (Bielefeld, Germany)
Ice machine	Ziegra Ice Machines Ltd. (Isernhagen, Germany)
Incubator, INCU-Line	VWR (Darmstadt, Germany)
Labtherm Heater	Gebr. Liebisch GmbH & Co. KG (Bielefeld, Germany)
Laminar air-flow device CA R 6	Clean Air (Minneapolis, MN, USA)
Liquid chromatograph ÄKTApurifier	GE Healthcare (Little Chalfont, United Kingdom)
Liquid chromatograph EASY-nLC 1000	Thermo Fisher Scientific (Waltham, MA, USA)
Mass spectrometer LTQ Orbitrap Velos	Thermo Fisher Scientific (Waltham, MA, USA)
Membrane filters (0.2 and 0.45 µm)	Sarstedt AG & Co. (Nümbrecht, Germany)
Micropipettes	Eppendorf AG (Hamburg, Germany)

Materials

Equipment and consumables	**Provider**
Microplate reader GENios	Tecan (Männerdorf, Switzerland)
Mini incubator INCU-line	VWR (Darmstadt, Germany)
Mini-PROTEAN Tetra cell casting stand	Bio-Rad Laboratories, Inc. (Hercules, CA, USA)
Multi-rotator multi RS-60	BioSan (Riga, Latvia)
Neubauer hemocytometer (Counting chamber)	Paul Marienfeld GmbH & Co. (Lauda-Königshofen, Germany)
Oasis HLB 10 mg cartridge	Waters Corporation (Milford, MA, USA)
Oasis HLB 400 mg cartridge	Waters Corporation (Milford, MA, USA)
Omnifix syringe 50 ml	B. Braun Melsungen AG (Melsungen, Germany)
P-2000 laser-based micropipette puller	Sutter Instruments (Novato, CA, USA)
Pasteur pipettes 230 mm	BRAND GMBH & Co. (Wertheim, Germany)
PC 4400 scale	METTLER TOLEDO (Greifensee, Switzerland)
PerfectBlue™ semi-Dry elektroblotter	VWR (Darmstadt, Germany)
pH-Meter, Calimatic 761	Knick Elektronische Messgeräte GmbH & Co. (Berlin, Germany)
Pipette tips	Greiner Bio-One GmbH (Frickenhausen, Germany)
Polymax1040 orbital shaker	Heidolph Instruments (Schwabach, Germany)
PolySULFOETHYL A 100 x 9.4 mm	PolyLC Inc. (Columbia, MD, USA)
PolyWAX LP 200 x 4.6 mm	PolyLC Inc. (Columbia, MD, USA)
PureLink™ HiPure plasmid midiprep kit	Thermo Fisher Scientific (Waltham, MA, USA)
PureLink™ Quick gel extraction kit	Thermo Fisher Scientific (Waltham, MA, USA)
QIAprep spin miniprep kit	Qiagen Inc. (Hilden, Germany)
QIAquick PCR purification kit	Qiagen Inc. (Hilden, Germany)
Reaction tubes 1.5 and 2 ml	Sarstedt AG & Co. (Nümbrecht, Germany)
Refrigerator 4°C	AEG AG (Berlin, Germany)
ReproSil-Pur 120 C18 AQ	Dr. Maisch GmbH (Ammerbuch-Entringen, Germany)
Rotamax 120 orbital shaker	Heidolph Instruments (Schwabach, Germany)
Rotamix RM1	ELMI Ltd. (Riga, Latvia)
RS-TR05 roller mixer	Carl Roth GmbH (Karlsruhe, Germany)
Sachtopore NP 5 µm 300 Å TiO_2 bulk material	Sachtleben Chemie GmbH (Duisburg, Germany)
Shaking water bath	GFL Gesellschaft für Labortechnik mbH (Burgwedel, Germany)
Specimen slide	Engelbrecht Medizin- und Labortechnik GmbH (Erdermünde, Germany)
Syringe needle, BD Microlane	Becton, Dickinson und Company (Franklin Lakes, NJ, USA)
Thermomixer Comfort	Eppendorf AG (Hamburg, Germany)
Branson Ultrasonics™ Sonifier S-250A with 2 mm tip	Branson Ultrasonics (Danbury, CT, USA)
Ultrasonic waterbath 2510	Branson Ultrasonics (Danbury, CT, USA)
Vacuum centrifuge RVC 2-18	Martin Christ Gefriertrocknungsanlagen GmbH (Osterode am Harz, Germany)
Vortex, UNIMAG ZX3	UniEquip Laborgerätebau- und Vertriebs GmbH (Leipzig, Germany)

3.3. Primers and oligonucleotides

All primers and oligonucleotides were synthesized by MWG Biotech (Ebersberg, Germany) or biomers.net GmbH (Ulm, Germany).

Primer internal name	Target gene	Sequence	Purpose	Tm* ºC
Fwd-Bnip3-E-042	Bnip3	TGGCGAGAAAAACAGCACTCTGGAAGAGGAAGATTATATTGAGAGAAG	SDM**	NA***
Rev-Bnip3-E-043	Bnip3	CTTCTCTCAATATAATCTTCCTCTTCCAGAGTGCTGTTTTTCTCGCCA	SDM	NA
Fwd-Bnip3-A-044	Bnip3	GCGAGAAAAACAGCACTCTGGCTGAGGAAGATTATATTGAGAG	SDM	NA
Rev-Bnip3-A-045	Bnip3	CTCTCAATATAATCTTCCTCAGCCAGAGTGCTGTTTTTCTCGC	SDM	NA
Fev-68-Bnip3	Bnip3	AAAATGCATATGGAACAAAAACTCATCTCAGAAGAGGATCTCATGTCGCAGAGCGGGGAG	Cloning	63.7
Rev-69-Bnip3	Bnip3	TTTAAGCTTTCAGAAGGTGCTAGTGGAAGTTGTC	Cloning	63.8
FwdIR-PuSmaI-010	IRES and Puromycin	AACCCGGGAAGCTTTTAAAACAGCTCTGGG	Cloning	58.8
RevIR-PuSpeI-011	IRES and Puromycin	TTTACTAGTTCAGGCACCGGGCTTG	Cloning	61.4
Fwd-Lamtor-E-46	LAMTOR1	GATGAGCAGGCCCTGCTTTCCGAAATCCTTGCCAAGACAGCTAGC	SDM	NA
Rev-Lamtor-E-47	LAMTOR1	GCTAGCTGTCTTGGCAAGGATTTCGGAAAGCAGGGCCTGCTCATC	SDM	NA
Fwd-Lamtor-A-48	LAMTOR1	ATGAGCAGGCCCTGCTTTCCGCCATCCTTGCCAAGACAGCTAG	SDM	NA
Rev-Lamtor-A-49	LAMTOR1	CTAGCTGTCTTGGCAAGGATGGCGGAAAGCAGGGCCTGCTCAT	SDM	NA
Fwd-66-Lmator1	LAMTOR1	AAATGCATATGGAACAAAAACTCATCTCAGAAGAGGATCTCATGGGGTGCTGCTATAGCA	Cloning	60.6
Rev-67-LAMTOR1	LAMTOR1	TTTAAGCTTTCATGGGATCCCAAACTGTAC	Cloning	59.1
Fwd-OSTM1-E-062	Ostm1	ATTCTACCCAAACGTCTCAAGTCGGAAACCGAATTTGCCAACATTCAAGAAAATGCCACC	SDM	NA
Rev-OSTM1-E-063	Ostm1	GGTGGCATTTTCTTGAATGTTGGCAAATTCGGTTTCCGACTTGAGACGTTTGGGTAGAAT	SDM	NA
Fwd-OSTM1-A-064	Ostm1	CTACCCAAACGTCTCAAGTCGGCCACCGCTTTTGCCAACATTCAAGAAAAT	SDM	NA
Rev-OSTM1-A-065	Ostm1	ATTTTCTTGAATGTTGGCAAAAGCGGTGGCCGACTTGAGACGTTTGGGTAG	SDM	NA
FWD-Rragc-038	RagC	AAAAAGCTTATGGAACAAAAACTCATCTCAGAAGAGGATCTCATGTCCCTGCAGTACGGG	Cloning	60.7
REV-Rragc-039	RagC	TTTGGATCCCTAGATGGCATTCCGAGGC	Cloning	59.4
FWD-Rragc-058	RagC	AAAATGCATATGGAACAAAAACTCATCTCAGAAGAGGATCTCATGTCCCTGCAGTACGGG	Cloning	60.7
REV-Rragc-059	RagC	TTTTCTAGACTAGATGGCATTCCGAGGC	Cloning	59.4
FWD-Rragc-A-70	RagC	GAAGCTGCAGTCATCAGACCGCTGCTCCAAGTCTGAAAGCCTT	SDM	NA
Rev-Rragc-A-71	RagC	AAGGCTTTCAGACTTGGAGCAGCGGTCTGATGACTGCAGCTTC	SDM	NA
FWD-Rragc-E-72	RagC	AGAAGCTGCAGTCATCAGACCGAAGCTCCAAGTCTGAAAGCCTTG	SDM	NA
Rev-Rragc-E-73	RagC	CAAGGCTTTCAGACTTGGAGCTTCGGTCTGATGACTGCAGCTTCT	SDM	NA
Fwd-Stard3n-E-50	Stard3nl	GCAGCTCATGGCCAGGATTGAGGAATATGAAGGAAGGGAAAAGAAAG	SDM	NA
Rev-Stard3n-E-51	Stard3nl	CTTTCTTTTCCCTTCCTTCATATTCCTCAATCCTGGCCATGAGCTGC	SDM	NA
Fwd-Stard3n-A-52	Stard3nl	AGCTCATGGCCAGGATTGAGGCCTATGAAGGAAGGGAAAAGAA	SDM	NA
Rev-Stard3n-A-53	Stard3nl	TTCTTTTCCCTTCCTTCATAGGCCTCAATCCTGGCCATGAGCT	SDM	NA
Fwd-Stard3nl-SalI-89	Stard3nl	AAAGTCGACATGAACCATCTTCCAGAACACAT	Cloning	59.7
Rev-Stard3nl-BglII-90	Stard3nl	TTTAGATCTTTAAACCTTATCGTCGTCATCCTT	Cloning	59.3
Fwd-Vamp8-E-54	Vamp8	AAGACAGAGGACTTGGAAGCCGAATCTGAACACTTCAAGACAACG	SDM	NA
Rev-Vamp8-E-55	Vamp8	CGTTGTCTTGAAGTGTTCAGATTCGGCTTCCAAGTCCTCTGTCTT	SDM	NA
Fwd-Vamp8-A-56	Vamp8	AAGACAGAGGACTTGGAAGCCGCGTCTGAACACTTCAAGACAAC	SDM	NA
Rev-Vamp8-A-57	Vamp8	GTTGTCTTGAAGTGTTCAGACGCGGCTTCCAAGTCCTCTGTCTT	SDM	NA

*: Melting temperature, **: Site directed mutagenesis

***: Not applicable. The annealing temperature for all site-directed mutagenesis PCRs was set at 60ºC.

3.4. Antibodies

Target name	Manufacturer	Host species	Product No.	Application	Dilution
LAMTOR1	Sigma-Aldrich (St. Louis, MO, USA)	Rabbit	HPA002997	WB*	1 to 1000
LAMTOR2	Cell Signaling Technology (Danvers, MA, USA)	Rabbit	#8145	WB	1 to 1000
LAMTOR3	Abcam (Cambridge, United Kingdom)	Rabbit	ab32134	WB	1 to 1000
LAMTOR4	Sigma-Aldrich (St. Louis, MO, USA)	Rabbit	HPA020998	WB	1 to 1000
LAMTOR5	Cell Signaling Technology (Danvers, MA, USA)	Rabbit	#14633	WB	1 to 1000
RagA	Cell Signaling Technology (Danvers, MA, USA)	Rabbit	#4357	WB	1 to 1000
RagB	Cell Signaling Technology (Danvers, MA, USA)	Rabbit	#8150	WB	1 to 1000
RagC	Cell Signaling Technology (Danvers, MA, USA)	Rabbit	#5466	WB	1 to 1000
RagD	Cell Signaling Technology (Danvers, MA, USA)	Rabbit	#4470	WB	1 to 1000
SLC38A9	Sigma-Aldrich (St. Louis, MO, USA)	Rabbit	HPA043785	WB	1 to 1000
Myc	Abcam (Cambridge, United Kingdom)	Rabbit	ab9106	WB and ICC**	WB(1:5000), ICC(1:400)
β-Actin	Sigma-Aldrich (St. Louis, MO, USA)	Mouse	A5316	WB	1 to 5000
p44/42 MAPK (Erk1/2)	Cell Signaling Technology (Danvers, MA, USA)	Rabbit	#9102	WB	1 to 10000
Phospho-p44/42 MAPK (Erk1/2)(Thr202/Tyr204)	Cell Signaling Technology (Danvers, MA, USA)	Rabbit	#9101	WB	1 to 5000
p70 S6 Kinase	Cell Signaling Technology (Danvers, MA, USA)	Rabbit	#9202	WB	1 to 1000
Phospho-p70 S6 Kinase (Thr389)	Cell Signaling Technology (Danvers, MA, USA)	Rabbit	#9205	WB	1 to 1000
Lamp2	The Developmental Studies Hybridoma Bank (DSHB) (Iowa, IA, USA)	Rat	ABL-93	ICC	1 to 50
mTOR	Cell Signaling Technology (Danvers, MA, USA)	Rabbit	#2983	ICC	1 to 50

*: Western blot, **: Immunocytochemistry

3.5. Enzymes

Enzyme	Provider
Conventional restriction enzymes	Thermo Fisher Scientific (Waltham, MA, USA)
FastDigest restriction enzymes	Thermo Fisher Scientific (Waltham, MA, USA)
Phusion high-fidelity DNA polymerase	Thermo Fisher Scientific (Waltham, MA, USA)
Sequencing grade modified trypsin, porcine	Promega (Madison, WI, USA)
T4 DNA ligase	Thermo Fisher Scientific (Waltham, MA, USA)
Taq DNA polymerase, recombinant	Thermo Fisher Scientific (Waltham, MA, USA)
Trypsin-EDTA solution 0.05%	Invitrogen Gibco (Paisley, United Kingdom)

3.6. Software

Software	Provider
FusionCapt Advance Solo 4 16.15	VilberLourmat (Eberhardzell, Germany)
GraphPad Prism 6.07	GraphPad Software Inc. (San Diego, CA, USA)
Office Professional Plus 2010	Microsoft Corporation (Redmond, WA, USA)
AxioVision SE64 Rel.4.9.1	Carl Zeiss AG (Oberkochen, Germany)
MaxQuant 1.5.2.8	Max Planck Institute of Biochemistry (Planegg, Germany)
Proteome discoverer 2.1	Thermo Fisher Scientific (Waltham, MA, USA)
Thermo Xcalibur 2.2	Thermo Fisher Scientific (Waltham, MA, USA)

4. Methods

4.1. Eukaryotic cell line culture-related methods

4.1.1. Cell maintenance

HEK293 and HeLa cell lines were cultured in Dulbecco's Modified Eagle's medium (DMEM) supplemented with 10% FCS, 100 IU/ml penicillin, 100 IU/ml streptomycin and 2 mM L-glutamine and were incubated at 37°C under 5% CO_2 at 100% air humidity. Cells were passaged before confluency by trypsinization.

4.1.2. MEF SILAC cells maintenance

Mouse embryonic fibroblasts (MEFs) were cultured in SILAC DMEM supplemented with 10% fetal bovine serum, 100 IU/ml penicillin, 100 IU/ml streptomycin and either unlabeled (light) (K0, R0) or heavy labeled lysine and arginine (K8: $^{13}C_6.^{15}N_2$; R10: $^{13}C_6.^{15}N_4$) at 37°C in a humidified atmosphere with 5% CO_2. MEF cells were cultured for at least 5 passages in the medium containing labeled amino acids before starting the experiment. U18666A was solubilized in DMSO prior to use and was added to the MEF cells at the final concentration of 3 µg/ml. The same amount of DMSO was administered to the control cells.

4.1.3. Transient transfection of the eukaryotic cells

Eukaryotic cells were transfected using TurboFect transfection reagent according to the manufacturer's instructions with some modifications. Briefly, cells were seeded 24 hours prior to transfection to reach 70-90% confluency at the time of transfection. For a 10-cm cell culture dish, 10 µg of purified plasmid DNA and 20 µl of TurboFect reagent were added to a tube containing 1 ml of serum-free medium and vortexed immediately. The mixture was added dropwise to the cells after 20 min of incubation at RT, and the cell culture dish was placed in a 37°C incubator after mild shaking.

4.1.4. Cell harvest

Cells were harvested by trypsinization or using a cell scraper. In either case, first, cells were washed with pre-warmed PBS once. In order to trypsinize a 10-cm culture dish, 1 ml of 0.05% (w/v) trypsin was added and cells were incubated for 5 min at 37° C. Thereafter, 10 ml of pre-warmed medium was added to the culture dish and cells were transferred to a 15 ml tube and

centrifuged for 5 min at 500× g at RT. Next, the supernatant was removed, and pelleted cells were employed for another passage or cryopreservation with 10% DMSO. To harvest cells using a cell scraper, after washing them with pre-warmed PBS, culture dishes were placed on ice and were rewashed with ice-cold PBS. Subsequently, 1 ml of ice-cold PBS was added, and cells were mechanically dissociated from the culture dish using a cell scraper and transferred into a 1.5 ml tube and pelleted down at 500× g for 5 min at 4° C. Cell pellets were snap-frozen using liquid nitrogen and stored at −80°C until further analysis.

4.2. Microscopy-related methods

4.2.1. Filipin staining

MEF cells were seeded at a density of 10,000 cells per 12 mm coverslip in a 24-well plate. On the following day, cells were treated with either 3 µg/ml of U18666A or the same volume of DMSO. After 24 h MEF cells were washed with PBS and fixed using 4% paraformaldehyde (PFA) for 10 min and washed thrice with PBS. Thereafter, the cells were permeabilized by incubation with 0.1% Triton X-100 for 30 min. Next, the cells were washed with PBS and stained with 125 µg/ml Filipin dissolved in PBS/10% FCS for 2 h in the dark at RT. Next, cells were washed thrice with PBS and mounted using DAPI-Fluoromount-G. The stained cells were observed using an Axiovert 200M microscope equipped with an AxioCamMR3.

4.2.2. Immunocytochemistry staining and microscopy of cells

For immunocytochemistry studies, eukaryotic cells were cultured on 12 mm coverslips and after washing with PBS were fixed with 4% PFA for 10 min at room temperature. Following fixing, coverslips were washed 3 times with PBS and transferred to a wet chamber. The cells were permeabilized with 0.1% Triton X-100 in PBS for 10 min and blocked using 10% FCS in PBS for 1 hour at RT. Diluted primary antibody in 1% FCS was incubated with the cells for 4 hours at RT or overnight at 4°C after washing them with PBS. Thereafter, cells were washed thrice with PBS and incubated with secondary antibody for 1 hour in the dark at RT. Afterwards, the coverslips were washed twice with PBS and once with water and mounted using DAPI-fluoromount-G. Immunocytochemistry images were acquired using the Axiovert 200M equipped with an AxioCamMR3 with the following filter sets: filter set 38 (excitation BP 470/40, beam splitter FT 495, emission BP 525/50) for green fluorescence; filter set 43 HE (excitation BP 550/25 (HE), emission FT 570 (HE), beam splitter BP 605/70 (HE)) for red fluorescence; filter set 49 (DAPI) (excitation G 365, beam splitter FT 395, emission BP 445/50) .

4.3. Molecular biology-related methods

4.3.1. Polymerase Chain Reaction (PCR)

Phusion High-Fidelity DNA Polymerase was used when PCR fragments were generated for cloning purposes. The following components were added to a PCR tube: 10 µl of 5× Phusion HF buffer, 1 µl of 10 mM dNTPs, 0.5 µM each of the forward and reverse primers, 10 ng of template DNA, 1.5 µl of DMSO, 0.5 µl of the Phusion DNA Polymerase (1U), and ddH_2O to a total volume of 50 µl. The PCR tube was vortexed and, after a brief centrifugation, was placed in a thermocycler and the DNA was amplified using the following PCR program: 2 min at 95℃ and 35 cycles of 30 sec at 95℃, 30 sec at X°C, and 30 sec/kb at 72℃ following with 10 min final extension at 72°C. The primer annealing temperatures (X) were adjusted to 3°C above their calculated melting temperatures (Tm) (Primers and oligonucleotides 3.3).

4.3.2. Site-directed mutagenesis

Candidate phosphosites were mutated (substituted) to either glutamic acid (E) or aspartic acid (D) and alanine (A) using polymerase chain reaction. Mutation points were placed in the middle of the primers and the melting temperature was designed to be more than 80°C. 10 µl of 5× Phusion HF buffer, 5 µl of 10 mM dNTPs, 20 pmol each of the forward and reverse primers, 10 ng of the template plasmid, 5 µl of DMSO, 0.5 µl of the Phusion DNA Polymerase (1U), and ddH_2O to a total volume of 50 µl were added to a PCR tube. The reaction tube was placed in a preheated thermocycler, with the following program: 1 cycle at 95°C for 2 min, 16 cycles of 50 sec at 95°C for, 50 sec at 60°C, and 30 sec/kb at 72°C, with a final 10 min extension at 72°C. Later, 1 µl of DpnI was added directly to the PCR products and incubated at 37°C for 4 h to digest the parental DNA template. The PCR products were purified using the protocol described in paragraph 4.3.3.

4.3.3. PCR products purification

Buffers and spin columns from QIAquick PCR purification kit were employed in order to purify and cleanup DNA PCR products. Binding buffer (PB buffer) was added to the PCR products with 3:1 ratio (PB buffer: PCR product) and the mixture was transferred into a fresh spin column. The column was centrifuged at 13000× g for 1 min and the flowthrough was collected and reloaded onto the column twice. Captured DNA was washed using wash buffer (PE buffer) and the flow-through was collected and reloaded onto the column once. The second flowthrough was discarded and the column was dried by centrifugation for 1 min at 13000× g. The collection tube

was changed and 35 µl of ddH_2O was added into the columns. After 5 min incubation at RT, dissolved DNA was collected by centrifugation at 13000× g for 1 min.

4.3.4. DNA digestion and ligation

DNA strand was cleaved at the restriction site of choice via restriction endonucleases. To that end, 10 units of restriction endonuclease(s) were incubated with 1 µg of DNA for 1 hour at 37°C in the corresponding buffer. In the case of double digestion, a reaction buffer compatible with both enzymes was chosen according to the manufacturer's recommendations. Subsequently, digested DNA was separated on an agarose gel to confirm the size of digested products or to purify the DNA fragment from the gel.

DNA fragments and the target vectors were digested using the same restriction endonucleases to generate sticky ends for ligation. 20 ng of the linear vector DNA was incubated with a 5-fold excess of the insert DNA in the presence of 1 unit of T4 DNA ligase for either 2 hours at RT or overnight at 16°C.

4.3.5. Bacterial transformation and culture

Bacterial cells were transformed using the heat shock method. Purified or ligated plasmid was mixed gently with 100 µl of chemically competent E. coli XL-1 Blue cells, and the mixture was incubated on ice for 30 min. Thereafter, heat shock was applied to the cells by incubating them for 45 seconds at 42°C followed by 2 min incubation on ice. Next, 900 µl of pre-warmed lysogeny broth (LB) medium (without antibiotic) was added to each sample, and samples were incubated at 37°C for 1 hour with 600 rpm on a Thermomixer. Then, 100 µl of the suspension was spread on LB-agarose plates containing ampicillin (150 µg/ml), and the plates were incubated at 37°C overnight. The next day, single clones were randomly picked and inoculated into 5 ml of LB-medium containing ampicillin (100 µg/ml) in glass tubes and incubated at 37°C in an orbital shaker at 200 rpm overnight. Then, the plasmid of interest was isolated from bacteria using QIAprep spin miniprep kit according to the manufacturer's protocol and was sent for sequencing verification. Correct clones were propagated and the plasmid DNA was purified using the plasmid PureLink HiPure plasmid midiprep kit according to the manufacturer's protocol.

4.4. Protein-related methods

4.4.1. Cell lysis

The following lysis buffer was used for all experiments in this study except otherwise stated. The lysis buffer is composed of 50 mM Tris-HCl pH 7.4, 500 mM NaCl, 2% TX-100, 0.4% SDS, 5 mM EDTA, 1 mM DTT, 1× protease inhibitor cocktail, and 1× phosphatase inhibitor cocktail. The lysis buffer was added to the cell pellets with 10:1 ratio (lysis buffer: cell pellet (v/v)) and the samples were placed on a rotator for 30 min at 4°C followed by brief probe sonication (2 pulses of 15 sec with 50% amplitude using 2 mm tip) to shear DNA into small fragments. Then, the lysates were centrifuged for 20 min at 16000× g at 4° C and supernatants were transferred to the new tubes for protein assay.

4.4.2. Protein concentration determination

Protein concentration was determined with the method based on the LOWRY assay protocol (LOWRY et al. 1951) using the Biorad DC assay kit according to the manufacturer's manual. Briefly, 20 µl of reagent S was added to 1 mL of reagent A to prepare reagent A'. 5 µL of diluted sample or bovine serum albumin (BSA) standard was placed in triplicates into a 96-well plate. 25 µL of working reagent A' and 200 µL of reagent B were added sequentially and the plate was incubated for 15 min at RT. Absorbance was measured at 750 nm using a TECAN microplate reader. Total protein amount was calculated using the BSA standard curve.

4.4.3. SDS-PAGE and Western blotting

10% SDS-PAGE gels were prepared using running and stacking gels (Table 4.1) and BioRad Mini-PROTEAN Tetra Cell Casting Stand. The gel was placed into an electrophoresis cell, and SDS-running buffer was added (Table 4.1). 10 – 50 µg of the protein samples were incubated for 10 min at 95°C after adding 1× Laemmli-buffer (Table 4.1), and were loaded onto the gel and the electrophoresis was performed at 120 V for ~1.5 h. Proteins separated on the gels were transferred to nitrocellulose membrane using the Perfect Blue semi-dry electro blotter according to the manufacturer instructions. The membranes were blocked with either 5% nonfat dry milk or 5% BSA in TBS containing 0.05% Tween 20 (TBS-T) for 1 hour. Subsequently, the membranes were washed thrice with TBS-T and incubated overnight at 4°C with the primary antibody. The proper secondary antibody was applied for 1 h after washing the membranes three times with TBS-T. The protein expression signals were detected using the enhanced chemiluminescence

(ECL) kit, visualized with the FUSION SOLO 4M system, and illustrated/analyzed by the FusionCapt advance software.

Table 4.1 SDS-PAGE electrophoresis buffers and solutions

Runing gel (10 ml for 2 Gels)	Stacking gel (5 ml for 2 gels)	4 x Lämmli buffer	10x SDS-running buffer, pH 8.6
Water: 4.89 ml	Water: 3.0 ml	4% (v/v) β-mercaptoethanol	1.9 M Glycine
1.5 M TRIS-HCl pH 8.8: 2.5 ml	0.5 M TRIS-HCl pH 6.8: 1.25 ml	8% (w/v) SDS	1% (w/v) SDS
10% (w/v) SDS: 100 µl	10% (w/v) SDS: 50 µl	40% (v/v) Glycerol	250 mM Tris-HCl
40% acrylamide: 2.5 ml	40% acrylamide: 625 µl	4% (w/v) Bromphenol blue	-
10% (w/v) APS: 100 µl	10% (w/v) APS: 50 µl	240 mM Tris-HCl	-
TEMED: 10 µl	TEMED: 10 µl	-	-

4.4.4. In-gel digestion of proteins

100 µg of each sample lysate was resolved on a 10% SDS-PAGE gel and the gel was stained with PageBlue protein staining solution for 1 hour. The SDS gel was washed with ddH_2O and each lane was excised into 10 pieces and each piece was further cut into 1-mm cubes. Coomassie dye was removed by washing the gel pieces with 30% ACN/0.O7 M ammonium bicarbonate (NH_4HCO_3). Afterwards, proteins were reduced with 20 mM DTT at 56°C for 45 min and alkylated using 1% acrylamide for 30 min in the dark at RT. Next gel pieces were washed with 0.1 M NH_4HCO_3, dehydrated using 100% ACN, and dried using vacuum centrifugation. Mass spectrometry grade trypsin was resuspended in 0.1 M NH_4HCO_3 and 1µg was added to each sample and incubated at 37°C, overnight. On the following day, the supernatants containing digested proteins were collected from the tubes and remaining peptides were extracted from the gel pieces by sequential addition of 50 µl of 0.1% TFA 50% ACN, 50 µl of 0.1 M NH_4HCO_3, and 100 µl of ACN. Peptides were dried using vacuum centrifugation.

4.4.5. Sample preparation for phosphopeptide enrichment

In order to perform phosphoproteomic studies, cell pellets were lysed in the following lysis buffer: 8 M urea, 75 mM NaCl, 50 mM Tris-HCl pH 8.2, 1 mM sodium fluoride, 1 mM β-glycerophosphate, 1 mM sodium orthovanadate, 10 mM sodium pyrophosphate, 1 mM PMSF, and 1× protease inhibitor cocktail. Ice-cold lysis buffer was added to the tubes containing cell pellets, and then samples were mixed by pipetting up and down. Lysates were centrifuged at 5000× g for 15 min at 4°C after brief sonication (2 pulses of 15 sec with 50% amplitude using 2 mm tip). Supernatants were transferred to new tubes and protein concentration was determined using the DC protein assay (4.4.2). Proteins were reduced using either 5 mM dithiothreitol (DTT) or 10 mM β-mercaptoethanol (β-ME) at 56° C, 800 rpm for 25 min and alkylated for 30 min in

either 20 mM acrylamide or 14 mM iodoacetamide in the dark. The reaction was quenched with the same amount of reducing reagent (DTT or β-ME) at room temperature (RT), 800 rpm for 15 min. The samples were diluted 1:5 by 25 mM Tris/HCl (pH 8.2) and $CaCl_2$ was added to a final concentration of 1 mM followed by addition of trypsin at an enzyme-to-substrate ratio of 1:200. Proteins were digested overnight at 37° C, and purified using 10 mg Oasis HLB cartridges, and the eluate fractions were dried in a vacuum centrifuge.

4.4.6. Co-immunoprecipitation (Co-IP) of Myc-tagged proteins

Co-IP experiments were carried out using Myc-Trap A beads according to the manufacturer's protocol with some modifications. Briefly, semi-confluent HEK293 cells were transfected with Myc-tagged LAMTOR1 and RagC constructs using Turbofect transfection reagent. After 48 h transfected cells were washed with PBS and harvested by a cell scraper in ice-cold PBS. The cells were pelleted at 500× g, 4°C and 400 µl of lysis buffer (40 mM HEPES pH 7.4, 1% Triton X-100, 10 mM β-glycerol phosphate, 10 mM pyrophosphate, 2.5 mM $MgCl_2$, and 2× of EDTA-free protease inhibitor cocktail) was added to each sample. The lysates were homogenized by passing through a 25G needle using a syringe once and then placed on ice for 30 min with extensive pipetting every 10 min. Thereafter, samples were centrifuged for 10 min at 20000× g, 4°C, supernatants were transferred to the new tubes, and the protein amount was measured for each sample. 3 mg of each lysate was transferred into the new tubes, and the volume was adjusted to 500 µl using dilution buffer (10 mM Tris/Cl pH 7.5, 150 mM NaCl, 0.5 mM EDTA, and 1× of protease inhibitor cocktail). The diluted lysate was added to the prewashed beads (20 µl of the Myc-trap slurry beads were washed thrice with ice-cold dilution buffer) and incubated at 4°C in a tube rotator for 3 h. Afterwards, supernatants were transferred into the new tubes, and Myc-trap beads were washed three times with the dilution buffer. To dissociate immunocomplexes from the beads, 100 µl of 2× laemmli buffer was added to each sample and incubated for 10 min at 95° C. Beads were collected by centrifugation for 2 min at 2500× g at RT and the supernatant was transferred into the new tube as an eluate. 10 µl of the fresh eluate (before freezing) was subjected to 10% SDS-PAGE gels for further analysis.

4.5. Peptide-related methods

4.5.1. Phosphopeptide enrichment

Peptides were desalted (4.5.6) and dried prior to phosphopeptide enrichment. Dried peptides were resuspended in 500 µl 80% ACN, 5% TFA, 1 M glycolic acid (Villén and Gygi 2008). TiO_2

beads were added at a ratio of 1:6 (peptides to beads, w/w) followed by incubation at RT, 1200 rpm for 15 min. Beads were pelleted by centrifugation at 13000× g for 1 min and the supernatant discarded. Subsequently, TiO_2 beads were transferred to new tubes using 1 ml of 80% ACN, 1% TFA, centrifuged, and the supernatant discarded. After washing the beads with 1 ml of 20% ACN, 0.1% TFA they were centrifuged, the supernatant was discarded and beads were dried using a vacuum centrifuge. Phosphopeptides were eluted from TiO_2 beads by adding 200 µl 1% NH_4OH and incubation at RT, 1200 rpm for 15 min. Beads were pelleted by centrifugation and supernatants transferred to new tubes followed by acidification using 10 µl formic acid (FA). Peptides were dried using a vacuum centrifuge and resolubilized in 500 µl 70% ACN, 0.1% TFA. TiO_2 was added again to each sample at a ratio of 1:6 (peptides to beads) and the beads were washed with 50% ACN, 0.1% TFA. Phosphopeptides were eluted by incubation with 200 µl 1% NH_4OH at RT, 1200 rpm for 15 min, acidified using 10 µl of FA and desalted with 10 mg Oasis HLB cartridges. The resulting elution fractions were dried using a vacuum centrifuge and stored at -20°C.

4.5.2. Strong Cation Exchange (SCX) Chromatography

Separation of peptides using SCX chromatography was performed on an Äkta Purifier system using a 100× 9.4 mm Polysulfoethyl A column as described initially by Villen et al. (Villén and Gygi 2008). The following solvents were used: solvent A: 7 mM KH_2PO_4, pH 2.65 and 30% ACN; solvent B: 7 mM KH_2PO_4, pH 2.65, 30% ACN, 350 mM KCl and solvent C: 50 mM K_2HPO_4, pH 7.5, 500 mM NaCl. pH values were adjusted using phosphoric acid (H_3PO_4) before addition of ACN. The column first was washed and equilibrated using solvent C by a linear gradient from 0 to 100% of 4 ml followed by 32 ml of 100% of C and a linear gradient from 100% to 0 of 4 ml. Finally, the column was primed with 80 ml of solvent A to be prepared for the loading of the sample. The peptides were loaded in 500 µl of solvent A followed by a washing step of 4 min. The flow rate was set at 2 ml/min and fractionation was performed at 8°C. Fractionation was performed with a linear gradient from 100% solvent A to 70% solvent A / 30% solvent B in 48 min followed by a linear gradient to 100% solvent B in 2 min, 2 min at 100% solvent B and 8 min of water. Across the gradient, 12 fractions of 12 ml each were collected for the experiment with 12 fractions and 6 fractions of 24 ml each, for comparison to the tip-based columns. Each fraction was lyophilized and peptides were desalted using Oasis cartridges followed by TiO_2 enrichment (fractionation of whole cell lysates).

4.5.3. Pipette tip-based strong cation-exchange (SCX) fractionation of peptides

Six elution buffers containing 7 mM KH_2PO_4 and 30% ACN were prepared with ascending concentrations of KCl (0 mM, 30 mM, 60 mM, 90 mM, 120 mM, and 350 mM) and pH values adjusted to 2.65 using H_3PO_4. 12 disks of Empore Cation-SR material were placed into 200 µl micropipette tips. Tip-columns were equilibrated by sequential application of 100 µl of methanol, elution buffer 6, water, equilibration buffer (50 mM K_2HPO_4, pH 7.5, 500 mM NaCl), water, and elution buffer 1, respectively, followed by centrifugation at RT, 2500× g for 3 min each. Samples were solubilized in 200 µl elution buffer 1 and loaded on the equilibrated tip-columns followed by centrifugation at RT, 2500× g for 3 min. The flow-through was collected as the first fraction and 5 more fractions were collected using 200 µl of elution buffers 2 to 6 followed by centrifugation at RT, 2500× g for 3 min. All fractions were dried using a vacuum centrifuge.

4.5.4. Pipette tip-based strong anion-exchange (SAX) fractionation of peptides

SAX fractionation was adapted from Wiesniwski et al. (Wiśniewski et al. 2009). Tip-columns were manufactured using 12 disks of Empore Anion-SR material. SAX buffers containing 20 mM AcOH, 20 mM H_3PO_4, and 20 mM boric acid were prepared with descending pH values (pH 11, 8, 6, 5, 4, 3) by the addition of NaOH. To the final elution buffer (pH 3) 0.25 M NaCl was added. Tip-columns were washed and equilibrated sequentially by the addition of 100 µl of MeOH, 1 M NaOH, and loading buffer (pH 11) followed by centrifugation at RT, 2500× g for 3 min. Samples were resuspended in 200 µl of loading buffer and loaded onto the column followed by centrifugation at RT, 2500× g for 3 min. The flow-through was collected as the first fraction followed by five subsequent fractions which were eluted using 200 µl of the buffers with descending pH value by centrifugation at RT, 2500× g for 3 min each. All samples were acidified with 10 µl of FA and dried using a vacuum centrifuge.

4.5.5. Pipette tip-based high-pH reversed-phase (Basic-RP) fractionation of peptides

We followed the strategy described by Han et al. (Han et al. 2014) with several changes concerning the type of reversed phase material used and the percentage of acetonitrile for elution of peptides in the single fractions. Tip-columns were prepared using twelve C18 Empore Extraction Disks. Buffers with 10 mM ammonium formate and increasing amounts of ACN were prepared for phosphopeptide elution and their pH value adjusted to pH 10 by the addition of 28% NH_4OH. Columns were equilibrated by sequential application of 100 µl of the following solutions and centrifugation at RT, 2500× g for 1 min: MeOH, 10 mM ammonium formate pH 10 with 50% ACN, 10 mM ammonium formate pH 10 with 2% ACN. Samples were solubilized

in 200 µl of 10 mM ammonium formate 2% ACN and the flow-through was collected as the first fraction. Subsequent fractions were eluted using 200 µl of ammonium formate buffers containing 6%, 10%, 12%, 14%, 16%, 18%, 20%, 22%, 24%, 26%, 28%, 30%, 33%, 36%, 40%, 50%, 60%, 70%, 80% and 90% ACN. Finally, tip-columns were eluted using 100% ACN. Later, these eluates were combined to form 6 fractions in the following way: fraction 1 consisted of eluates with 6%, 18%, 28%, and 50% ACN; fraction 2 of eluates with 10%, 20%, 30%, and 60% ACN; fraction 3 of eluates with 12%, 22%, 33%, and 70% ACN; fraction 4 of eluates with 14%, 24%, 36%, and 80% ACN; fraction 5 of eluates with 16%, 26%, 40% and 90% ACN; and fraction 6 was the combination of the flow-through of the sample loading step and the last eluate fraction (100% ACN). After sample pooling, all fractions were dried using a vacuum centrifuge.

4.5.6. Peptide purification methods

Depending on the amounts, peptides were purified using either StageTips or solid-phase extraction (SPE) cartridges. For the samples containing less than 10 µg of peptides, StageTips were applied as described elsewhere (Rappsilber et al. 2003). Briefly, 4-6 discs of C18 Empore extraction disks were placed in 200 µl micropipette tips and equilibrated by sequential application of 20 µl of MeOH, 80% ACN 0.5% AcOH, and 0.5% AcOH and centrifugation at RT, 2500× g for 1 min in between. In the case of phosphopeptides, StageTips columns were also primed with 20 µl of 50 mM citrate prior to loading the samples (Winter et al. 2009b). Dried peptides were resuspended in 20 µl of 5% ACN 5% FA solution, and later 80 µl of water was added to dilute ACN amount. Resuspended peptides were applied to the StageTips and washed using 100 µl of 0.5% AcOH and finally eluted using 2× 20 µL 80% ACN 0.5% AcOH. Between each step StageTips were centrifuged at RT, 2500× g for 1 min. For the larger amount of peptides (>10 µg), 10 mg Oasis HLB cartridges were applied. The cartridges were equilibrated using 1 ml of following solutions,100% ACN, 50% ACN 0.5% AcOH, and 0.1% TFA, respectively. Dried peptides were resuspended in 1 ml 1% AcOH and loaded 2× to the columns and washed using 2 ml of 0.5% AcOH. Purified peptides were eluted using 1 ml of 50% ACN 0.5% AcOH.

4.6. Mass spectrometry analysis of the samples

4.6.1. LC-MS/MS data acquisition

All samples were desalted using C18 STAGE tips as described before and dried using a vacuum centrifuge. Desalted samples were resuspended in 5% ACN, 5% FA solution and loaded on in-

house manufactured analytical columns at a flow rate of 1 µl/min solvent A (0.1% FA in water) using a nanoflow UHPLC system. Columns were prepared by packing a 100 µm ID fused silica spray tip pulled with a P2000 laser puller with 5 µm ReproSil-Pur 120 C18-AQ particles. In the case of phosphopeptides, columns were equilibrated with several injections of 50 mM citrate before running phospho-samples (Winter et al. 2009b). Separation was performed at a flow rate of 400 nl/min with 60 or 90 min gradients from 99% solvent A (water with 5% DMSO (Hahne et al. 2013), 0.1% FA) 1% solvent B (ACN with 5% DMSO, 0.1% FA) to 65% solvent A 35% solvent B. 240 min segmented gradients were used for the analyses of unfractionated samples. Segmented gradients consisted of a 200 min linear gradient from 1% to 25% solvent B, followed by a 30 min step to 30% solvent B and a 10 min step to 35% solvent B at 400 nl/min. Peptides eluting from the column were ionized at 1.6 kV in the positive ion mode in the nanosource of an LTQ Orbitrap Velos mass spectrometer. Survey scans were acquired in the Orbitrap analyzer from m/z 400 to 1200 at a resolution of either 30000 or 60000 followed by fragmentation of the 10 most abundant ions in the LTQ part of the instrument. Singly charged ions and such with unassigned charge states were excluded from MS/MS fragmentation. The repeat count was set to 1 and dynamic exclusion to 30s for all gradients. Multi-Stage Activation (MSA) (Schroeder et al. 2004) was activated for phosphosamples triggered by neutral-losses of phosphoric acid (m/z 24.5, 32.7, 49, and 98).

4.6.2. Mass spectrometry data analysis

The generated mass spectrometry raw files were processed using MaxQuant (version 1.5.2.8) using the Andromeda search engine (Cox and Mann 2008). The database used was either UniProt human (including SwissProt and TrEMBL, release 2015_04, 68485 entries) for human cell lines or Uniprot mouse (including SwissProt and TrEMBL, release 2015_05, 53297 entries) for murine cell lines. The enzyme specificity was set to trypsin with maximum of two missed cleavages allowed and quantification was performed using default parameters for 2 states (light and heavy (K8, R10)) SILAC in MaxQuant. Fixed modifications were set to carbamidomethyl (in the case of alkylation with iodoacetamide), or propionamide (in the case of alkylation by acrylamide) at cysteine residues. Variable modifications were as follows: acetylation at protein N-termini, oxidation at methionine, carbamylation at lysine and peptide N-termini (in the case of urea based lysis buffer), as well as phosphorylation at serine, threonine, and tyrosine. Matching between runs was used with default settings. The minimal score for modified peptides was set to 40 and the minimal delta score for modified peptides to 9.

4.6.3. Bioinformatic and statistical analysis

MaxQuant-processed data were further analyzed using the Perseus toolbox (version 1.6.0.7) and Microsoft Excel (2010). For Gene Ontology (GO) analysis GOrilla (Gene Ontology enRIchment anaLysis and visualization (http://cbl-gorilla.cs.technion.ac.il)) (Eden et al. 2009)) and PANTHER (Protein Analysis Through Evolutionary Relationships (http://www.pantherdb.org)) (Ashburner et al. 2000) tools (free online GO tools) were employed to identify enriched GO terms. Using Gorilla, differentially expressed proteins were implemented as a target group and other proteins found in all replicates were applied as background and gene ontology annotation was performed for biological process. Functional GO enrichment analysis of biological processes and cellular component was carried out using the PANTHER tool. Statistical processing of data and graphing were performed using Prism software (GraphPad Prism version 6.07) and Microsoft Excel 2010.

5. Chapter 1: Tip-based fractionation of batch-enriched phosphopeptides

5.1. Introduction

5.1.1. Large-scale phosphoproteomics

Protein phosphorylation plays an important role in a multitude of cellular functions such as signal transduction, regulation of enzyme activity, and protein–protein interactions (Pawson 2004). Since the first development of workflows for large-scale phosphoproteome analysis using mass spectrometry, a significant variety of protocols has been established for the enrichment and fractionation of phosphopeptides (Kanshin et al. 2012; Engholm-Keller and Larsen 2013). This led to the identification and quantification of phosphorylation sites in a plethora of cells and tissues providing valuable information for the identification of cellular mechanisms (Hornbeck et al. 2015). The development of these workflows was motivated by technical challenges preventing the identification of phosphopeptides in complex peptide mixtures resulting from the proteolytic digestion of whole proteomes. The most important to mention are low abundance and altered detection efficiencies compared to those of nonphosphorylated peptides in the sample. The latter can be due to altered ionization of phosphorylated peptides as well as loss of phosphopeptides caused by unspecific binding to metal ions on reversed-phase columns (Seidler et al. 2011; Winter et al. 2009b; Winter et al. 2012).

5.1.2. Phosphopeptide enrichment methods and workflows

For enhancing the detection of phosphopeptides, several methods have been established for their enrichment based on the negatively charged phosphorylation group. These methods can be grouped into three categories: (i) immobilized metal ion affinity chromatography (IMAC), (ii) metal oxide affinity chromatography (MOAC), and (iii) immunoaffinity chromatography

(Kanshin et al. 2012; Engholm-Keller and Larsen 2013; Rush et al. 2005; Rikova et al. 2007). Besides these affinity methods, liquid chromatography (LC)-based approaches have been used for separating phosphopeptides from their nonphosphorylated counterparts. The most popular ones are ion exchange chromatography (SAX (Han et al. 2008) and SCX (Beausoleil et al. 2004)), hydrophilic interaction liquid chromatography (HILIC) (McNulty and Annan 2008), and electrostatic repulsion-hydrophilic interaction chromatography (ERLIC) (Alpert 2008). Similar to IMAC and MOAC, the negative charge of the phosphate group allows for separation of phosphopeptides from their nonphosphorylated counterparts in these approaches (Kanshin et al. 2012). Although the mentioned chromatographic separations can be used as a stand-alone method for phosphopeptide enrichment in large-scale phosphoproteomic studies, the combination of peptide fractionation (usually by SCX, SAX, or high-pH reversed-phase chromatography) with an enrichment for phosphopeptides by IMAC or MOAC are most common (Kanshin et al. 2012; Engholm-Keller and Larsen 2013). Although sample fractionation can principally be performed either before or after phosphopeptide enrichment, the vast majority of studies employed fractionation followed by enrichment of phosphopeptides for each fraction (Kanshin et al. 2012; Engholm-Keller and Larsen 2013). These approaches are very laborious and time-consuming because each of the generated fractions has to be processed individually. Therefore, enrichment of phosphopeptides prior to fractionation would be more cost-effective and less time-consuming, as for each sample only a single phosphopeptide enrichment has to be performed. Furthermore, it would be possible to miniaturize fractionation equipment as the samples to be fractionated are several micrograms of phosphopeptides rather than several milligrams of whole cell lysate digests. So far only a handful of studies have been published performing fractionation of phosphopeptides after their enrichment. Engholm-Keller et al. developed a workflow that consists of SIMAC (Thingholm et al. 2008) enrichment of phosphopeptides followed by their fractionation by HILIC (TiSH workflow) (Engholm-Keller et al. 2012), and Wiśniewski et al. performed filter-aided sample preparation (FASP) and TiO_2 enrichment prior to phosphopeptide fractionation using SAX tip-based columns (Wiśniewski et al. 2010). Batch-enrichment of phosphopeptides using TiO_2 followed by TMT labeling and high-pH reversed-phase fractionation was first used by Erickson et al. (Erickson et al. 2015) and later by Possemato et al. (Possemato et al. 2017), and Iesmantavicius et al. was the first to use SCX tip-based fractionation after batch enrichment of phosphopeptides using TiO_2 (Iesmantavicius et al. 2014). Adachi et al. developed an alternative fractionation strategy by SCX tips of IMAC batch-enriched phosphopeptides

(Adachi et al. 2016). Furthermore, for samples enriched for other PTMs, SCX tip-based fractionation has been shown to be successful. Weinert et al. (Weinert et al. 2013), for example, used SCX tips to fractionate succinylated peptides, and Iesmantavicius et al. employed this strategy for ubiquitinated peptides (Iesmantavicius et al. 2014). Tip-based fractionation of peptides follows the principle of STAGE tips, which are micro columns manufactured using chromatographic beads immobilized in a Teflon meshwork (Rappsilber et al. 2003). In this context, the advantages of this method over conventional chromatographic methods are, for example, their low cost, ease-of-use, reproducibility, and flexibility. For the fractionation of peptide samples in general, tip-based columns are by now well-established, especially in the format of strong anion exchange tips (e.g., refs (Wiśniewski et al. 2009) and (Zarei et al. 2016)).

In this study, methods for the analysis of batch-enriched phosphopeptide samples were compared. This includes analysis of unfractionated samples using long gradients, fractionation by tip-based SAX, SCX, and BRP columns as well as the commonly used setup using a high-capacity SCX column in combination with a chromatography system.

5.2. Results

5.2.1. Fractionation of batch-enriched peptides by SCX chromatography leads to substantial loss of phosphopeptides

Initially, to minimize experimental variation induced by sample preparation, ~70 mg of HeLa whole cell lysate digest was prepared and stored after desalting as dried aliquots of 3 mg each at −20 °C. We first set a benchmark following the well-established protocol by Villen et al. (Villén and Gygi 2008). Instead of IMAC, we used TiO_2 phosphopeptide enrichment as it performed better in our hands, resulting in higher numbers of identified phosphorylation sites and less unspecific enrichment of nonphosphorylated peptides (data not shown). Using SCX chromatography, we generated 12 fractions and enriched each of them using TiO_2 (SCX-TiO_2) followed by LC–MS/MS analyses. With this approach, we were able to identify 10908 nonredundant phosphorylation sites with a phosphopeptide enrichment efficiency (purity) of 93% (Figure 5.1, Supplementary tables 5.1 and 5.2). Next, we tested if it is possible to perform first phosphopeptide enrichment and then fractionation by SCX chromatography. This would allow for conducting only one phosphopeptide enrichment and reducing the complexity of the obtained SCX fractions. We performed TiO_2 phosphopeptide enrichment of 3 mg of whole cell lysate tryptic digest and fractionated the phosphopeptide-enriched sample using SCX (TiO_2-SCX) followed by LC–MS/MS analyses using the same setup as used for the SCX-TiO_2 experiments. We could identify only 1291 phosphorylation sites showing a dramatically decreased performance (Figure 5.1, Supplementary tables 5.1 and 5.2). To investigate if the enrichment of phosphopeptides from the unfractionated samples led to lower enrichment efficiencies, and therefore lower numbers of identifications, we performed 4 h gradient LC–MS/MS analyses of unfractionated phosphopeptide-enriched samples.

5.2.2. Performance of single gradient analysis of enriched phosphopeptides is limited by the binding capacity of the analytical C18 column

The binding capacity of the analytical C18 columns in our LC–MS/MS setup should be in the range of several μg of peptide. We therefore questioned if 3 mg of peptide is too much as starting material for phosphopeptide enrichment when analyzing the unfractionated sample by 4 h gradients, as the amount of enriched phosphopeptides may exceed the capacity of the column.

We therefore performed phosphopeptide enrichment of 0.5, 1, 2, and 3 mg of whole cell lysate

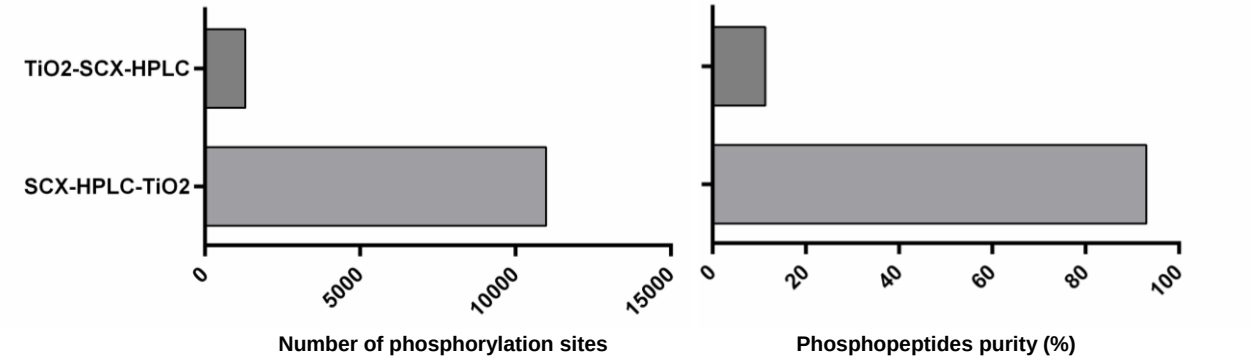

Figure 5.1 Comparison between TiO_2-SCX-HPLC and SCX-HPLC-TiO_2 methods.
Comparison between the strong cation exchange (SCX) fractionation of 3 mg tryptic HeLa whole cell lysate digest prior to phosphoenrichment by TiO_2 (SCX-HPLC-TiO_2) and SCX fractionation of the same sample after batch-enrichment of the phosphopeptides by TiO_2 (TiO_2-SCX-HPLC). Shown are numbers of identified phosphorylation sites (left panel) and the enrichment efficiency (purity) of the phosphopeptides (right panel).

digest using TiO_2 and analyzed the resulting phosphopeptide-enriched fractions by LC–MS/MS. We were able to identify 1349, 3980, 4984, and 5061 phosphorylation sites for 0.5, 1, 2, and 3 mg of cell lysate digest, respectively (Figure 5.2). We had the impression that the capacity of the system was already approaching its maximum using phosphopeptides enriched from 1 mg of starting material as doubling and tripling this amount both resulted in an increase of identified phosphorylation sites by only ~25% with virtually no difference between 2 and 3 mg of starting material. We achieved for 3 of the 4 samples a purity of more than 80% observing a slight reduction with increasing amounts of starting material: 86.2, 84.6, 81.3, and 77.1% phosphopeptides for 0.5, 1, 2, and 3 mg, respectively. From these results, we conclude that fractionation is a mandatory step for the phosphoproteomics analysis of highly complex samples. Therefore we compared three tip-based fractionation methods.

5.2.3. Fractionation of batch-enriched phosphopeptides using tip-based columns

We evaluated three different types of chromatographic material covering the most common resins used for the preparation of tip-based chromatography columns: strong anion exchange (SAX) (Wiśniewski et al. 2010), strong cation exchange (SCX) (Rappsilber et al. 2007), and C18 reversed-phase material (Possemato et al. 2017) for basic reversed-phase (BRP) fractionation (Figure 5.3 (B)).

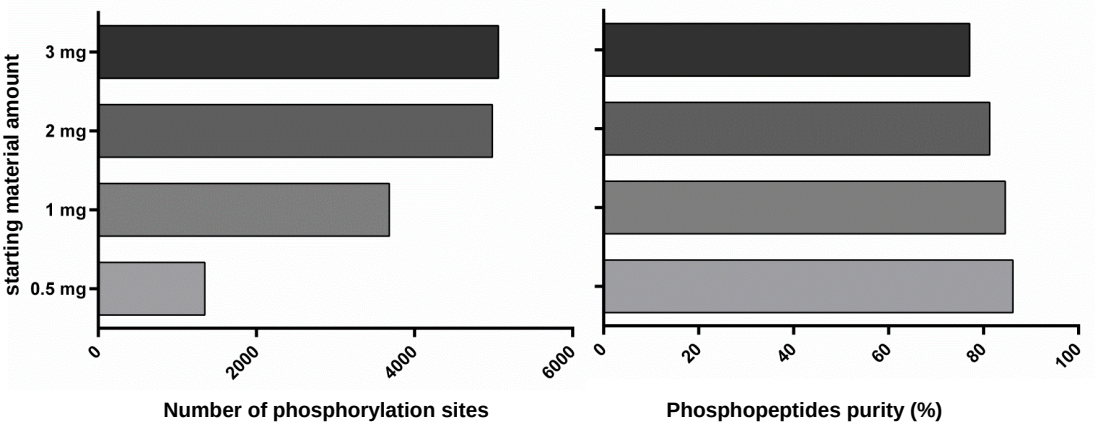

Figure 5.2 Performance of single gradient analysis of enriched phosphopeptides.
The number of identified phosphorylation sites (left panel) and the enrichment efficiency (purity) of phosphopeptides (right panel) in unfractionated phosphopeptide enriched samples analyzed with 4 hour LC-MS/MS gradients. 0.5, 1, 2, and 3 mg of HeLa whole cell lysate tryptic digest were used as the starting material for TiO_2 phosphopeptide enrichment. n=1

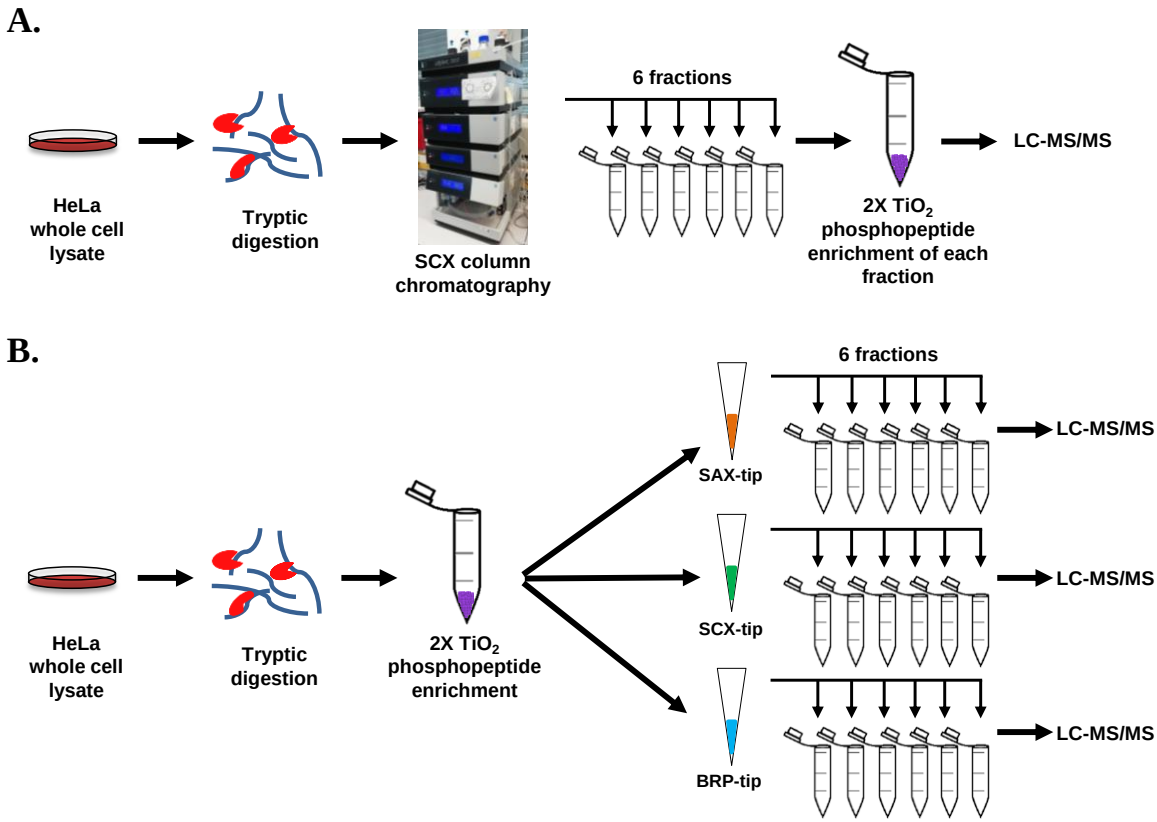

Figure 5.3 Schematic view of the workflow for phosphoenrichment and fractionation methods.
A. Digested peptides were fractionated using SCX column chromatography, and subsequently, phosphopeptide enrichment was performed for each fraction (CSCX method) **B.** Enriched phosphopeptides were fractionated using three tip-based fractionation methods, and the results were compared.

We generated tip-columns following the principle of STAGE tips (Rappsilber et al. 2003) using an increased number of disks to allow for higher binding capacity. SAX and BRP tip fractionation was carried out following published protocols (Wiśniewski et al. 2010; Han et al. 2014) employing decreasing pH value (SAX) and increasing acetonitrile content (BRP) for

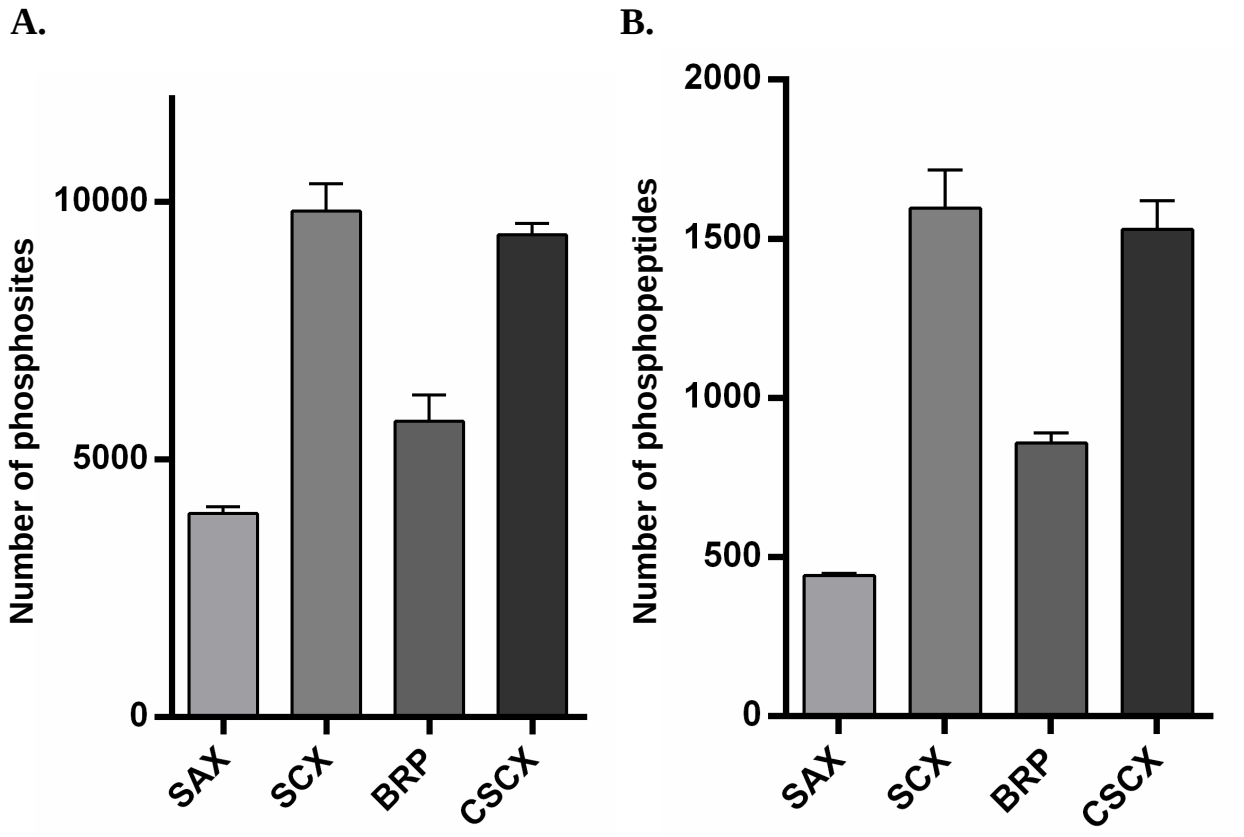

Figure 5.4 SCX tip-based fractionation outperforms the other approaches.
A. Identified phosphorylation sites for strong cation exchange (SCX), strong anion exchange (SAX) and basic reversed phase (BRP) tip-fractionated batch-enriched phosphopeptides. Column chromatography SCX (CSCX) samples were first fractionated followed by phosphopeptide enrichment of the single fractions. **B.** Identified unique multiply phosphorylated peptides for each of the tip-based methods as well as CSCX. Shown are mean values + SD; n=3

elution of peptides, respectively. For SCX tips, we designed our own buffers reflecting the gradient we used for SCX fractionation of whole cell lysate digests with the chromatography system (SCX-TiO_2), eluting peptides with increasing salt concentration. For each approach, we fractionated the enriched phosphopeptides from 3 mg of whole cell lysate tryptic digest to six fractions. Additionally, we performed fractionation using an SCX column in combination with a

chromatography system, generating six fractions that were then enriched for phosphopeptides to be able to compare the performance of our approach to the common SCX-TiO_2 procedure

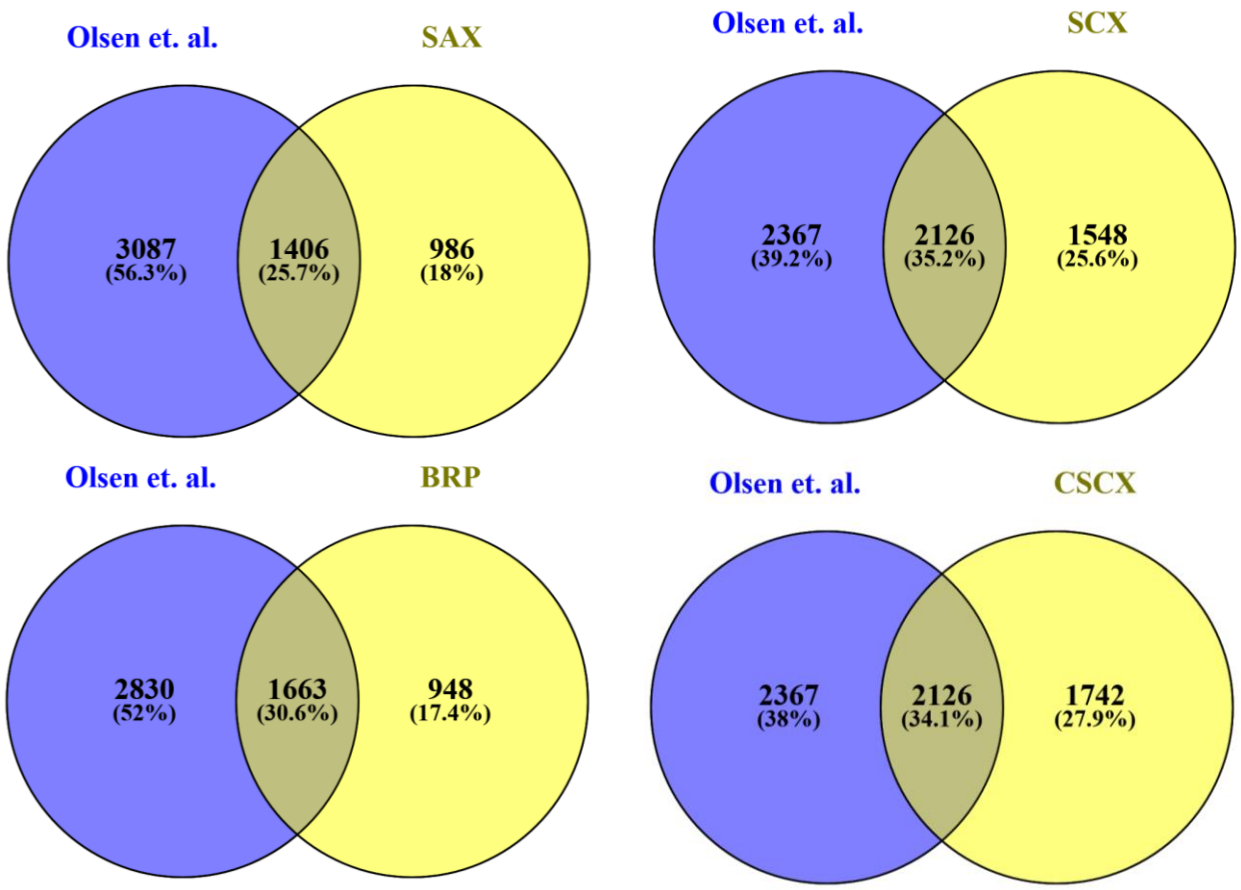

Figure 5.5 Comparison of the phosphoproteins identified with the different fractionation methods to the dataset published by Olsen et al (Olsen et al. 2010).
Percentages show the proportion of phosphoproteins that are specific for each study or are common among studies. Venn diagrams were constructed using the open-access online tool Venny (Juan Carlos Oliveros).

(Figure 5.3 (A), column-SCX, CSCX). Each experiment was carried out in three independent replicates, and eluate fractions were analyzed by LC–MS/MS.

5.2.4. SCX tip-based fractionation outperforms the other approaches

SCX tips resulted with 9812 identified phosphorylation sites on average in the highest number of identifications followed by CSCX, BRP tips, and SAX tips with 9354, 5740, and 3950 sites, respectively (Figure 5.4 (A), Supplementary tables 5.1 and 5.2). This corresponds to with the identification of 3674, 3868, 3611, and 2392 phosphoproteins. Out of the 5315 detected phosphoproteins in total, 34.2% overlap with a data set published by Olsen et al. (Olsen et al. 2010), who performed SCX-TiO_2-based analysis of the HeLa phosphoproteome, whereas the

phosphoproteins identified in the individual approaches overlap between 26 and 35% with these data (Figure 5.5).

For both SCX and BRP, we identified 54% of phosphopeptides in all three replicates. The CSCX- and SAX-fractionated samples resulted in slightly lower values, identifying 51 and 45% of phosphopeptides in all replicates, respectively (Figure 5.6 (A)). When comparing the overlap between the different approaches, out of ~16,400 phosphosites identified in total, only 17% were detected with all four approaches. CSCX and SCX tips led to the identification of the highest number of unique phosphopeptides (17.7 and 17.3%, respectively) followed by BRP (6.1) and SAX (5.3) (Figure 5.6 (B)). For multiply phosphorylated peptides, SCX and CSCX performed similarly. They outperformed the other two methods by leading on average to 3.6- (SAX) and 1.8- (BRP) times the number of identified multiply phosphorylated peptides (Figure 5.4 (B)). The distribution of identified phosphopeptides across fractions (Figure 5.7 (A)) followed a similar pattern for SAX and BRP, with the first fraction resulting in the highest number of identifications (~25% of identified phosphopeptides), and all of the following fractions resulted in substantially lower numbers. The only exception was the last BRP fraction, which also contained a high number of phosphopeptides. This is most likely due to the fact that it was composed of the first (flow-through) and the last fraction of elution (4.5.5), indicating that a substantial amount of phosphopeptides do not bind to the C18 material under these conditions, as the last fraction (elution with 100% ACN) should not contain a high number of phosphopeptides.

For the SCX samples, the distribution was more even with the second fraction containing the highest number of phosphopeptides. CSCX-fractionated samples showed a high amount of phosphorylated peptides in the first three fractions, whereas identifications in the following three fractions decreased substantially. These results were quite surprising to us, as we expected the SAX material to bind the acidic phosphorylated peptides very efficiently (Dai et al. 2009) and therefore did not expect to find the highest numbers of phosphopeptides in the flow-through. It seems that the phosphate group is not able to result in strong binding to the ion exchanger resin for all peptides. This may be improved by changing the buffer system used. For multiply phosphorylated peptides (Figure 5.7 (B)), we observed similar behavior as for singly phosphorylated peptides for the BRP samples, whereas in this case, the presence of phosphopeptides in the fraction consisting of the flow through and the last elution was even more

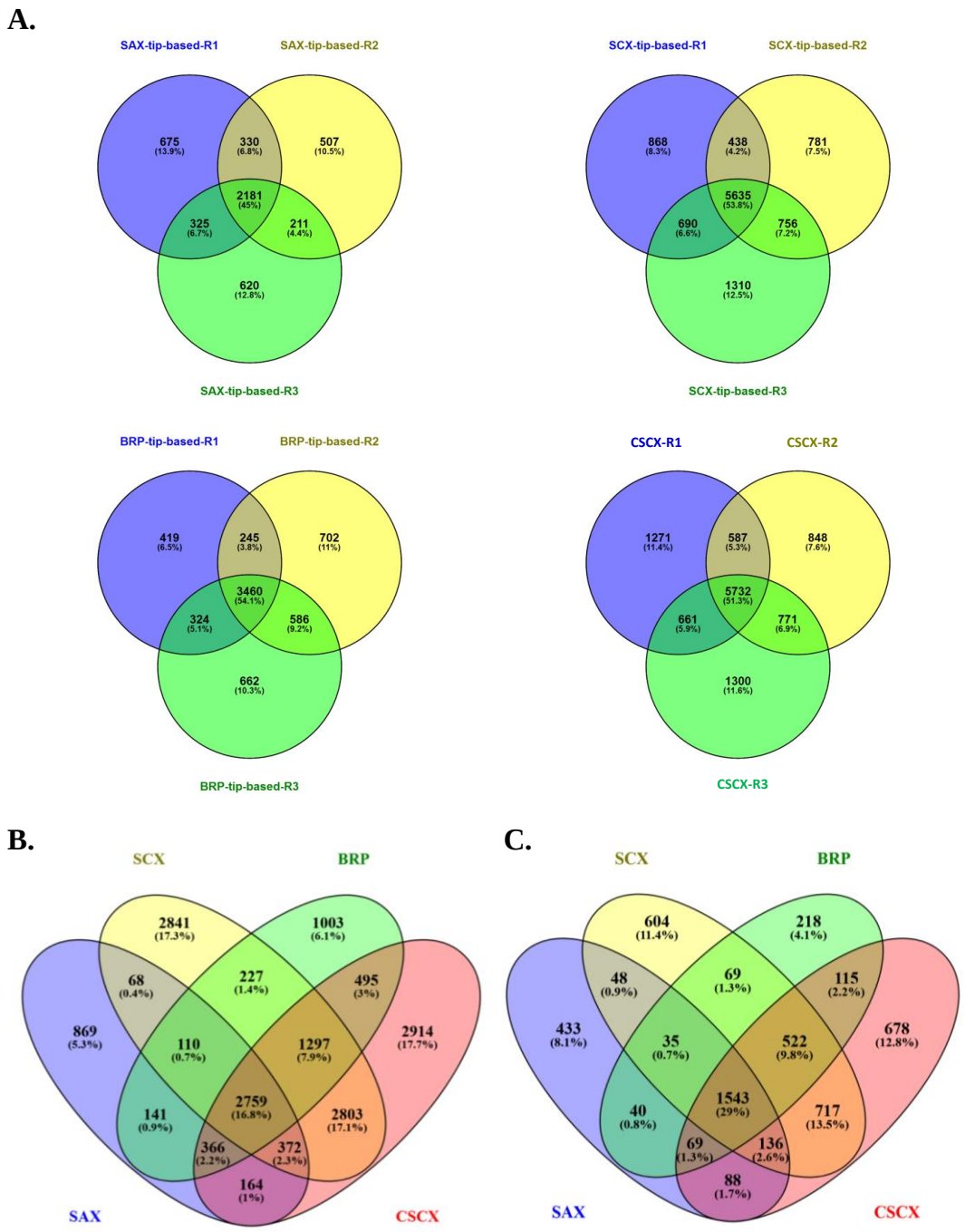

Figure 5.6 The overlap between different replicates and fractionation methods.
A. Overlap of identified phosphopeptides in 3 independent replicates for the fractionation of phosphopeptides enriched from 3 mg HeLa whole cell tryptic digest by strong anion exchange (SAX) tips, strong cation exchange (SCX) tips, basic reversed phase (BRP) tips and column SCX (CSCX) fractionation of whole cell lysate tryptic digest followed by enrichment of the individual fractions. **B.** Overlap of phosphopeptides identified in the 4 different methods. (C) Overlap of phosphoproteins identified in the 4 different methods. R1: replicate 1, R2: replicate 2, R3: replicate 3. Venn diagrams were constructed using the open-access online tool Venny (Juan Carlos Oliveros).

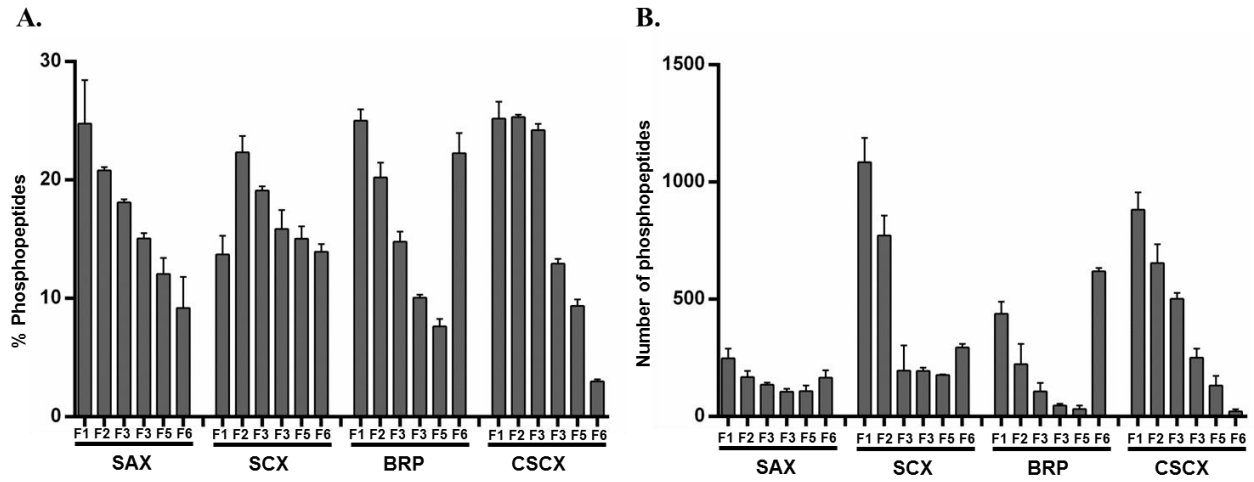

Figure 5.7 The distribution of identified phosphopeptides across fractions (F1 to F6).
A. Distribution of phosphorylated peptides across six fractions (F1 to F6) of the tip-based SAX, SCX, BRP fractionation and Column chromatography SCX (CSCX) of batch-enriched phosphopeptides (displayed as a percentage of the total number of identified phosphopeptides). **B.** Distribution of multiply phosphorylated peptides across the six fractions of each tip-based method and column chromatography SCX (CSCX). Shown are mean values + SD; n=3

pronounced. In the SCX samples, the majority of multiply phosphorylated peptides eluted in the first two fractions, which is in accordance with the literature (Mohammed and Heck 2011). In the CSCX-fractionated samples, the initial fraction contained the highest number of peptides, which decreased steadily with increasing fraction number. SAX, surprisingly, performed the worst, and no big differences for the numbers of identified multiply phosphorylated peptides between the individual fractions were observed. A possible reason for this bad performance is a very strong binding of multiply phosphorylated peptides to the SAX resin preventing their elution with the buffers used in our experimental setup. In general, the significant differences observed between the different resins were quite surprising to us as the input and number of fractions were the same for all approaches. In particular, the results obtained for the BRP-fractionated samples were quite unexpected as it had been shown before that BRP outperforms SCX in the classical "fractionation followed by enrichment" format (Yue and Hummon 2013; Batth et al. 2014). A possible reason for these discrepancies may be the material used for generating the BRP tip columns, as different resins may exhibit varying stabilities under the basic conditions used. Furthermore, we only generated six fractions with discontinuous steps increasing by 2% ACN each for elution of phosphopeptides, whereas most column-based approaches employ continuous gradients and

collect higher numbers of fractions. This also results in a substantially different concatenation

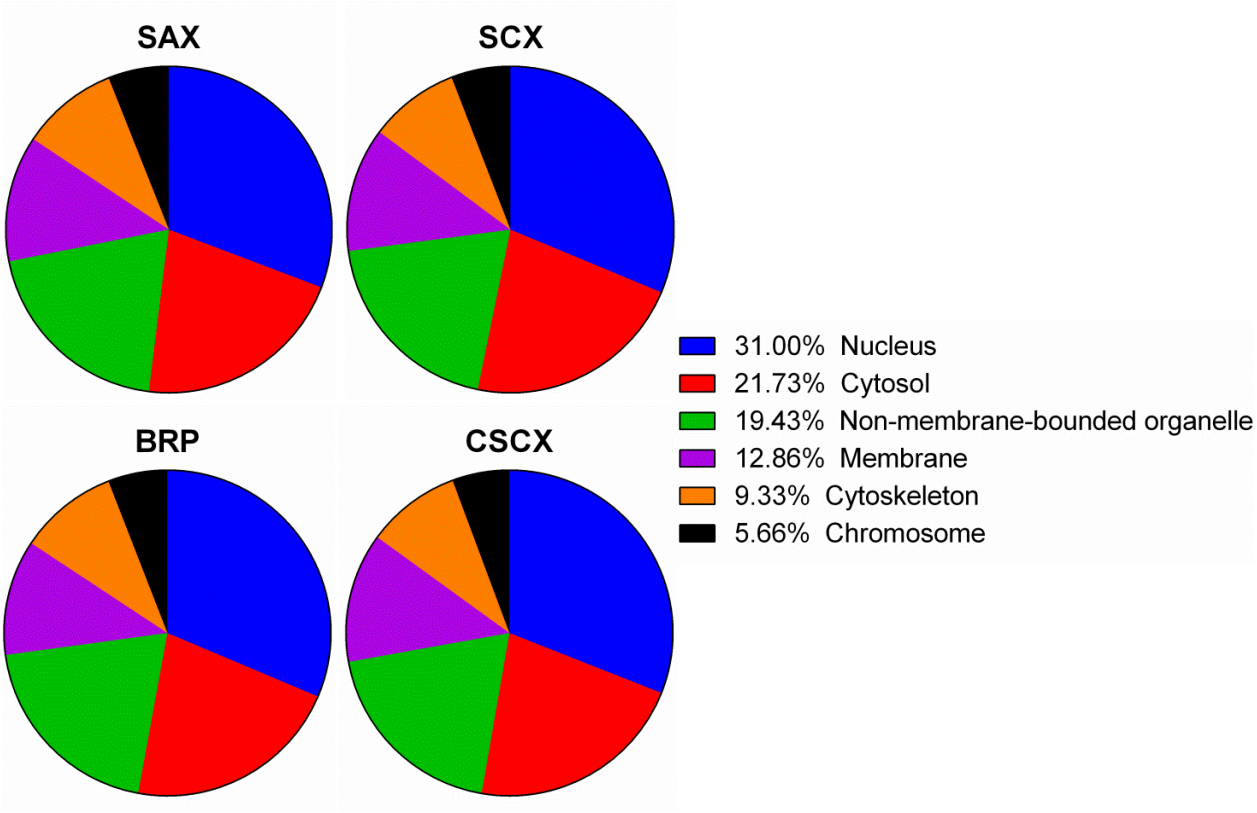

Figure 5.8 Gene ontology (GO) analysis of phosphoproteins.
GO analysis of identified phosphoproteins using the strong anion exchange (SAX) tips, strong cation exchange (SCX) tips, basic reversed phase (BRP) tips, and column SCX (CSCX). GO analysis was performed using PANTHER (Mi et al. 2017; Mi et al. 2013).

pattern compared to our approach, possibly improving separation power and reducing redundancy. For the strong differences observed between SAX- and SCX/CSCX-fractionated samples, the presence of salt in the elution buffer may be essential, and the use of salt gradients for SAX tips may therefore improve their performance. To further evaluate possible reasons for the discrepancies observed between the SAX-, SCX-, BRP-, and CSCX-fractionated samples, we performed gene ontology (GO) analyses of the phosphoproteins identified in the individual datasets (Figure 5.8, Supplementary table 5.3). We could not observe any differences in the GO categories assigned. This indicates that the physicochemical properties of the proteins from which the identified peptides originate are not likely to be the reason for the discrepancies observed. We therefore argued that the observed effects must be due to the properties of the individual peptides and their interaction with the resins in the different approaches.

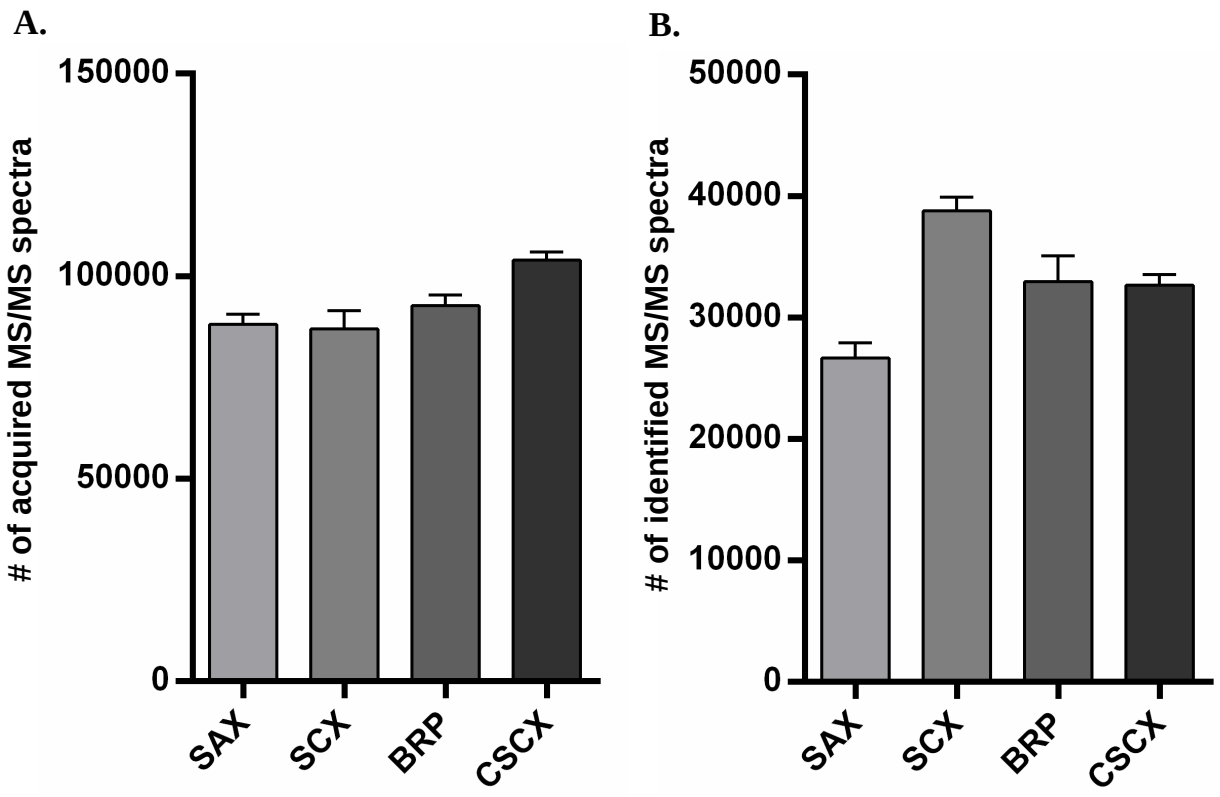

Figure 5.9 Identification efficiency of fragment ion spectra.
A. Acquired MS/MS spectra for SAX, SCX and BRP tip fractionated and column chromatography SCX (CSCX) tryptic digests of HeLa whole cell lysate. **B.** Identified MS/MS spectra for each tip-based methods and CSCX. Shown are mean values + SD; n=3

5.2.5. Identification efficiency of fragment ion spectra

A possible reason for the observed discrepancies is a difference in data acquisition. We therefore investigated the number of MS/MS spectra acquired, which was the lowest for SCX and the highest for CSCX (Figure 5.9 (A)). In terms of identified MS/MS spectra, however, the SCX-fractionated samples outperformed the other samples, resulting in increases of 15, 18, and 45% compared to BRP, CSCX, and SAX, respectively (Figure 5.9 (B)).

A possible reason for these observations is differences in signal intensity for the fragmented phosphopeptides as high-intensity precursor ions will lead more likely to the identification of the respective peptides. Possible reasons leading to higher intensities are (i) a better distribution of high-abundance ions across fractions in the SCX samples resulting in lower complexities of individual fractions and, therefore, no undersampling in the data-dependent acquisition (DDA) mode or (ii) better resolution leading to higher concentrations of peptides in single fractions,

preventing redundant fragmentation. For the SAX-, BRP-, and CSCX-fractionated samples, we

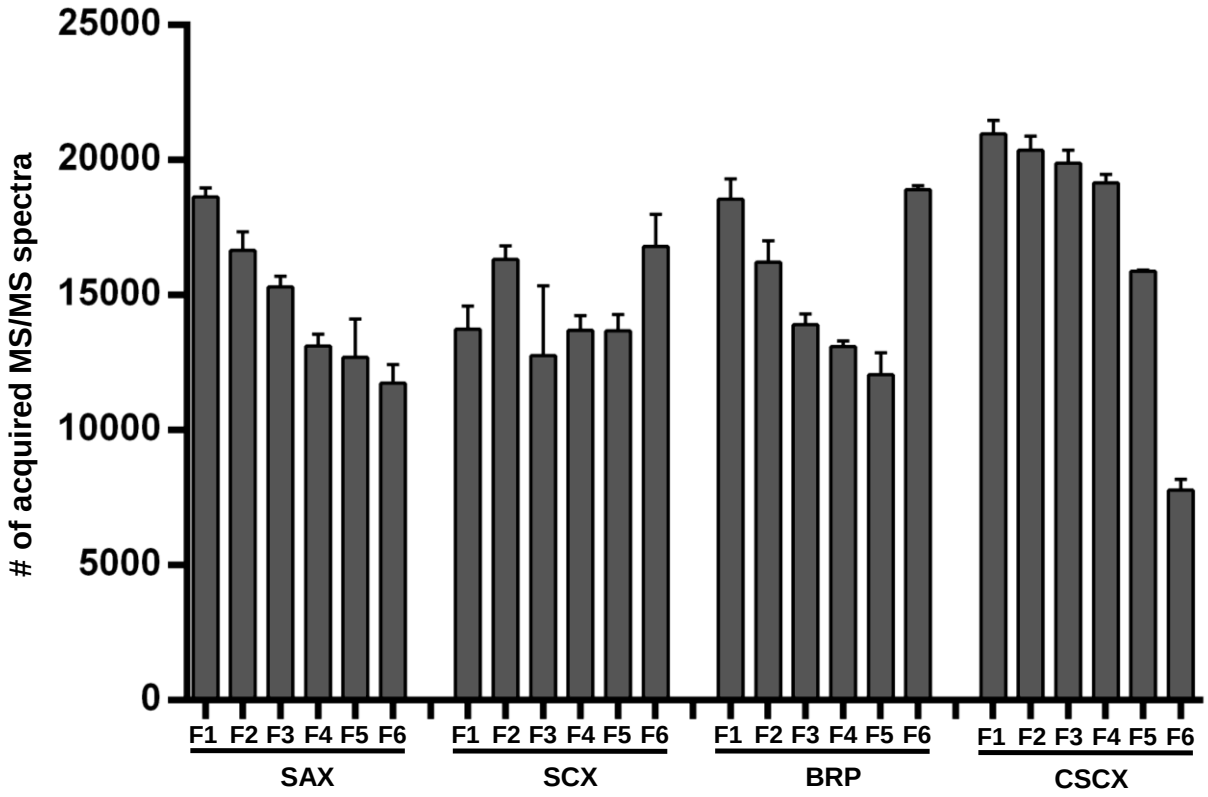

Figure 5.10 Distribution of acquired MS/MS spectra across the fractions.
The number of acquired MS/MS spectra in single fractions (F1 to F6) of strong anion exchange (SAX) tips, strong cation exchange (SCX) tips, basic reversed phase (BRP) tips, and column chromatography SCX (CSCX). 3 mg of HeLa whole cell lysate tryptic digest were enriched by TiO_2 followed by tip-based fractionation of the phosphopeptides. For CSCX, whole cell lysate digests were fractionated and the generated fractions were enriched individually. Shown are mean values + SD; n=3

observed a decrease of acquired MS/MS spectra with increasing fraction number whereas no such effect could be seen for SCX (Figure 5.10), indicating a more homogeneous distribution of phosphopeptides for the SCX-fractionated samples. Additionally, we observed higher redundancy in the SAX-fractionated samples compared to SCX and BRP, which resulted in roughly similar values (Figure 5.11): more than 50% of the peptides in the SAX-fractionated samples were detected more than 4 times. This implies that SAX fractionation leads to a broader distribution of peptides across fractions. This results in reduced signal intensities in the individual fractions and therefore reduces the likelihood for fragmentation (and identification) in the LC–MS/MS experiments. For CSCX-fractionated samples, however, the redundancy was significantly lower

across all data sets showing superior fractionation compared to all tip-based approaches. It also,

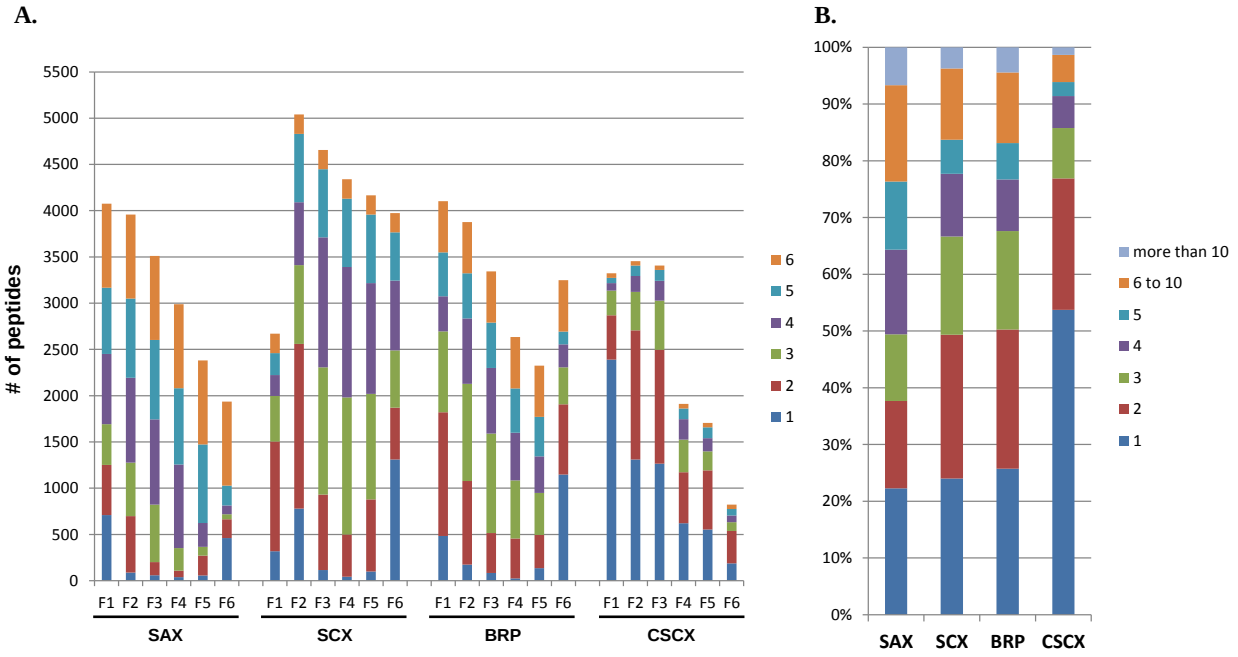

Figure 5.11 Peptide redundancy observed in the tip-based fractionation of batch enriched phosphopeptides and the enrichment of single fraction generated by column SCX chromatography (CSCX).
3 mg of HeLa whole cell lysate tryptic digest were used for each experiment. Fractionation of batch enriched phosphopeptides was performed by strong anion exchange (SAX), strong cation exchange (SCX) and basic reversed phase (BRP) tips, and column chromatography SCX (CSCX). **A.** Peptide redundancy observed in each fraction of tip-based methods and CSCX. Numbers in the legend (1 to 6) refer to the number of fractions the same peptide has been identified in. **B.** Peptide redundancy observed in whole datasets displayed as relative values normalized to the total number of peptides identified for the respective stationary phase, also mutiple identifications in the same fraction are included.

however, indicates a higher loss of phosphorylated peptides during sample preparation as the reduced redundancy should facilitate the identification of more phosphorylation sites compared to that of the tip-based SCX approach, which is not the case. In the tip-based approaches, a broader dilution of the sample should lead to more features identified because the same peptide will be recognized in the survey scan of multiple runs. We therefore investigated how many peptide features (all detected LC-MS features) were detected by MaxQuant in the SAX-, SCX-, BRP-, and CSCX-fractionated samples (Figure 5.12). The SAX-fractionated samples resulted in ~22000 and the BRP fractionated samples in ~31000 more features than in the SCX- and CSCX-fractionated samples, which resulted in similar values (increase of 9 and 12% relative to SCX and CSCX, respectively), confirming a broader distribution of peptides for the SAX and BRP tip-fractionated samples.

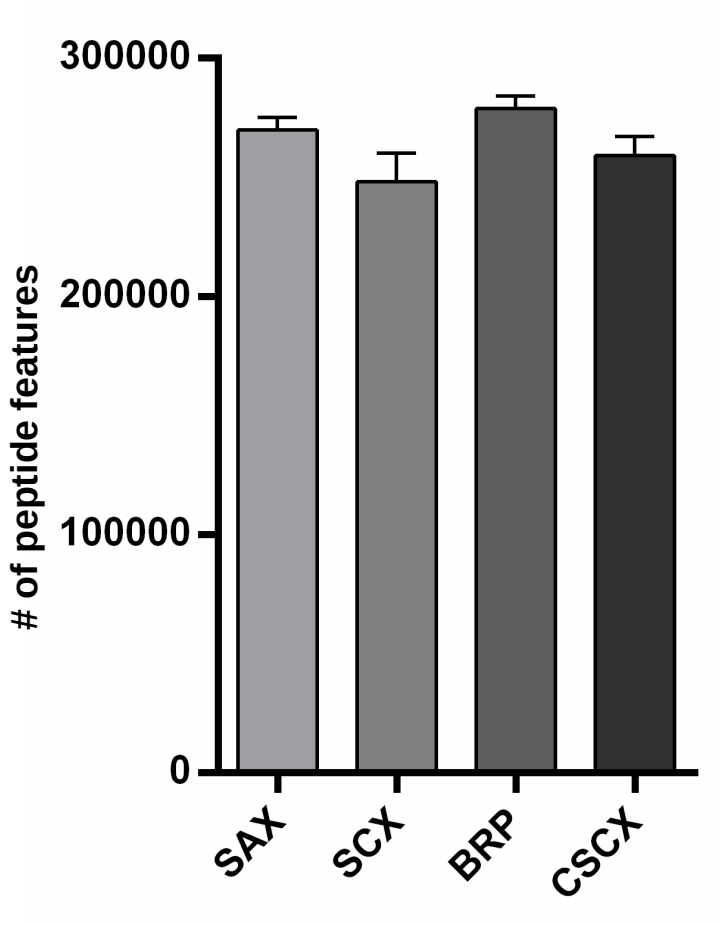

Figure 5.12 Comparison of the number of peptide features (all detected LC-MS features) among different methods.
Peptide features detected by MaxQuant in the strong anion exchange (SAX), strong cation exchange (SCX), basic reversed phase (BRP) tip-based fractionation, and column chromatography SCX (CSCX) samples. Phosphopeptides were enriched from tryptic digests of 3 mg HeLa whole cell lysate using TiO_2 followed by fractionation using different methods. Shown are mean values of the sum of the 6 individual fractions + SD; n=3.

5.2.6. Identification of nonphosphorylated peptides

Next, we investigated the purity of phosphopeptides by comparing numbers of identified phosphorylated and nonphosphorylated peptides. Surprisingly, the purity varied strongly between SAX (62%)-, SCX (86%)-, BRP (66%)-, and CSCX- (84%)-fractionated samples (Figure 5.13).

Across single fractions, the percentage of phosphorylated peptides was constantly ~60% for SAX-fractionated samples but varied between fractions of the SCX (97 to 80%)-, BRP (84 to 43%)-, and CSCX (96 to 46%)-fractionated samples (Figure 5.14). The strong difference between fractions we observed in the BRP samples reflects the influence of phosphate groups on retention

behavior in reversed-phase chromatography. Peptides carrying a phosphate group elute earlier

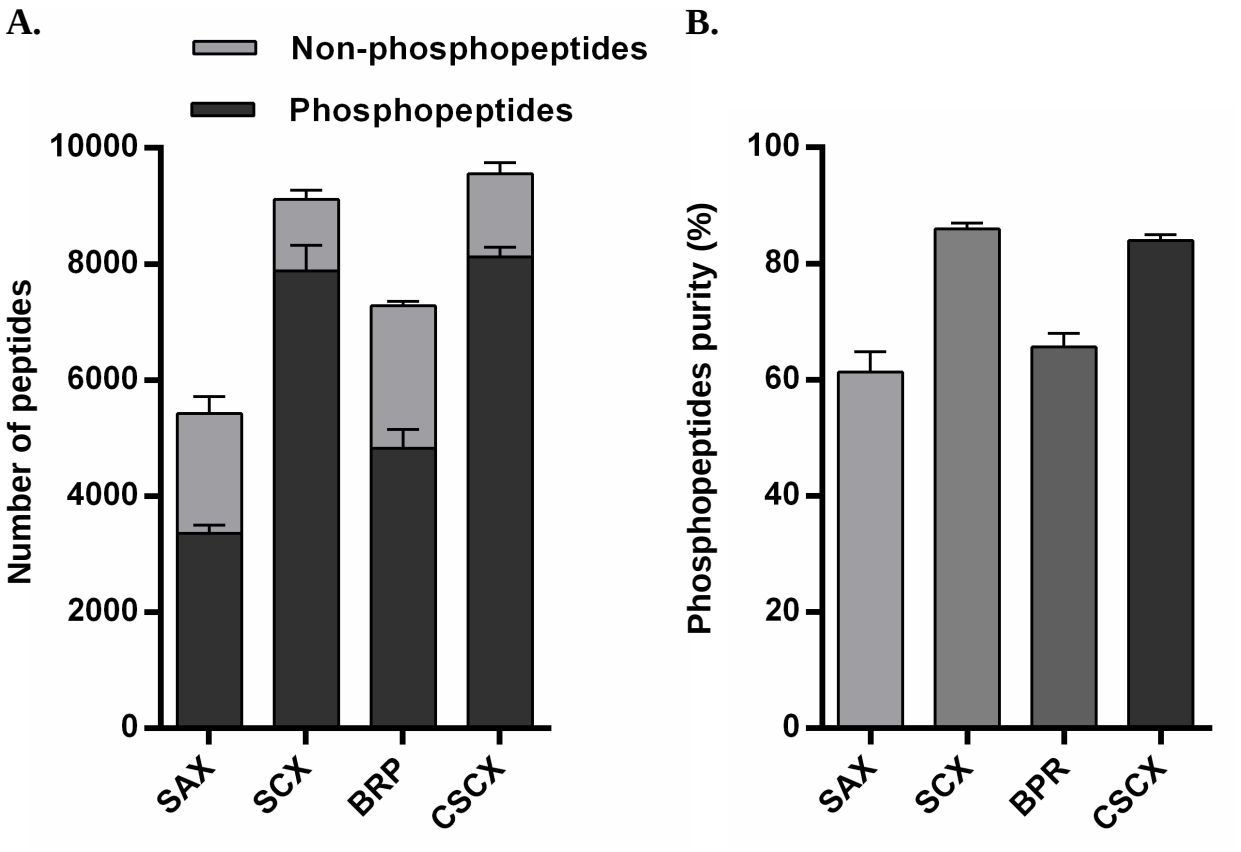

Figure 5.13 The number and percentage of phosphorylated peptides.
A. Average number of phosphorylated and non-phosphorylated peptides identified in SAX, SCX ,BRP, and CSCX fractionated samples. **B.** Purity of phosphopeptide enriched fractions (%) for the different tip-based fractionation and CSCX methods. Shown are mean values + SD; n=3

due to their increased hydrophilicity allowing unspecifically enriched nonphosphorylated peptides to be detected in the later fractions. Earlier elution of phosphorylated peptides compared to their unmodified counterparts can also be seen for C18 reversed-phase material under acidic conditions (Mohammed and Heck 2011). The discrepancies between SCX and CSCX were quite surprising to us because we used the same solutions for elution of peptides in both approaches. They are most likely due to stronger binding of the stationary phase used in the tip-based approaches. The higher redundancy of SCX compared to CSCX cannot explain the observation, as just the number of phosphopeptides identified solely in fraction 6 of the SCX samples was higher than all combined identifications in the last fraction of the CSCX experiment.

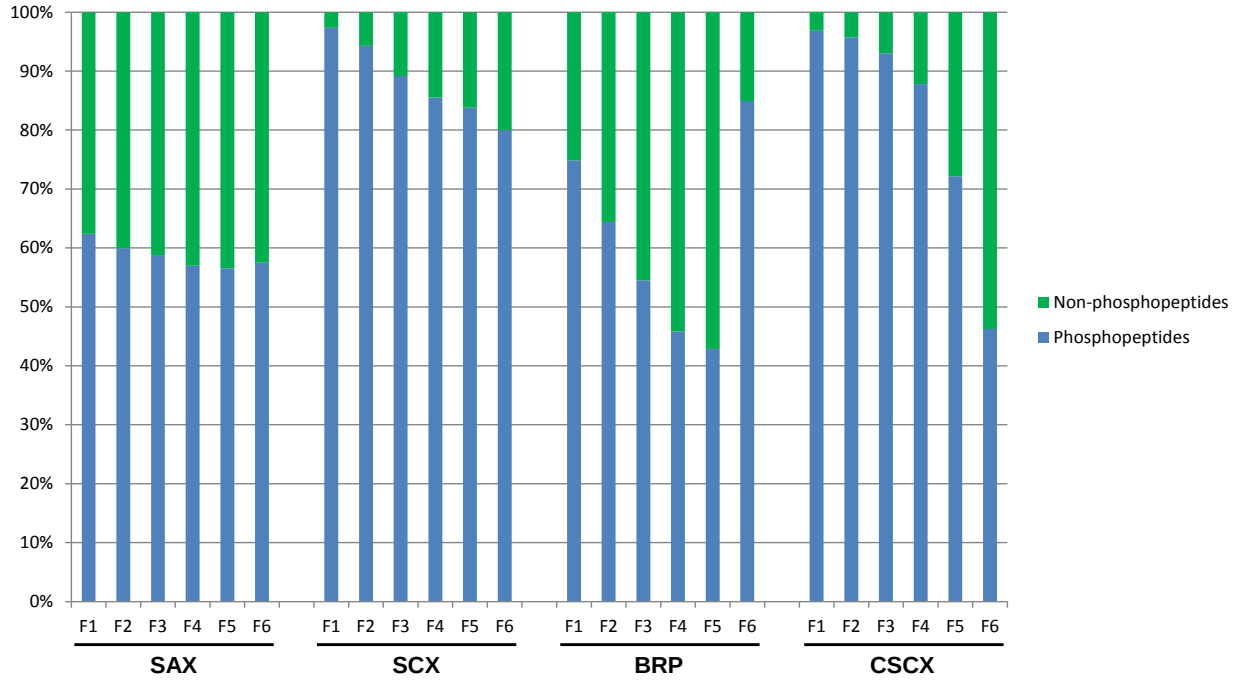

Figure 5.14 Phosphopeptide purity across the fractions.
Comparison of the phosphopeptide purity across the six fractions (F1 to F6) of the strong anion exchange (SAX), strong cation exchange (SCX), and basic reversed phase (BRP) tip-based fractionated batch enriched phosphopeptides, as well as column chromatography SCX (CSCX) fractionated samples followed by enrichment of the individual fractions. Shown are the combined values of 3 replicates of TiO_2 enrichment experiments of 3 mg HeLa whole cell tryptic digests.

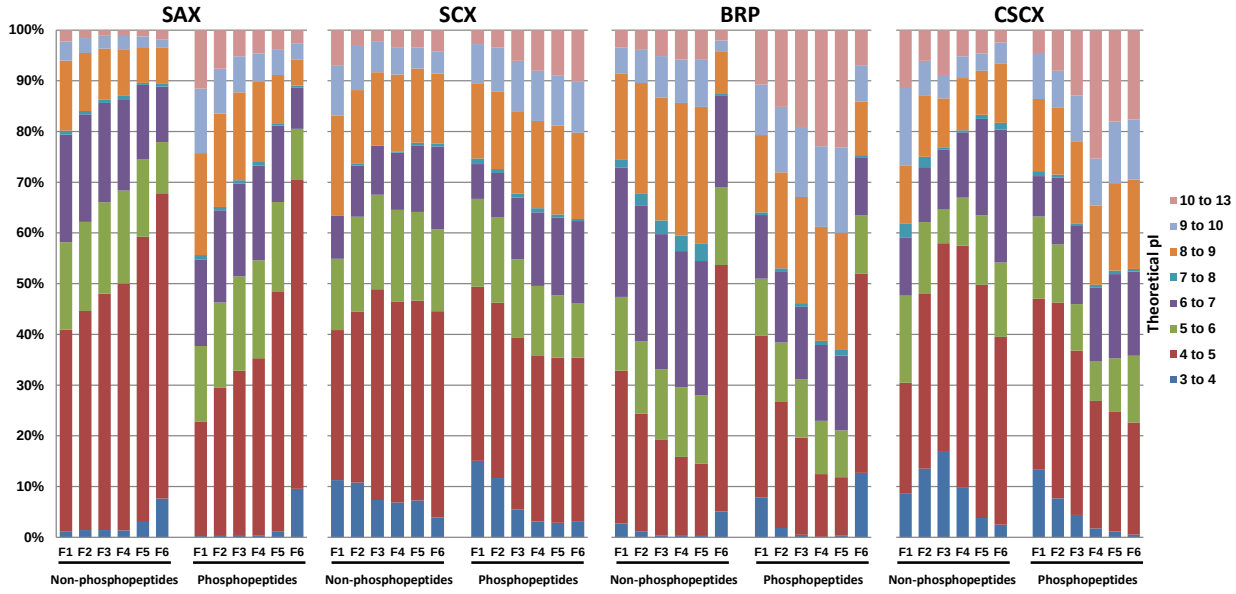

Figure 5.15 Distribution of theoretical isoelectric points (pI) of peptides across the fractions (F1 to F6).
Theoretical pI of peptides detected in each fraction of the strong anion exchange (SAX), strong cation exchange (SCX), and basic reversed phase (BRP) tip-based fractionated batch

enriched phosphopeptides, as well as column chromatography SCX (CSCX) fractionated samples followed by enrichment of the individual fractions. Shown are the combined values of 3 replicates of TiO_2 enrichment experiments of 3 mg HeLa whole cell tryptic digests.

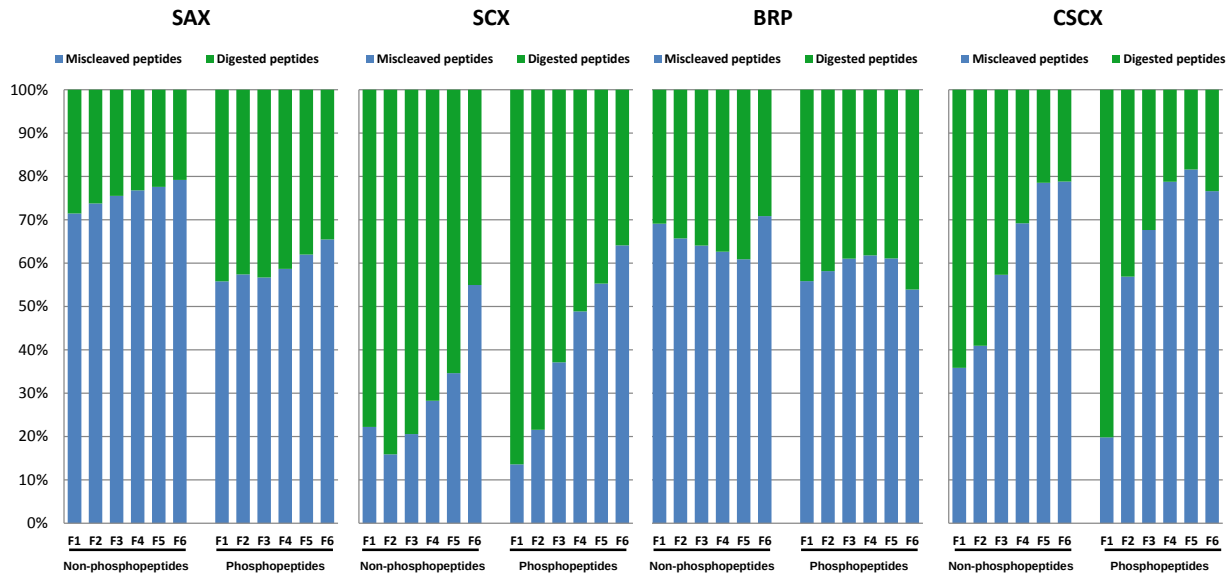

Figure 5.16 Distribution of the miscleaved peptides across the fractions (F1 to F6).
Distribution of the miscleaved peptides in each fraction of the strong anion exchange (SAX), strong cation exchange (SCX), and basic reversed phase (BRP) tip-based fractionated batch enriched phosphopeptides, as well as column chromatography SCX (CSCX) fractionated samples followed by enrichment of the individual fractions. Shown are the combined values of 3 replicates of TiO_2 enrichment experiments of 3 mg HeLa whole cell tryptic digests.

5.2.7. Analysis of fraction-specific peptide properties

To better understand the broad distribution of phosphopeptides across SAX fractions and the high variations in phosphopeptide purity, we investigated the isoelectric point, length, and the number of missed cleavage sites of the identified peptides across the fractions of the different approaches. For SAX in particular, we observed a strong correlation of the fraction number and isoelectric point (Figure 5.15) of the peptides, and acidic peptides presented the most abundant population. The BRP-fractionated samples contained more neutral and basic peptides, whereas the SCX and CSCX samples resulted in a rather uniform distribution. When investigating the missed cleavage sites, we observed roughly similar cleavage rates for the SAX- and BRP-fractionated samples (Figure 5.16). For SAX, the rate of miscleaved peptides increased with the fraction number, whereas the opposite was the case for the BRP samples. The SCX samples showed significantly lower miscleavage rates and a clear distribution with small amounts of miscleaved peptides in the first fraction (15 and 22%), which increased steadily to high numbers in the last fraction (64 and

55%) for the phosphorylated and nonphosphorylated peptides, respectively. This is most likely due to the increased interaction of the SCX material with the additional basic amino acid present in the miscleaved peptides. A similar trend was observed for the CSCX samples with a higher number of observed missed cleavage sites both for phosphorylated (20 to 77%) and nonphosphorylated peptides (36 to 79%). In total, as expected, the percentage of missed cleavage sites among phosphopeptides was higher than among nonphosphopeptides (Winter et al. 2009a). When investigating the length of peptides (Figure 5.17), we found that SCX and CSCX identified on average shorter peptides than BRP and SAX. A possible reason may be that the interaction with the stationary phase in SAX and BRP is due to the whole peptide backbone, whereas in SCX it is mainly based on the basic groups present at the N- and C-termini of tryptic peptides.

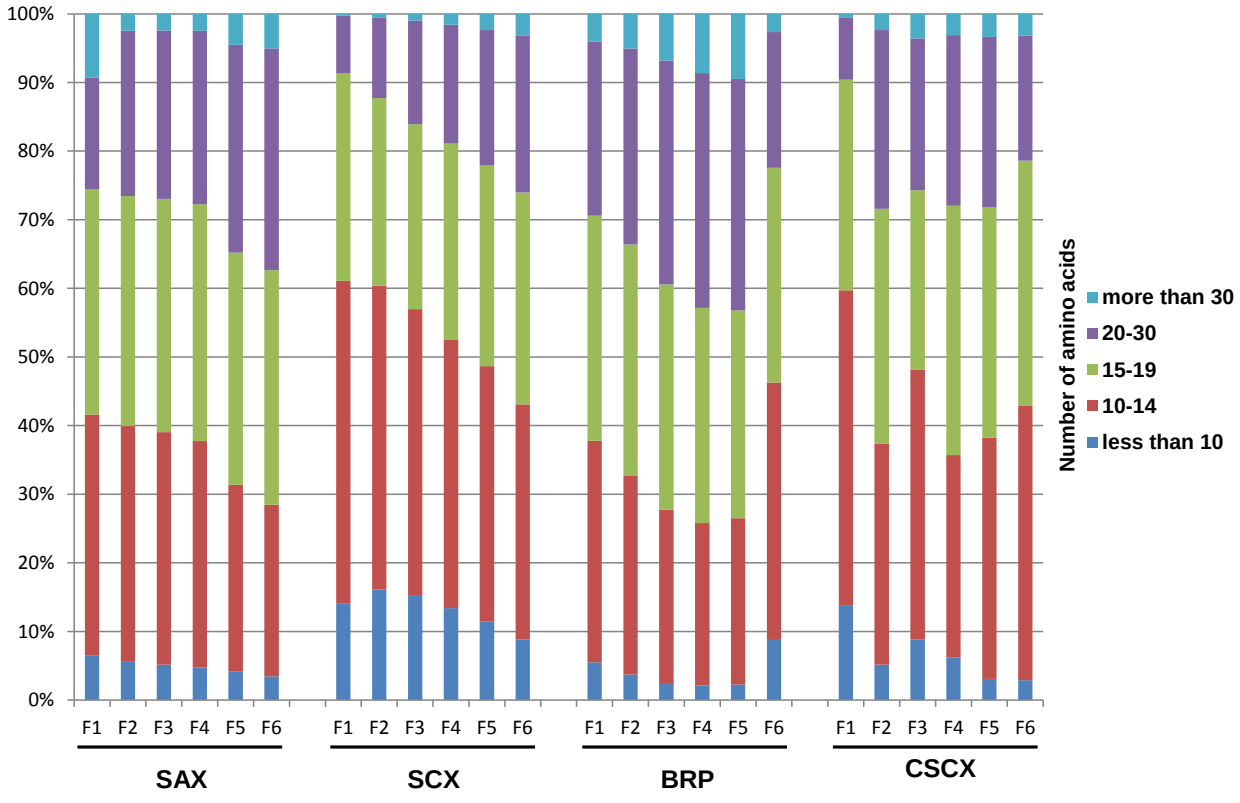

Figure 5.17 Distribution of peptide lengths across the fractions (F1 to F6).
Distribution of peptide lengths for each fraction of the strong anion exchange (SAX), strong cation exchange (SCX), and basic reversed phase (BRP) tip-based fractionated batch enriched phosphopeptides, as well as column chromatography SCX (CSCX) fractionated samples followed by enrichment of the individual fractions. Shown are the combined values of 3 replicates of TiO_2 enrichment experiments of 3 mg HeLa whole cell tryptic digests.

5.3. Discussion and conclusion

The goal of this study was to establish a workflow that allows for the identification of large numbers of phosphorylation sites with minimal effort. The standard method for large-scale phosphoproteomic experiments comprises peptide fractionation using SCX chromatography followed by phosphopeptide enrichment for each fraction (SCX-IMAC/TiO_2). The most laborious step of this approach is the lyophilization, desalting, and phosphopeptide enrichment of the fractions generated during SCX fractionation as every step has to be carried out 12 (or 24) times and the fractions are of high volume and complexity. Therefore, we wondered whether we can perform first phosphopeptide enrichment and afterwards fractionation by SCX chromatography (TiO_2-SCX). However using this method, the number of detected phosphosites was dramatically reduced in comparison to the standard method. This may be due to loss of phosphopeptides in the chromatographic system caused by nonspecific interaction with metal ions present on surfaces of the LC system and in the chromatographic column (Winter et al. 2009b) or decreased enrichment efficiency due to the high complexity of the sample.

Next, we asked if it is mandatory to fractionate phosphopeptides or if LC-MS/MS runs with a long-gradient (240 min) would be enough for detecting a relatively high amount of the phosphopeptides in a sample. Our results indicated that the system was approaching its maximum capacity using phosphopeptides enriched from 1 mg of starting material and there is no difference in detected phosphopeptides between 2 and 3 mg of starting material. Compared to the SCX-TiO_2 sample, we achieved similar enrichment efficiencies with long gradient analyses. We therefore conclude that the reduced number of peptides identified when performing TiO_2-SCX was rather due to losses in the chromatography system than a decreased performance of TiO_2 enrichment. Furthermore, it is not possible to completely omit a fractionation step because single run analyses approach a maximal number of identifiable peptides that is most likely due to a limited capacity of the analytical C18 column. We therefore evaluated tip-based fractionation methods, as it is possible to miniaturize the chromatography conditions by this approach, which should result in virtually no loss of phosphopeptides and allows for using large amounts of starting material.

We compared three tip-based fractionation methods and on the basis of the results of our analyses, we have the impression that, for the tip format, the SCX material is superior to SAX and BRP due to a more efficient distribution of the phosphorylated peptides across the single

fractions. This results in higher intensities and lower fraction complexity and therefore a better identification in the DDA mode. We believe that the underrepresentation of short phosphopeptides in SAX and BRP is due to an insufficient interaction with the chromatographic material resulting in highly complex initial fractions and therefore undersampling in these LC–MS/MS runs. Longer peptides are retained more efficiently but are also not fractionated with a sufficient resolution resulting in elution across several fractions. This results in redundant identification of abundant peptides and dilution effects reducing precursor intensities of low abundance ions, preventing their identification. This favors the identification of nonphosphorylated background peptides leading to the observed reduced phosphopeptide purity in SAX and BRP, which is less pronounced in the SCX samples. CSCX-fractionated samples show similar characteristics and performance compared to such fractionated by SCX tips. The main difference is the reduced redundancy of CSCX, which however fails to result in increased numbers of identified phosphorylation sites. We believe this is due to an increased loss of phosphopeptides during sample fractionation, and phosphopeptide enrichment in CSCX, and better retention of phosphopeptides on the tip SCX resin.

Here we showed that the fractionation of phosphopeptides using pipet tip-based columns leads to similar results as the common approach using liquid chromatography-based approaches at a fraction of the cost and time. Among tip-based fractionation, SCX clearly outperforms SAX and BRP, leading to increases in the number of identified phosphorylation sites of 148% and 71%, respectively. We believe that this is due to a stronger interaction of the phosphopeptides with the SCX material leading to more efficient retention and better resolution. Because the individual resins cover different fractions of the phosphoproteome, the number of identified phosphorylation sites of a sample can be expanded by fractionating it with several tip-based columns. For research groups not specialized in the analysis of phosphopeptides in particular, the tip-based fractionation of batch-enriched phosphopeptides should be of value as it allows for performing large-scale phosphoproteomic experiments even for unexperienced operators. Compared to the common approach, which requires expensive chromatography systems and SCX columns as well as high amounts of desalting cartridges, plasticware, and TiO_2, the tip-based system comes at a fraction of the cost and offers high robustness, simplicity, and reproducibility. Furthermore, the sample processing time is reduced from 1 week to only 2 days at a comparable performance. Because all materials involved are single-use items, there is no possibility for carry over increasing the purity

of samples processed together, and it is possible to fractionate high amounts of samples in parallel. We therefore believe that the fractionation of batch-enriched phosphopeptides using SCX tip-based columns is a valuable approach for the large-scale characterization of phosphopeptides from complex samples.

6. Chapter 2: Phosphoproteome changes in altered cholesterol metabolism

6.1. Introduction

6.1.1. Lysosomes

Nearly all animal cells possess the membrane-bound organelles called lysosomes. The number of lysosomes differs in various cell types; mammalian cells contain several hundred lysosomes under normal conditions (Valm et al. 2017). Due to the presence of the V-type adenosine triphosphate (ATP) dependent membrane proton pumps in the lysosomal membrane which constantly pump protons inside the lysosomes, the pH in the lysosomal lumen is acidic. This low pH (4.5 to 5.0) is optimal for the activity of the hydrolases in the lumen which are responsible for the primary function of lysosomes that is degradation of the waste macromolecules from different sources into their constituent components with low molecular weight (Ohkuma et al. 1982). More than 60 different hydrolases, proteases, lipases, sulfatases, phosphatases, glycosidases, and nucleases can be found in lysosomes (Luzio et al. 2007). The acidic pH-optima of the hydrolytic enzymes ensure that, in the case of lysosomal rupture, these enzymes do not digest cellular components. The luminal membrane of lysosomes is protected against the lysosomal hydrolases through a thick glycocalyx formed by glycosylated membrane proteins (Kundra and Kornfeld 1999). Hydrolysis capability of the lysosomes has earned them the cellular incinerators title; however, in recent years it has been shown that lysosomes are involved in several other fundamental cell processes such as signaling, energy metabolism, secretion and plasma membrane repair (Settembre et al. 2013).

6.1.2. Lysosomes and signal transduction

Lysosomes are the intracellular site for the master regulator of cell growth and metabolism, the mechanistic target of rapamycin complex 1 (mTORC1) (Sancak et al. 2010). In recent years mTORC1 has emerged as a pivotal signaling node which connects nutrient and energy sensing through regulation of cellular anabolic and catabolic processes. When nutrients and energy are abundant, mTORC1 is recruited from the cytosol to the lysosomal surface through a multi-protein complex composed of the amino acid transporter SLC38A9, the vATPase, the Rag GTPases, and

the Ragulator complex (Figure 6.1) (Shimobayashi and Hall 2016). SLC38A9 is an arginine sensor that activates the Ragulator complex in the presence of this amino acid. Ragulator complex consists of five subunit proteins, LAMTOR1 (p18), LAMTOR2 (P14), LAMTOR3 (MP1), LAMTOR4 (C7orf59), and LAMTOR5 (HBXIP) (Bar-Peled et al. 2012). After stimulated by amino acids, the Ragulator complex acts as a guanine nucleotide exchange factor (GEF) for the Rag GTPase heterodimer (RagA/B-RagC/D) complex. Ragulator complex converts Rags to their active state, in which RagA/B are loaded with guanosine triphosphate (GTP) and RagC/D are bound to guanosine diphosphate (GDP) and thereafter Rags complex localizes mTORC1 at the lysosomal surface (Bar-Peled et al. 2012). In addition to the Rag GTPase complex, another GTPase (Rheb GTPase) is needed for maximal mTORC1 activity in the presence of growth factors and abundant nutrients. Rheb GTPase resides at the cytoplasmic surface of lysosomes and activates mTORC1 through direct interaction with mTOR catalytic domain (Long et al. 2005). This interaction can be interrupted via the heterotrimeric TSC complex composed of tuberous sclerosis complex 1 (TSC1), TSC2, and TBC1 domain family member 7 (TBC1D7) (Figure 6.1). TSC2 has GTPase-activating protein (GAP) activity towards Rheb and therefore can interfere with its interaction with mTORC1 by promoting GTP to GDP hydrolysis (Dibble et al. 2012). TSC1 and TBC1D7 are crucial for the stability of the TSC complex (Dibble et al. 2012). AMPK and AKT regulate TSC2 activity by phosphorylation, in a way that in the presence of growth factors and energy, TSC2 is deactivated and therefore is not interfering with Rheb and mTORC1 interaction (Figure 6.1) (Shimobayashi and Hall 2016). Castellano et al. showed that lysosomal cholesterol can also activate mTORC1 through the SLC38A9-NPC1 complex (Castellano et al. 2017).

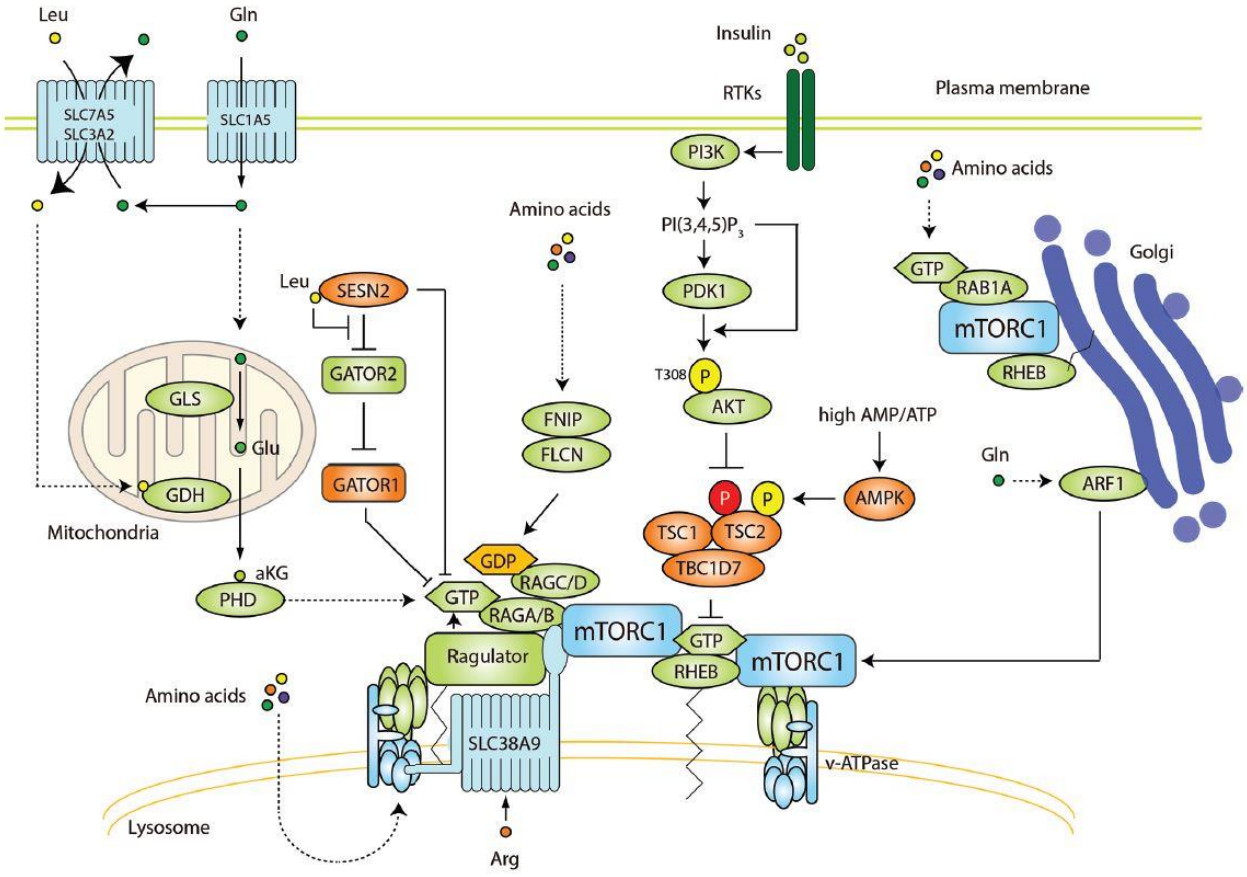

Figure 6.1 mTORC1 signaling pathway. Adopted from Shimobayashi and Hall (Shimobayashi and Hall 2016).

6.1.3. Lysosomal storage disorders (LSDs)

Having more than 60 soluble hydrolases, lysosomes are able to break down almost all types of macromolecules, including proteins, nucleic acids, carbohydrates, and lipids into their constituent components (Ballabio and Gieselmann 2009). Genetic defects in lysosomal proteins can lead to the accumulation of the substrate of the affected enzyme in the lysosomes and therefore progressive lysosomal dysfunction in different organs and tissues. These rare inherited disorders are known as Lysosomal Storage Diseases (LSDs) and represent about 50 genetic disorders (Ballabio and Gieselmann 2009). Although most of the LSDs occur due to the deficiency of one of the lysosomal hydrolases, a mutation in the non-enzymatic proteins such as lysosomal membrane proteins can also lead to LSDs (Platt et al. 2012). LSDs result in various pathogenic events such as oxidative stress, altered calcium homeostasis, altered lipid trafficking, inflammation, autophagy, autoimmune responses, and endoplasmic reticulum stress (Vitner et al. 2010). These effects result in impaired cell and tissue function which lead to severe symptoms

and premature death. Despite many years of research, little is known about the molecular mechanisms by which the accumulated un-metabolized substrates lead to cellular dysfunction (Settembre et al. 2013; Futerman and van Meer 2004). A better understanding of the molecular mechanisms of LSDs can lead to finding new therapeutic methods and drugs which will help patients suffering from these diseases.

6.1.4. Niemann Pick Disease Type C (NPC)

Niemann Pick diseases are autosomal recessive LSDs which can be categorized into three main groups: types A, B, and C. Types A and B are caused by the inherited genetic deficiency of lysosomal acid sphingomyelinase. Type C is an atypical lysosomal storage disease as it doesn't occur as a result of an enzyme deficiency, but is associated with mutations in either NPC1 (the majority of the cases (95%)) or NPC2 genes (Vanier 2010). NPC is a progressive neurodegenerative disease with broad clinical heterogeneity from an early neonatal fatal outcome to a chronic neurodegenerative disease in adults (Vanier 2010). The molecular functions of NPC1 and NPC2 proteins are still incompletely known (Vanier 2010; Vance and Karten 2014). It has been shown that both of the proteins are involved in the transport of unesterified cholesterol from lysosomes into other cell compartments such as the ER. Therefore, the main feature of the NPC disease is an impaired egress of cholesterol from lysosomes, leading to unesterified cholesterol accumulation inside late endosomes/lysosomes (Vanier 2015). Several reports have shown that although cholesterol is the primary storage molecule in NPC disease, other lipids such as sphingolipids are also involved and accumulate (Vanier 2015). NPC1 is an intracellular cholesterol transporter with 13 transmembrane domains, that is localized on the late endosomal/lysosomal membranes and NPC2 is located in the lysosomal lumen (Kwon et al. 2009). NPC1 and NPC2 function in concert with each other, NPC2 binds to released unesterified cholesterol from low-density lipoproteins (LDLs) and transfers it to the cholesterol-binding pocket at the N-terminal domain (NTD) of NPC1. NPC1 helps the bound cholesterol to pass across the lysosomal membrane by interacting with the NPC1 transmembrane domain (Figure 6.2) (Kwon et al. 2009).

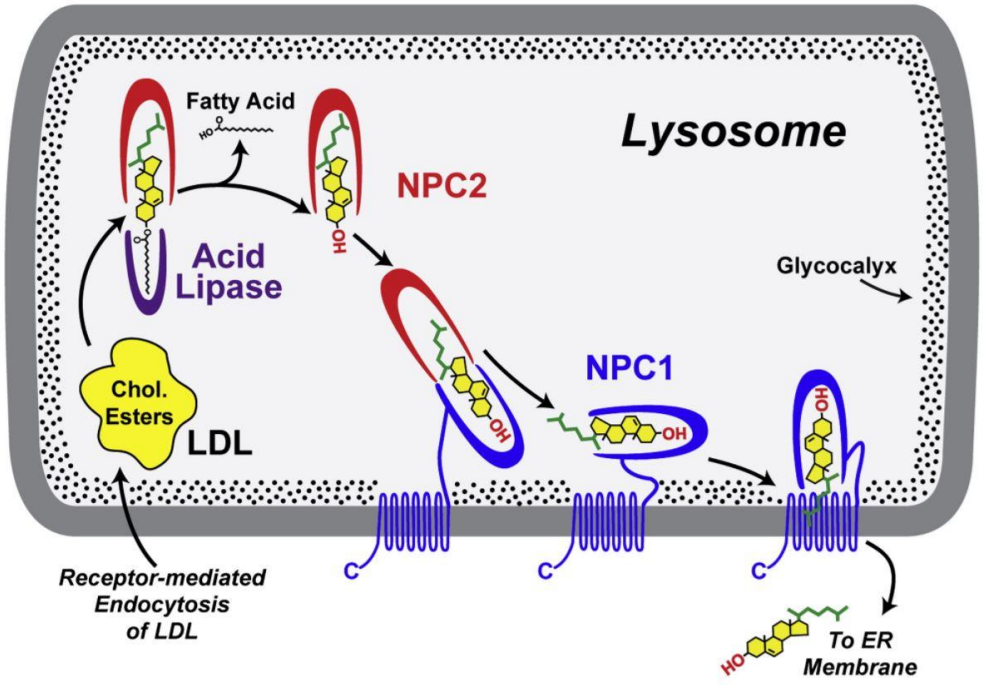

Figure 6.2 NPC1 and NPC2 function in concert with each other to catalyze the mobilization of cholesterol from late endosomes to other cell compartments. Adopted from Kwon et al. (Kwon et al. 2009).

6.1.5. Common research models for studying NPC disease

To gain a better insight into the pathology of NPC disease and the function of NPC1 and NPC2 proteins different model systems have been developed. Obtaining fibroblast cells from human patients suffering from NPC was one of the first established models for studying this disease (Liscum 1989; Sokol et al. 1988). Other groups employed different NPC mutant cell lines from other organisms such as Chinese hamster (Cadigan et al. 1990), yeast (Malathi et al. 2004), and drosophila (Huang et al. 2005). Moreover, several knock-out mouse models for NPC1 (Loftus et al. 1997; Miyawaki et al. 1986) or NPC2 (Nielsen et al. 2011) have been generated and used in different studies. Besides these models, some chemical compounds such as amphiphilic amines can mimic the NPC defect in the cell culture systems (Rodriguez-Lafrasse et al. 1990). The amphipathic steroid 3-b-[2-(diethylamino)ethoxy]androst- 5-en-17-one (with the commercial name U18666A) is the most widely used chemical for mimicking the NPC phenotype. The mechanism of U18666A inhibiting the NPC1/NPC2 complex is not yet completely understood. The blockage could be a result of direct interaction of U18666A with NPC1 and/or NPC2 or alterations in the NPC protein function induced by the effects of U18666A on the lysosomal membrane (Cenedella 2009). Various combinations of genomics and proteomics techniques have been applied to study these models systems including mass spectrometry.

6.1.6. Mass spectrometry-based studies of LSDs

LC-MS-related techniques have been employed in a wide range of studies related to LSDs from large-scale proteomic studies to targeted multiple reaction monitoring (MRM) studies. Beside research applications, in recent years, thanks to the triple quadrupole analyzers, tandem mass spectrometry has been established as a reliable alternative to biochemical methods for diagnosis and screening of LSDs based on detecting lipids and metabolites in clinical samples (Piraud et al. 2018).

MS-related methods also have been employed for Niemann-Pick disease research studies. Rauniyar et al. employed NPC1-mutated primary fibroblast cells and investigate the proteomic alterations resulting from NPC1 mutation in these cells. In total, they identified 4308 distinct proteins, of which 281 were differentially expressed (113 proteins showed up-regulation and 168 proteins down-regulation in NPC1-mutated cells) (Rauniyar et al. 2015). The differentially expressed proteins were associated with various biological processes such as reactive oxygen species (ROS) metabolic process, cholesterol metabolism, lipid localization, steroid metabolic process, antioxidant activity, and apoptosis (Rauniyar et al. 2015). In another study Cologna et al. compared the cerebellar proteome profiles of the NPC1 WT and mutant mouse. Using two-dimensional gel electrophoresis following with MALDI-TOF/TOF and LC-ESI-MS/MS, they found 77 differentially expressed proteins including 49 upregulated and 22 downregulated proteins (Cologna et al. 2012). In the follow-up experiments, they confirmed their MS results for glutathione S-transferase alpha, superoxide dismutase, and fatty acid binding protein (FABP3) by comparing the expression of these proteins in cerebrospinal fluid of NPC1 patients relative to controls (Cologna et al. 2012). Byun et al. also employed two-dimensional gel electrophoresis and MALDI-TOF mass spectrometry to compare differentially expressed hippocampal protein profiles between $NPC^{+/+}$ and $NPC^{-/-}$ mice at the age of 4 and 8 weeks. Although they did not find any significant difference in protein profiles after four weeks, after eight weeks several proteins such as Glutamate receptor 2 (Gria2) were differentially expressed (Byun et al. 2006). In another proteomic study, Sarkar et al. compared the whole proteome obtained from NPC1-KO and WT MEF cells. They found in total 21 and 12 upregulated proteins in NPC1-KO and WT MEFs, respectively. The upregulated proteins in NPC1-KO cells were linked to lysosome, endocytosis, and autophagy (Sarkar et al. 2013). Annaert and colleagues developed a method for isolating late endosomes/lysosomes using acid-coated superparamagnetic iron oxide nanoparticles (SPIONs) (Tharkeshwar et al. 2017). They employed their method to perform a proteomic and lipidomic

study of WT and NPC1-deficient cells. They showed that besides cholesterol, which is the hallmark of the NPC disease, other lipids such as glycerophospholipids (GPLs), glycosphingolipids (GSLs), ceramide (Cer), hexosylceramide (HexCer) and sphingomyelin (SM) also get accumulated in LE/LYS of NPC1 KO cells. In their proteomic study, they found 36 proteins upregulated in NPC1 mutant cell line out of which many were involved in autophagy and the catabolic functions of lysosomes (Tharkeshwar et al. 2017). Only a handful of NPC1 interaction partners and binding proteins have been identified so far. Macias-Vidal et al. used a NPC1 peptide (amino acids 1032–1066) as bait to capture and identify NPC1 binding proteins. Using LC-MS/MS they isolated 31 lysosomal proteins along with the bait peptide which most of them were involved in lipid catabolism and proteolysis (Macías-Vidal et al. 2016).

6.1.7. Niemann-Pick disease type C and phosphoproteomic studies

There have been several reports which indicate that in knock-down/out or inhibited NPC1/NPC2 cells or animals, the activity of several kinases or phosphorylation state of various proteins are changed. Xu et al. using HUVECs cells showed that blockade of cholesterol trafficking using U18666A inhibitor or siRNA knockdown of NPC1/2 leads to mTORC1 inhibition, but no alterations in the activity of kinases such as mitogen-activated protein kinases (MAPK) and AKT was observed (Xu et al. 2010). Sawamura et al. have reported contradictory findings. They employed NPC1 mutated Chinese hamster ovary (CHO) cell line and showed that the lack of NPC1 protein activates MAPK which in turn promotes tau phosphorylation (Sawamura et al. 2003). Saito et al. investigated phosphorylation state of tau and Alpha-synuclein proteins in the brains of twelve NPC1 patients, and their results showed aberrant phosphorylation of both proteins in the patient's brains (Saito et al. 2004). Garver et al. measured the expression of several protein kinases in murine NPC livers (NPC1-mutated), and concluded that the expression level of protein kinase C alpha, protein kinase C zeta, proto-oncogene tyrosine-protein kinase Src, and protein kinase C delta increase significantly in comparison to the wild-type murine livers (Garver et al. 1999). Despite these findings, which suggest significant alterations in the phosphoproteome of the NPC cells, no large-scale phosphoproteomic study has been conducted to investigate phosphorylation state in this disease.

6.2. Results

Using the method that was described in chapter one (fractionation of phosphopeptides using SCX pipet tip-based columns), the phosphoproteome changes in perturbed cholesterol metabolism system was investigated. U18666A chemical was employed to induce the conditions same as Niemann-Pick Disease Type C (NPC), which is one of the most frequent lysosomal storage diseases (LSDs).

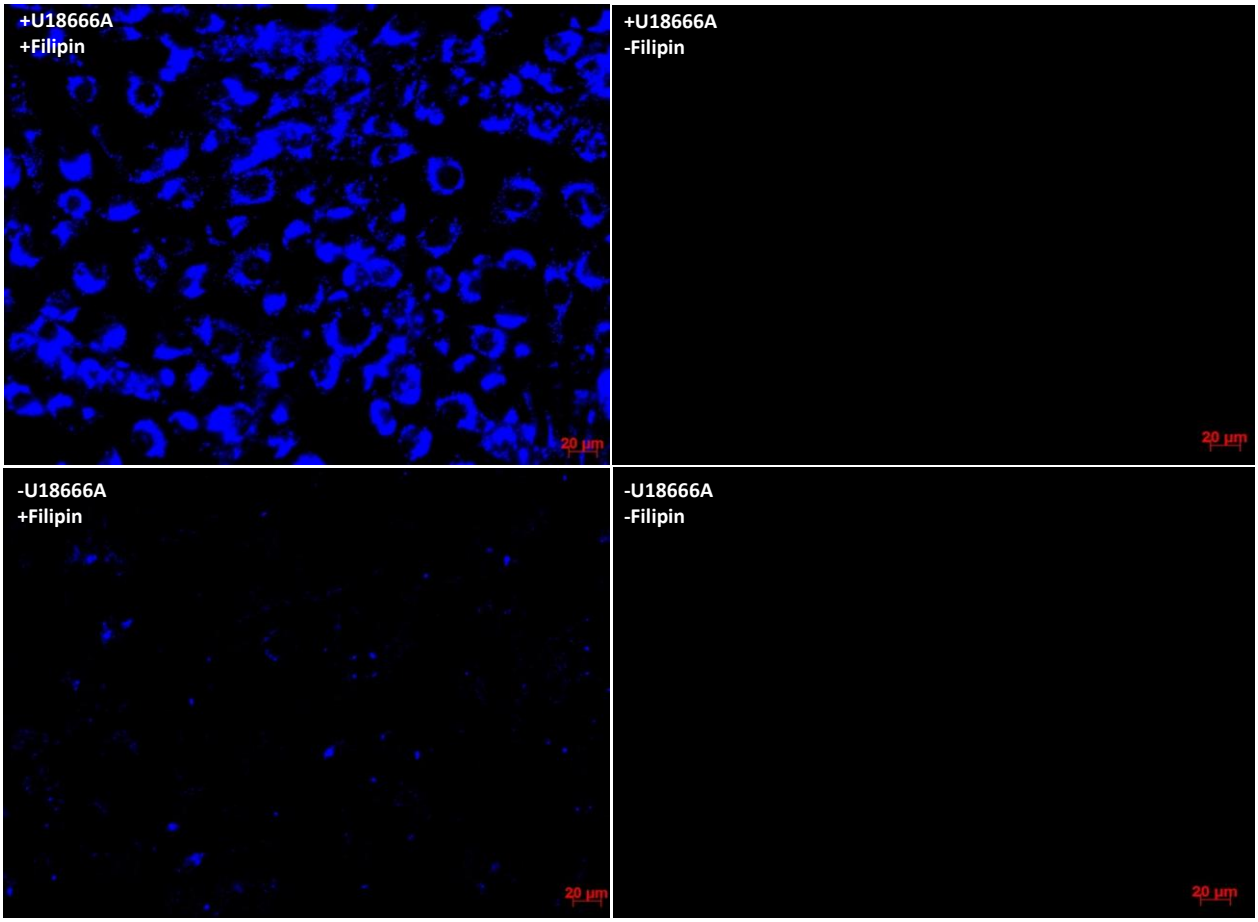

Figure 6.3 Filipin staining of MEFs.
MEFs were cultured on coverslips and incubated with either U18666A (3 µg/ml) or DMSO for 24 hours. Afterward, the cells were fixed and stained with or without filipin before imaging with the Axiovert 200 M microscope, using an objective with 20x magnification. Images were recorded with an exposure time of 350 ms. Blue color indicates the accumulation of cholesterol.

6.2.1. U18666A treatment of the mouse embryonic fibroblast (MEF) cells

To induce NPC1 phenotype, SILAC-labeled MEF cells were treated with the cholesterol transport inhibitor U18666A and accumulation of cholesterol inside the lysosomes was monitored

by filipin staining. Filipin is a combination of chemical compounds with fluorescence properties

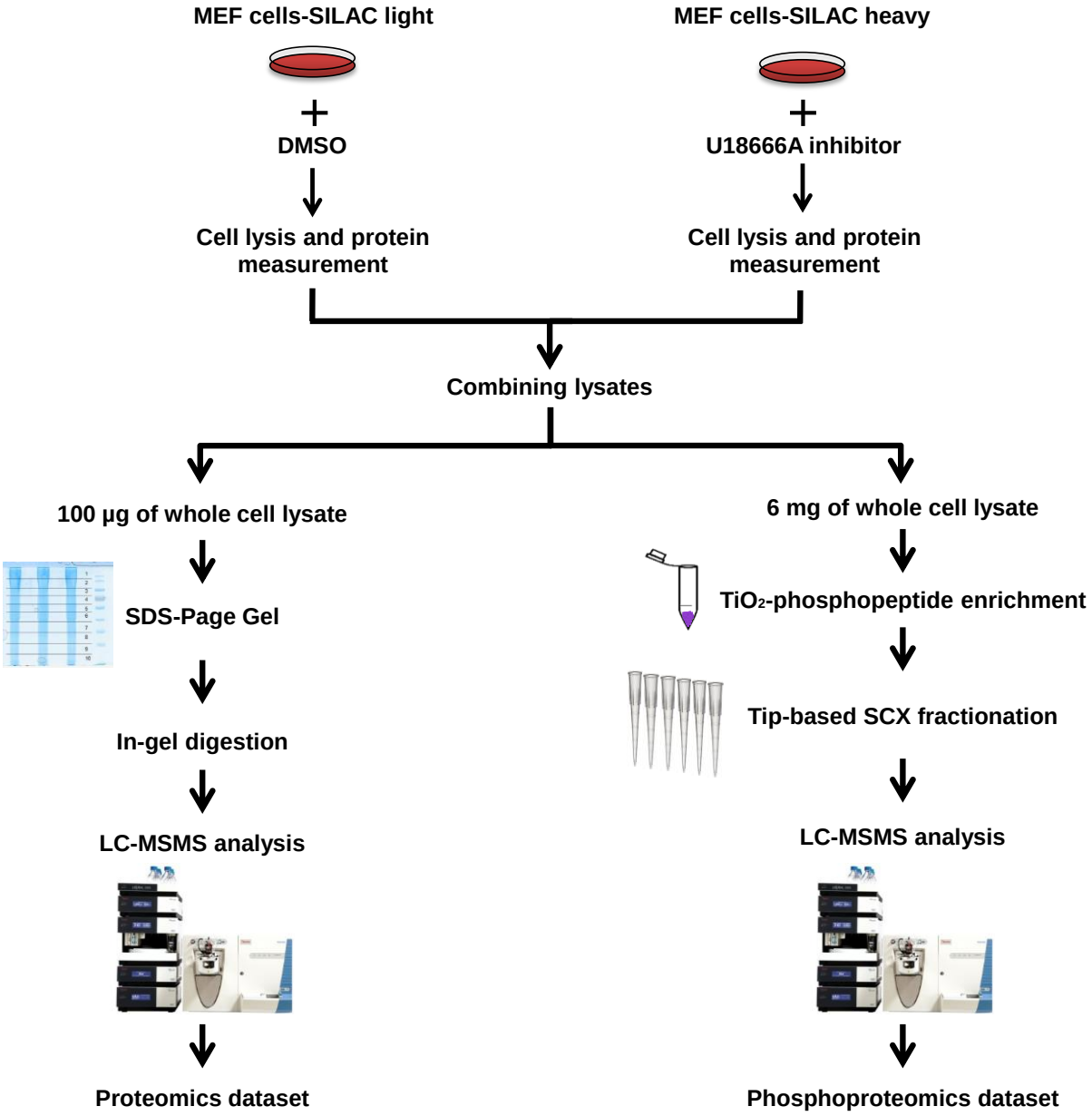

Figure 6.4 Schematic view of the proteomics and phosphoproteomics experimental procedure. SILAC-labeled MEF cells were treated with either U18666A (cholesterol transporter inhibitor) or DMSO (control). The same amount of the cell lysates (heavy and light labeled) was combined. 100 µg and 6 mg of the combined lysate was used for the proteomic and the phosphoproteomic study, respectively.

that specifically binds to the unesterified cholesterol (Arthur et al. 2011). MEF cells were cultured on coverslips and incubated either with U18666A or DMSO for 24 hours and afterwards fixed and stained with filipin before imaging with fluorescence microscopy. Figure 6.3 shows cholesterol accumulation inside the lysosomes in U18666A-treated cells.

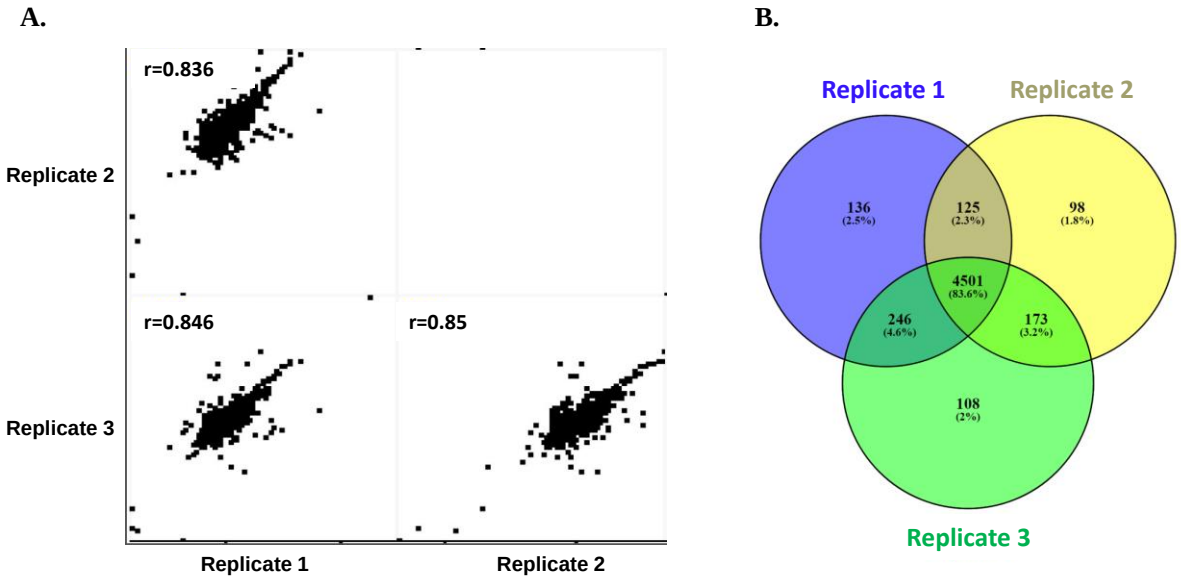

Figure 6.5 Comparing the results obtained from three biological replicates of the proteomics dataset.
A. MaxQuant software outputs regarding the proteomics dataset were further evaluated by Perseus software. Correlation between the three biological replicates was assessed using Pearson's correlation coefficient (r). **B.** The overlap between the proteins found in three replicates is shown using a Venn diagram. Venn diagrams were constructed using the open-access online tool Venny (Juan Carlos Oliveros).

6.2.2. Proteomic and phosphoproteomic study of NPC disease

MEF cells were labeled using stable isotopes (SILAC) with either heavy or light arginine and lysine (Blagoev et al. 2003). Light and heavy labeled MEF cells were cultured in 10-cm dishes and treated with DMSO or U18666A for 24 hours, respectively. Afterwards, cells were harvested and lysed using urea-based lysis buffer, and the protein amount was determined. The same amounts of the lysates were combined, and 100 µg and 6 mg of the combined lysates were taken for the proteomic and phosphoproteomic experiments, respectively (Figure 6.4).

6.2.2.1.Large-scale proteomics analysis of U18666A-treated cells

100 µg of the combined whole cell lysate was resolved by 10% SDS-PAGE gel and each lane of the SDS-PAGE gel was excised into 10 slices. Each slice was subjected to in-gel tryptic digestion after reduction and alkylation. Afterwards, resulting peptides were analyzed using an LTQ Orbitrap Velos mass spectrometer, and raw data were processed by the MaxQuant software (Figure 6.4). This experiment was conducted in 3 independent biological replicates and in total 5502 proteins and 49255 peptides were detected (Supplementary table 6.1). This dataset is named as “Proteomics dataset” in this chapter. The results from MaxQuant software were further

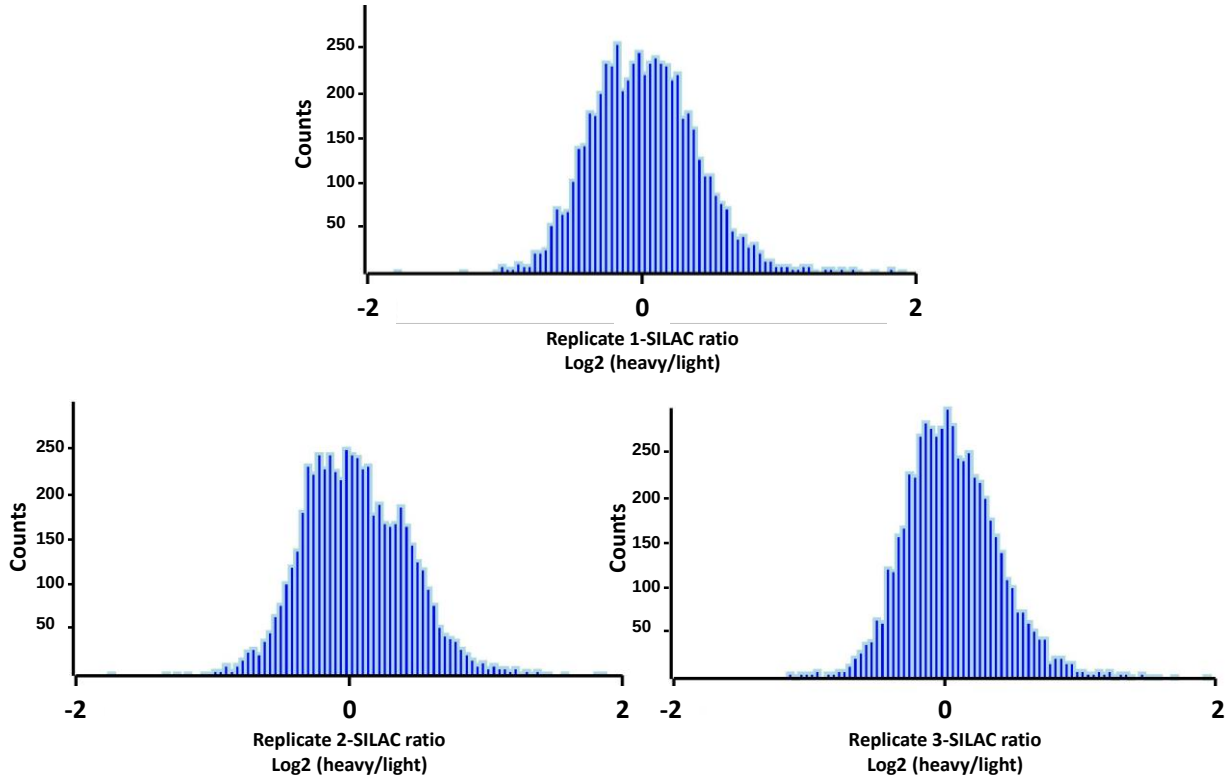

Figure 6.6 Normal distribution of H/L SILAC ratios for each replicate of the proteomics dataset. Normalized ratios acquired from the MaxQuant software were converted to log (base 2) values and using these values distribution of SILAC ratios for each replicate was assessed using Perseus (from MaxQuant software package). Y-axis (counts) shows the number of counts in each bin in the histogram.

analyzed and evaluated by Perseus software. Correlations between the three biological replicates were assessed using Pearson's correlation coefficient (r) (Puth et al. 2014). The Pearson's r was determined to be 0.836, 0.846, and 0.850 between replicate 1 and 2, 1 and 3, and 2 and 3, respectively, as shown in figure 6.5 (A) scatter plots. These relatively high Pearson's correlation coefficients indicate the high reproducibility among the three replicates. The high reproducibility can also be observed by comparing proteins found in each replicate (Figure 6.5 (B)). More than 83% of the proteins were common to all three replicates, and just 6.3% were detected in only one replicate. Next, normalized ratios acquired from the MaxQuant software were converted to log (base 2) values and using these values distribution of SILAC ratios for each replicate were assessed. Figure 6.6 shows that in all 3 replicates SILAC ratios for the quantified proteins are normally distributed around 0.

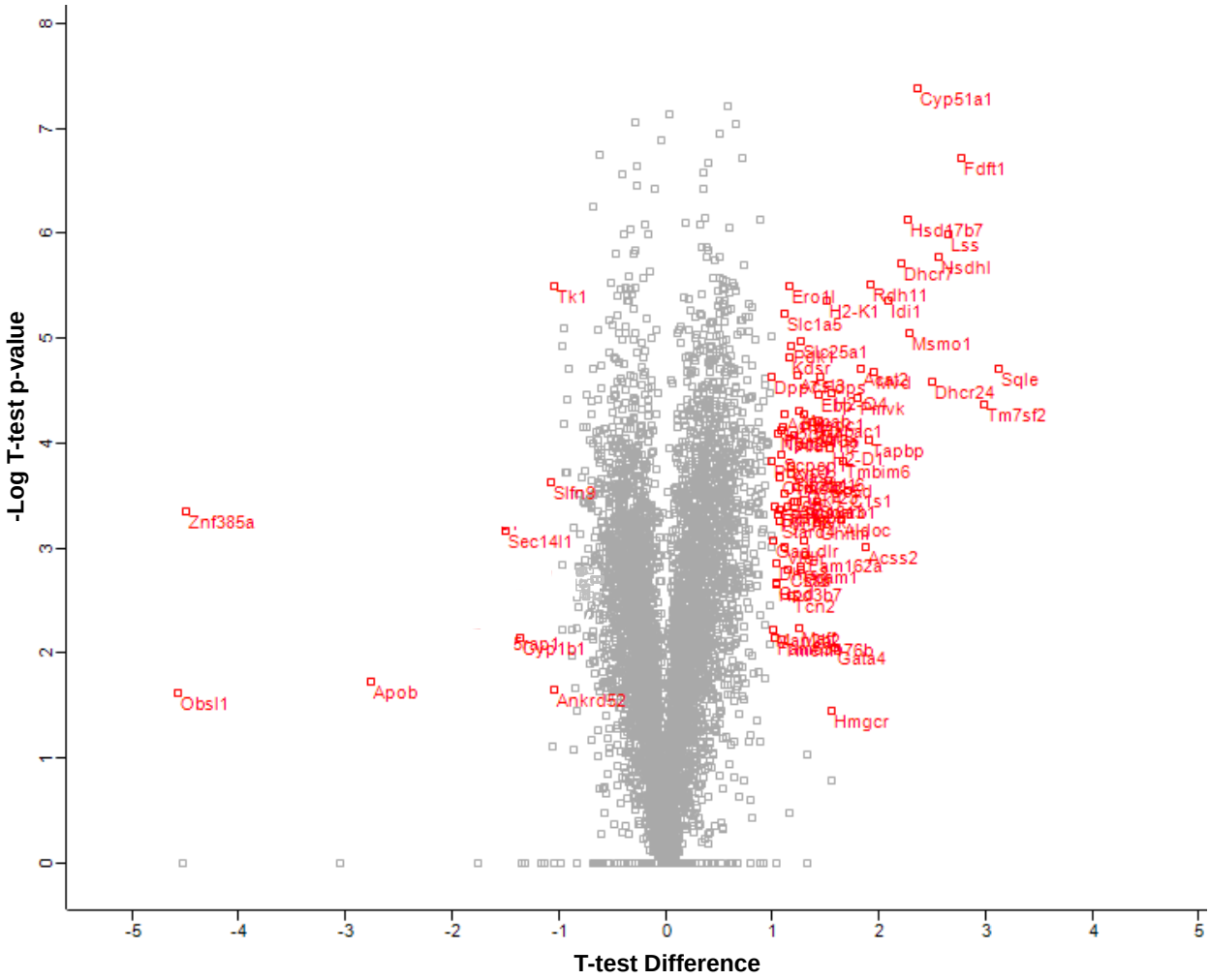

Figure 6.7 Differentially expressed proteins in the proteomics dataset.
Detected proteins in the proteomics dataset were searched for the up- and down-regulated proteins upon addition of U18666A to the culture medium. Only proteins were considered regulated that were detected in at least two biological replicates with P-values less than 0.05 and had log2 transformed SILAC ratios higher or lower than +1 and -1 (the arbitrary cut off), respectively. T-test differences of proteins were plotted against -Log t-test P-value using Perseus (from MaxQuant software package).

Next, the proteomics dataset was examined for differentially expressed proteins. Only proteins were accepted in the protein list that were detected in at least two biological replicates with p-values below 0.05 and more than one unique peptide. The SILAC ratios +1 and -1 (log 2 values) were selected as cutoff values for up- and downregulation, respectively. Applying the mentioned criteria, 66 and 8 differentially expressed proteins were found in the dataset (with ratios higher and lower than 1 (log 2 values), respectively) (Figure 6.7, Table 6.1, and Supplementary table 6.1).

Table 6.1 Downregulated proteins in the proteomics dataset.
Eight downregulated proteins upon addition of U18666A to the culture medium in the proteomics dataset with more than 1 detected peptide, and P-values less than 0.05 are shown in the table. The number of unique peptides identified for each protein is shown in the "peptides" column.

Protein names	Gene names	Log 2 Ratio	Peptides
Thymidine kinase, cytosolic	Tk1	-1.03	5
Schlafen family member 9	Slfn9	-1.09	9
Serine/threonine-protein phosphatase 6 regulatory ankyrin repeat subunit C	Ankrd52	-1.20	2
SEC14-like protein 1	Sec14l1	-1.45	2
Cytochrome P450 1B1	Cyp1b1	-1.58	5
Apolipoprotein B-100;Apolipoprotein B-48	Apob	-2.88	2
Obscurin-like protein 1	Obsl1	-4.17	3
Zinc finger protein 385A	Znf385a	-4.60	2

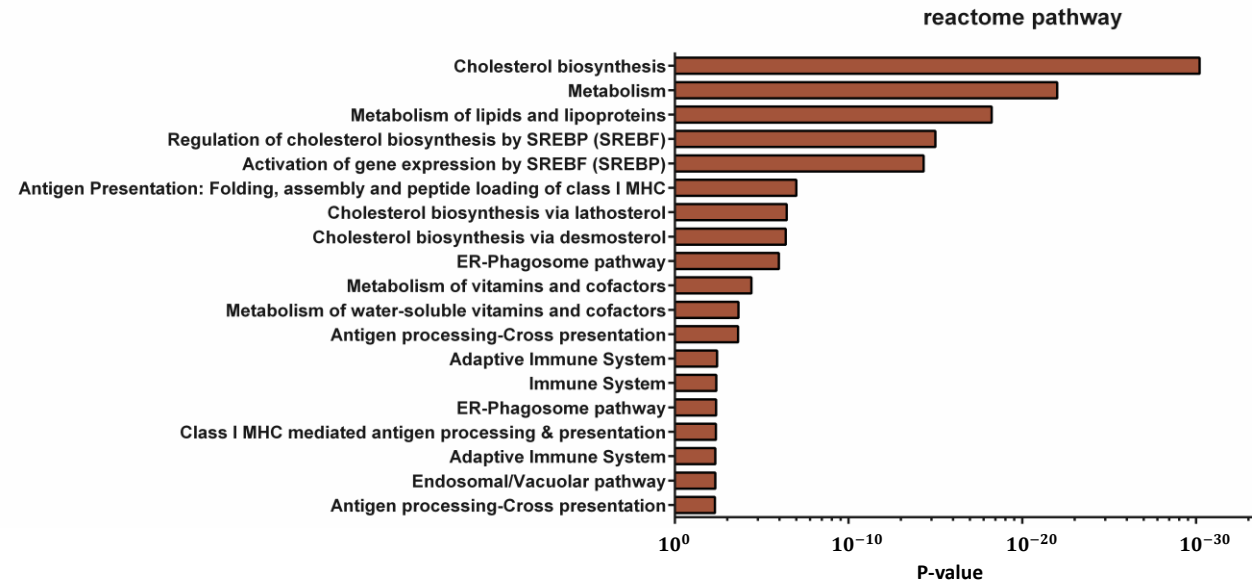

Figure 6.8 GO term enrichment analysis of the upregulated proteins.
Functional GO enrichment analysis of biological processes was carried out with the PANTHER Classifications system (Mi et al. 2017; Mi et al. 2013). The 66 detected upregulated proteins upon addition of U18666A to the culture medium in the proteomics dataset were searched for Reactome pathways (target proteins) against all mouse reference proteins in the PANTHER database as background (22262 reference proteins). P-value was calculated using the Fisher test. The diagram shows enriched GO terms with P-values < 0.05 with the appertaining P-values (x-axis) in decreasing order.

6.2.2.2. Gene ontology (GO) analysis of the upregulated proteins in the proteomics dataset

PANTHER online software was employed to conduct GO analysis for the 66 upregulated proteins. Figure 6.8 shows all the Reactome pathways which were significantly overrepresented (FDR < 0.05) according to the PANTHER data. Three groups with the lowest p-values (highest

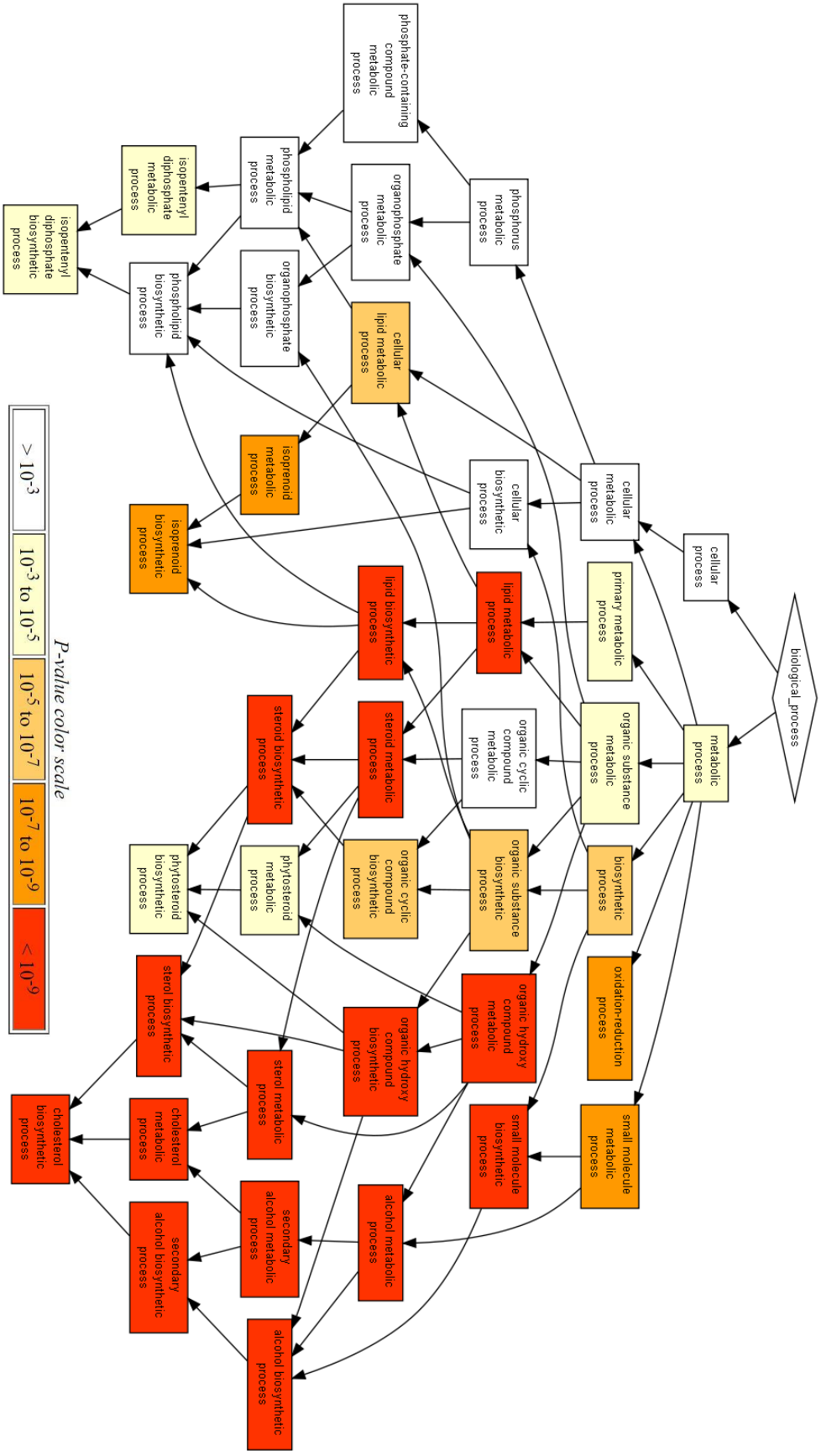
biological_process
cellular process
metabolic process
cellular metabolic process
primary metabolic process
organic substance metabolic process
phosphorus metabolic process
phosphate-containing compound metabolic process
cellular biosynthetic process
lipid metabolic process
organic cyclic compound metabolic process
organophosphate metabolic process
phospholipid metabolic process
isopentenyl diphosphate metabolic process
biosynthetic process
oxidation-reduction process
small molecule metabolic process
cellular lipid metabolic process
organophosphate biosynthetic process
phospholipid biosynthetic process
isopentenyl diphosphate biosynthetic process
isoprenoid metabolic process
isoprenoid biosynthetic process
lipid biosynthetic process
steroid metabolic process
steroid biosynthetic process
organic substance biosynthetic process
organic cyclic compound biosynthetic process
phytosteroid metabolic process
phytosteroid biosynthetic process
organic hydroxy compound metabolic process
organic hydroxy compound biosynthetic process
small molecule biosynthetic process
sterol metabolic process
sterol biosynthetic process
alcohol metabolic process
secondary alcohol metabolic process
cholesterol metabolic process
cholesterol biosynthetic process
secondary alcohol biosynthetic process
alcohol biosynthetic process
P-value color scale
> 10-3
10-3 to 10-5
10-5 to 10-7
10-7 to 10-9
< 10-9

Figure 6.9 GO term enrichment analysis of the top 20 upregulated proteins.
Gene ontology clustering was performed using Gorilla analysis (Eden et al. 2009). The top 20 detected upregulated proteins upon addition of U18666A to the culture medium in the proteomics dataset were searched for enriched GO terms as the target set against 5199 all other proteins detected in protein dataset as background. P-value was calculated using the Fisher test. The diagram is color-coded to illustrate the P-value according to the P-value scale.

significance) are "Cholesterol biosynthesis", "Metabolism", and "Metabolism of lipids and lipoproteins". GO analysis of the upregulated proteins was also performed using the Gorilla gene ontology tool. Upregulated proteins were subjected to GO analysis as target genes, and the remaining 5482 proteins found in all three replicates as background. Similar to the results obtained from PANTHER, again the groups with the lowest p-values are related to the cholesterol and lipid biosynthesis (Figure 6.9). 8 downregulated proteins were also subjected to the PANTHER and Gorilla software; however, no significant relation was found between them.

Table 6.2 Top 20 upregulated proteins in the proteomics dataset.
Top 20 upregulated proteins upon addition of U18666A to the culture medium in the proteomics dataset with more than 1 detected peptide, and P-values less than 0.05. The number of unique peptides identified for each protein is shown in the table. Proteins which according to the literature are related to cholesterol metabolism are illustrated in green, and for 4 proteins (here shown in red) a direct relation between them and cholesterol metabolism was not found.

Protein names	Gene names	Log 2 Ratio	Peptides
Squalene monooxygenase	Sqle	3.17	11
Delta(14)-sterol reductase	Tm7sf2	3.00	3
Squalene synthase	Fdft1	2.79	16
Lanosterol synthase	Lss	2.63	28
Sterol-4-alpha-carboxylate 3-dehydrogenase	Nsdhl	2.55	21
Delta(24)-sterol reductase	Dhcr24	2.54	12
Lanosterol 14-alpha demethylase	Cyp51a1	2.37	25
Methylsterol monooxygenase 1	Msmo1	2.28	5
3-keto-steroid reductase	Hsd17b7	2.25	11
7-dehydrocholesterol reductase	Dhcr7	2.22	6
Acetyl-coenzyme A synthetase, cytoplasmic	Acss2	2.06	2
Isopentenyl-diphosphate Delta-isomerase 1	Idi1	2.05	13
Tapasin	Tapbp	1.93	11
Diphosphomevalonate decarboxylase	Mvd	1.92	9
Retinol dehydrogenase 11	Rdh11	1.90	13
3-hydroxy-3-methylglutaryl-coenzyme A reductase	Hmgcr	1.89	3
Acetyl-CoA acetyltransferase, cytosolic	Acat2	1.83	15
Phosphomevalonate kinase	Pmvk	1.79	11
Complement C1s-A subcomponent	C1sa	1.78	3
Fructose-bisphosphate aldolase C	Aldoc	1.68	10

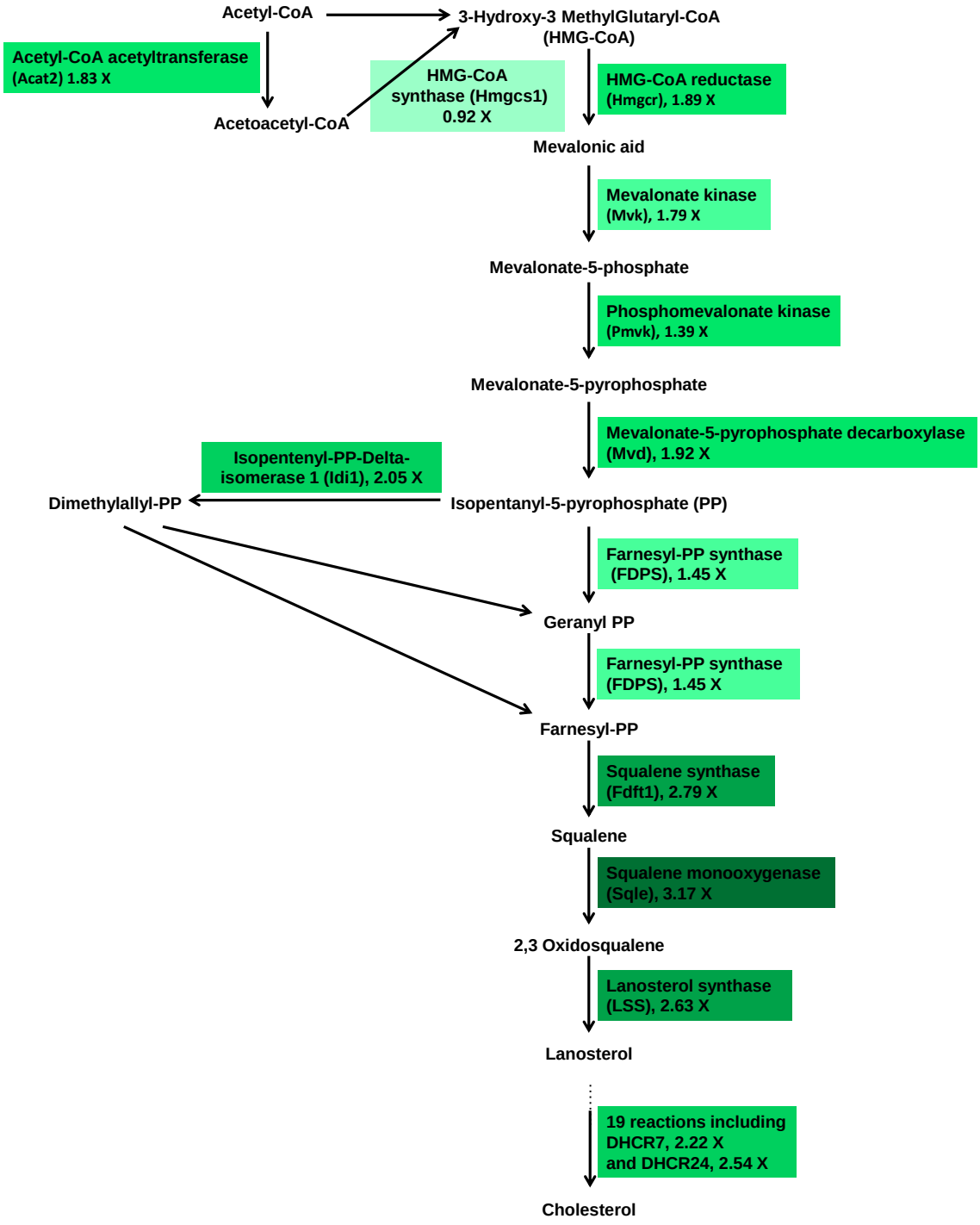

Figure 6.10 All enzymes involved in the cholesterol metabolism are upregulated.
The proteomics dataset was interrogated for enzymes involved in the cholesterol metabolism pathway. All proteins involved in the cholesterol metabolism pathway were found in the proteomics dataset, and all are upregulated upon addition of U18666A to the culture medium. The log2 expression ratios are illustrated in a colored scale, with low values colored in light green and higher values colored in dark green.

Table 6.2 shows the top 20 upregulated proteins with more than one unique peptide in the proteomics dataset. 16 proteins in the list are related to cholesterol metabolism. As shown in figure 6.10, all enzymes involved in cholesterol synthesis pathway are upregulated in the proteomics dataset. Next, the dataset was interrogated for the kinases and phosphatases. Searching for the word "kinase" and "phosphatase" resulted in finding 266 kinases and 116 phosphatases. Five kinases and one phosphatase were recognized to be differentially expressed in U18666A-treated cells (Table 6.3).

6.2.2.3.Large-scale phosphoproteomics analysis of U18666A-treated cells

The aim of this study was to investigate the phosphorylation alterations in U18666A-treated cells. To that end, 6 mg of the combined (3 mg sample (U18666A-treated cells) + 3 mg control (DMSO-treated cells)) whole cell lysate was subjected to double TiO_2 phosphopeptide enrichment. Enriched phosphopeptides were fractionated using the tip-based SCX fractionation method and later were subjected to quantitative analysis by LC-MS/MS (Figure 6.4). MaxQuant and Perseus software packages were employed for data analysis. In total, 3428 phosphoproteins,

Table 6.3 Differentially expressed phosphatases and kinases in the proteomics dataset.
The proteomics dataset was searched for phosphatases and kinases that were differentially expressed upon addition of U18666A to the culture medium more than 1 fold (log 2 ratio) with more than 1 unique peptide. The number of unique peptides identified for each protein is shown in the table.

Protein names	Gene names	Log 2 Ratio	Peptides
Phosphomevalonate kinase	Pmvk	1.79	11
Mevalonate kinase	Mvk	1.39	8
Adenylate kinase 4, mitochondrial	Ak4	1.39	6
[Pyruvate dehydrogenase (acetyl-transferring)] kinase isozyme 1, mitochondrial-1	Pdk1	1,18	4
Thymidine kinase, cytosolic	Tk1	-1.04	5
Serine/threonine-protein phosphatase 6 regulatory ankyrin repeat subunit C	Ankrd52	-1.20	2

9504 phosphopeptides, and 12881 phosphorylation sites were detected (Supplementary table 6.2). Although the reproducibility of the replicates was lower in the phosphoproteomics dataset in comparison to the proteomics dataset, the correlation between the three replicates of the phospho-study was still relatively high. The Pearson's r (Puth et al. 2014) was found to be 0.726, 0.755, and 0.787 between replicates 1 and 2, 1 and 3, and 2 and 3, respectively (Figure 6.11 (A)). More than 55% of the phosphosites were detected in all 3, and 23.9% were found exclusively in only one replicate (Figure 6.11 (B)). The distribution of the heavy over light (H/L) SILAC ratios for

total quantified phosphosites in each replicate is shown in figure 6.12. Most of the quantified phosphosites showed a ratio around 1 (log 2 (ratios) = 0) as it was expected.

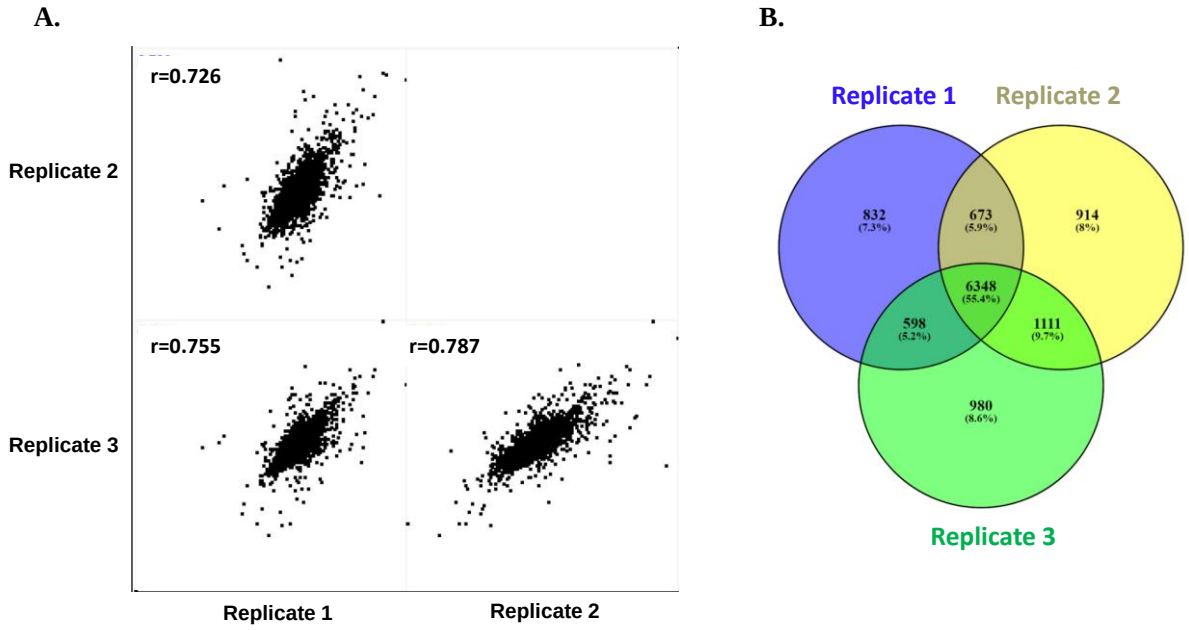

Figure 6.11 Comparing the results obtained from three biological replicates of the phosphoproteomics dataset.
A. MaxQuant software outputs of the phosphoproteomics dataset were further evaluated by Perseus software. Correlations between the three biological replicates were assessed using Pearson's correlation coefficient (r). **B.** The overlap between the proteins found in three replicates is shown using a venn diagram. Venn diagrams were constructed using the open-access online tool Venny (Juan Carlos Oliveros).

9695 of the 12881 detected phosphosites were classified as class I phosphosites (certainty of phosphosite localization p > 75%). 120 and 168 of the class I phosphosites were up- or downregulated, respectively, more than 1 fold (log 2 values) and found in at least two biological replicates with p-values less than 0.05 (Supplementary table 6.2). Table 6.4 shows the top 20 differentially expressed phosphorylation sites (up and down). One of the mitogen-activated protein kinase 1 (MAPK1) phosphosites (Y185) is among the downregulated phosphosites (Table 6.4). Phosphorylation at this phosphosite (Y185) activates the MAPK1 enzyme (Dalby et al. 1998). Due to the importance of this phosphosite, there are commercially available antibodies against the phosphorylated form of the Y185 residue. Phospho-p44/42 MAPK antibody was exploited to corroborate the mass spectrometry results. Phospho-p44/42 MAPK (Erk1/2) antibody was employed for Western blot analysis of U18666A-treated samples. Figure 6.13

shows that in line with the MS data, Y185 phosphorylation dramatically reduces upon U18666A treatment and therefore MAPK1 is deactivated.

6.2.2.4.GO analysis of the differentially expressed phosphorylation sites

104 phosphoproteins corresponding to 120 upregulated phosphosites were subjected to the GO analysis for the "GO biological process" using the PANTHER software. Figure 6.14 (A) indicates the top 20 GO terms with the lowest p-values. The top three enriched GO terms were found to be "regulation of cellular localization", "establishment of localization", and "localization". GO terms associated with "localization" are enriched in the upregulated phosphoproteins (10 groups out of 20 are associated with localization). Other overrepresented GO terms are including: "regulation of response to stimulus", "regulation of cellular pH", "lipid biosynthetic process", and "sterol biosynthetic process" (Figure 6.14 (A)).

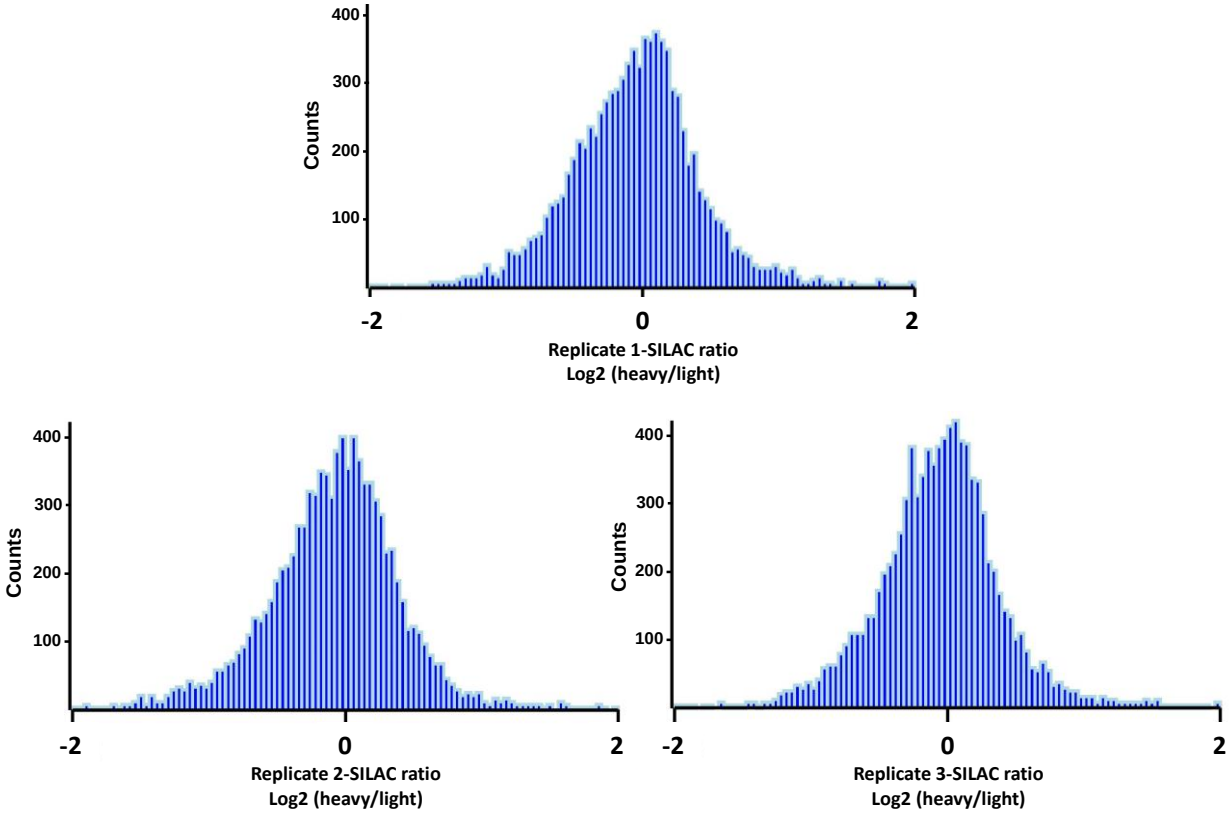

Figure 6.12 Normal distribution of H/L SILAC ratios for each replicate of the phosphoproteomics dataset.
Normalized ratios acquired from the MaxQuant software were converted to log (base 2) values and using these values distribution of SILAC ratios for each replicate was assessed using Perseus (from MaxQuant software package). Y-axis (counts) shows the number of counts in each bin in the histogram.

GO analysis was also performed for the downregulated phosphosites. 135 phosphoproteins associated with 168 downregulated phosphosites were analyzed using the PANTHER software for the "GO biological process". As it is shown in figure 6.14 (B), 5 out of top 20 enriched GO terms are related to localization. "Regulation of cellular component organization", "cellular component organization or biogenesis", and "localization" were found to be top three enriched GO terms. In general, among the top 20 enriched GO terms, six GO terms were associated with the organization of different cellular components and five were associated with "transport" (Figure 6.14 (B)).

6.2.3. Six phosphoproteins were selected for further analysis

Regulated phosphosites were subjected to manual investigation and literature review and six lysosomal-associated phosphoproteins (ragulator complex protein LAMTOR1, ras-related GTP-binding protein C (RagC), osteopetrosis-associated transmembrane protein 1 (OSTM1),

Table 6.4 Top 20 differentially expressed phosphosites in the phosphoproteomics dataset.
Top 20 up- or down-regulated phosphorylation sites upon addition of U18666A to the culture medium in the phosphoproteomics dataset. Phosphorylation sites with localization probability > 75% are shown. "Protein level ratio" shows the relative intensity of the correspondent protein in the proteomics dataset.

Upregulated phosphosites					Downregulated phosphosites				
Gene names	Position within protein	Localization prob	Ratio H/L (log2)	Protein level ratio (log2)	Gene names	Position within protein	Localization prob	Ratio H/L (log2)	Protein level ratio (log2)
Pex1	1142	0.92	5.27966	-	Csrnp2	280	1	-3.12205	-
Akt2	126	0.99	4.45536	-0.22	Fam65a	875	0.98	-3.11004	-0.70
Pkhd1	3258	0.99	4.41691	-	Wdr13	79	0.99	-3.05086	-
Stim1	257	1	3.92039	0.41	Aak1	554	1	-2.8667	-0.46
Cbfa2t2	235	0.97	3.79743	-	Cdc42ep2	3	0.95	-2.72786	-
Arpp19	6	0.96	3.25985	-	Asap1	819	0.99	-2.30116	-0.34
Ccdc115	100	0.99	3.15557	0.41	Bnip3l	167	0.99	-2.12967	-0.09
Agpat9	68	0.99	3.05108	-	Mapk1	185	0.99	-2.08749	-0.23
Dock7	963	0.90	3.04663	-0.19	Synrg	989	0.99	-2.03617	-
Shroom3	969	1	3.03958	-0.15	Ubap1	253	0.99	-1.97336	-0.36
Fdft1	53	1	2.99271	2.79	Palld	650	0.97	-1.94669	-0.48
Slc4a2	55	1	2.83479	0.65	Map3k7	415	0.85	-1.9422	-
Mfsd1	20	1	2.82652	0.56	Rps6	247	0.99	-1.92413	-0.26
Flnb	885	0.75	2.81223	-0.20	Rps6	244	0.99	-1.88082	-0.26
Vamp2	80	0.99	2.76977	0.46	Sec61b	49	0.99	-1.86581	-
Taok1	445	0.99	2.63923	0.05	Raph1	192	0.99	-1.86412	0.16
Spag5	12	1	2.61967	-	Txlna	515	1	-1.79912	-0.64
Spag5	14	1	2.61967	-	Nup205	1165	0.99	-1.79266	0.05
Hmox1	176	0.76	2.40504	1.23	Cbx3	99	0.99	-1.69825	0.27
Tmem106b	34	0.99	2.40242	0.60	Tsc22d4	165	0.99	-1.68971	-

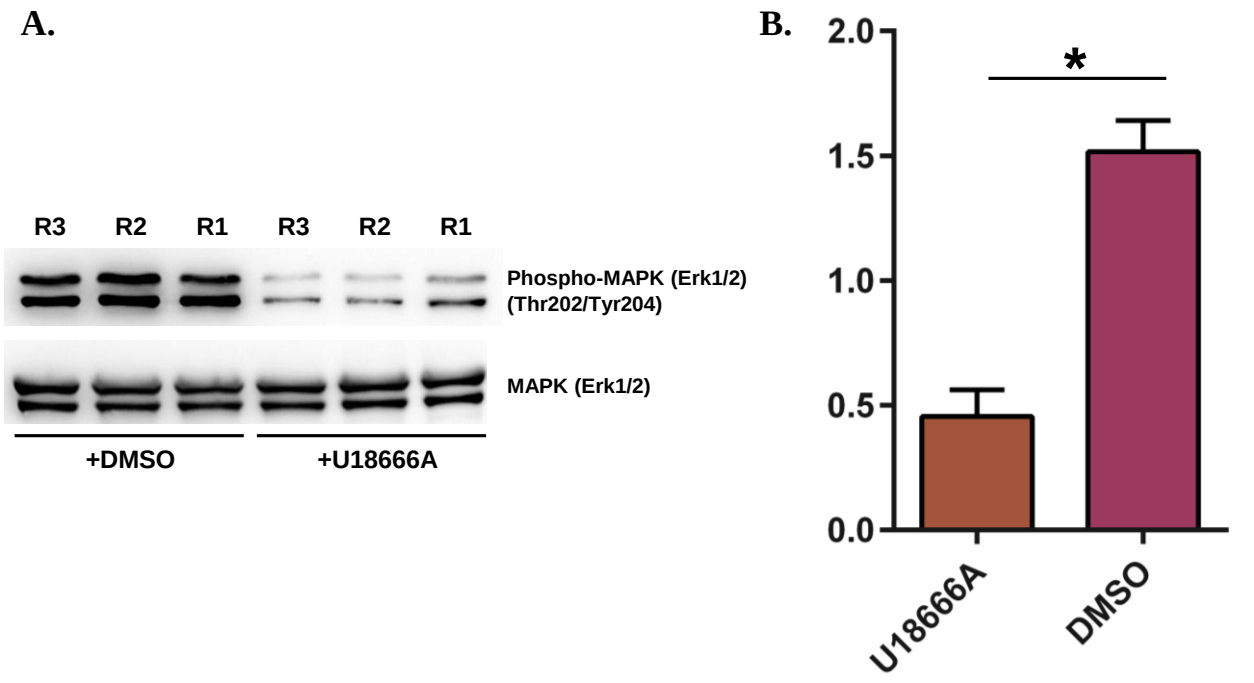

Figure 6.13 Evaluation of ERK1/2 activity in MEF cells treated with U18666A.
A. Mouse embryonic fibroblast (MEF) cells were treated with either U18666A (3 µg/ml) or DMSO and after 24 h harvested and lysed. 20 µg of protein lysate was applied to each lane of an SDS-PAGE gel. Subsequently, the gel was semi-dry blotted, and the blots were blocked using 5% BSA (wt/vol) in Tris-buffered saline containing 0.1% Tween 20. Next, blots were incubated with either Phospho Erk1/2 (Thr202/Tyr204) (#9101 Cell Signaling Technology) as a readout for ERK1/2 activity or total Erk1/2 (#9102 Cell Signaling Technology) primary antibodies. After incubation with proper secondary antibodies, protein signals were visualized using FUSION system. The figure shows the results of 3 independent biological experiments. **B.** The Fusion software was employed for quantification of protein signals. Phospho Erk1/2 intensity in each condition was normalized against total Erk1/2. Statistical analysis was conducted using the GraphPad Prism 6 software. Shown are mean values + SEM; n=3; *,$p < 0.05$-paired T-test (P-value: 0.0159).

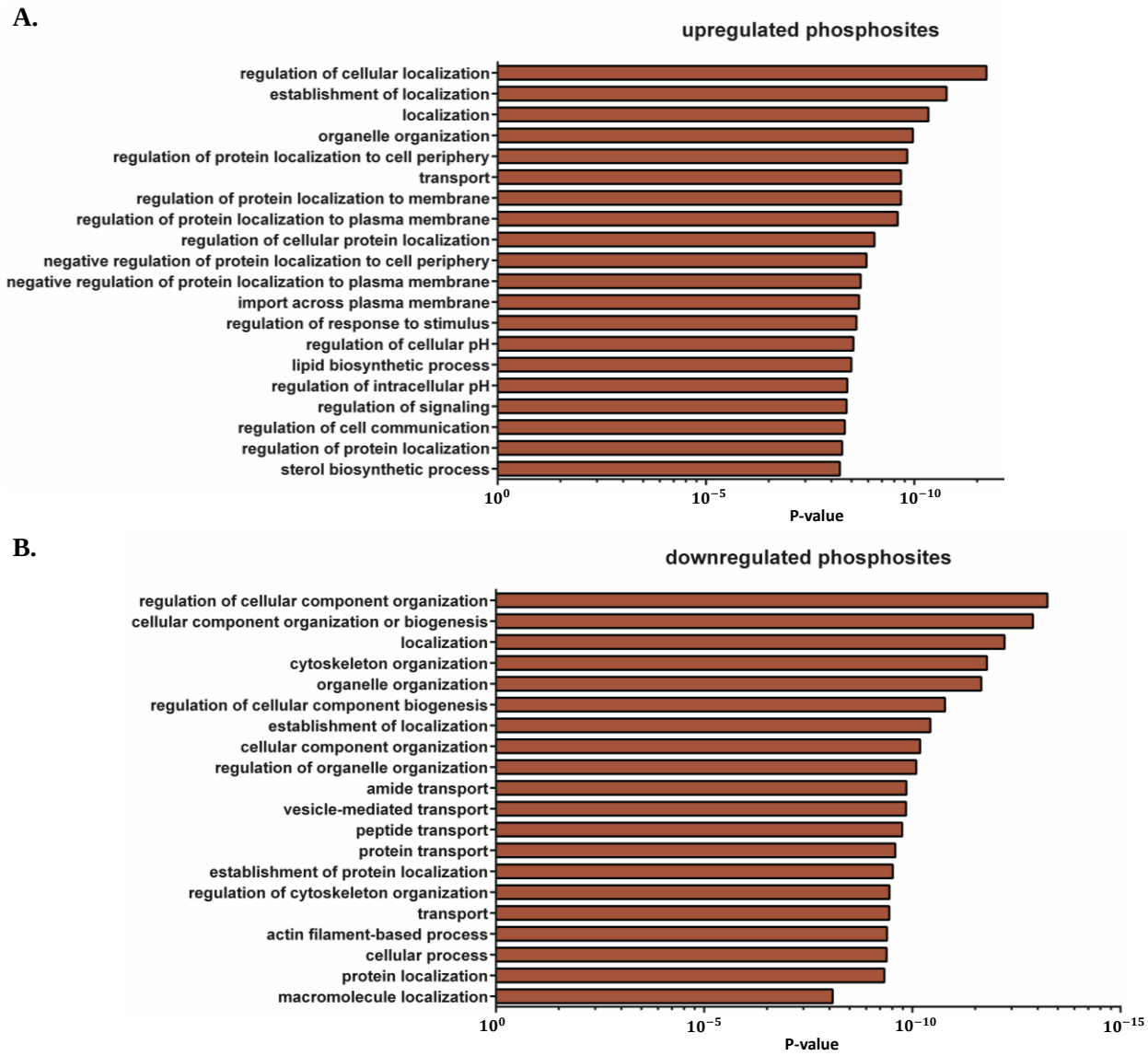

Figure 6.14 GO term enrichment analysis of the differentially expressed phosphosites.
Gene ontology clustering was performed using PANTHER analysis (Mi et al. 2017; Mi et al. 2013). Phosphoproteins harboring the 120 upregulated phosphosites (**A**) or 135 downregulated phosphosites (**B**) upon addition of U18666A to the culture medium in the phosphoproteomics dataset were subjected to the PANTHER software for the "GO biological process complete". Top 20 enriched GO terms with a false discovery rate < 0.05 are shown here. Raw P-values were calculated using the Fisher test. The diagram shows GO terms with the appertaining P-values (x-axis) in decreasing order.

Table 6.5 List of the candidate phosphorylation sites for subsequent biological follow-up experiments.
Differentially expressed phosphorylation sites upon addition of U18666A to the culture medium in the phosphoproteomics dataset were manually analyzed and evaluated for their relatedness to lysosomes and their importance for cell function. Table 6.5 shows the candidate phosphopeptide sequences and their fold-change expression. Moreover, the proteomics dataset was searched for the correspondent proteins and fold-change was mentioned in the table if detected in the proteomics dataset. (N.I. : Not Identified)

Protein	Position within proeins	Sequence	Fold change (log 2)	P-value	Related protein (log 2 fold change)
LAMTOR1	S56	TDEQALLSS(ph)ILAK	1.97	1.54E-005	0.67
RAGC	S381	SCSHQTS(ph)APSLK	-1.44	0.007062	0.28
OSTM1	S327,S329	LKSS(ph)TS(ph)FANIQENAT	2.05	0.000563	N.I.
STARD3NL	S39	IES(ph)YEGR	1.55	0.000298	N.I.
BNIP3	S88	NSTLS(ph)EEDYIER	1.82	0.005374	N.I.
VAMP8	T54	NKTEDLEAT(ph)SEHFK	1.97	8.39E-005	N.I.

STARD3 N-terminal-like protein (STARD3NL), BCL2/adenovirus E1B 19 kDa protein-interacting protein 3 (BNIP3), and vesicle-associated membrane protein 8 (VAMP8)) (containing seven phosphosites) were chosen for follow-up experiments (Table 6.5). Six candidate phosphosites were chosen among the upregulated phosphosites, as well as S381 of RagC which was the only downregulated phosphorylation site. The MS spectra of the candidate phosphosites were manually inspected for the heavy/light ratios to eliminate the false positive ratios due to spectral overlap or software errors. Spectra of LAMTOR1 and BNIP3 phosphopeptides associated with S58 and S88 phosphosites, respectively, are shown as examples in the figure 6.15 (A and B). The proteomics dataset was also examined to determine whether the candidate phosphoproteins were detected in the proteomic study. LAMTOR1 and RagC are the only proteins which were found in the proteomics dataset (Table 6.5), the intensities of these proteins did not significantly change after U18666A stimulation (0.67, and 0.28 (log 2 values), respectively).

6.2.4. Effects of phosphomimetic mutation on the stability of the candidate phosphoproteins

Phosphorylation can lead to a variety of changes in proteins, such as alteration in degradation rate. Therefore, for all candidate phosphoproteins, first, the effect of phosphorylation on their degradation rate was investigated. To that end, phosphorylated residues were mutated to either

phosphomimetic glutamic acid (E) or phosphoresistant alanine (A) residues using PCR

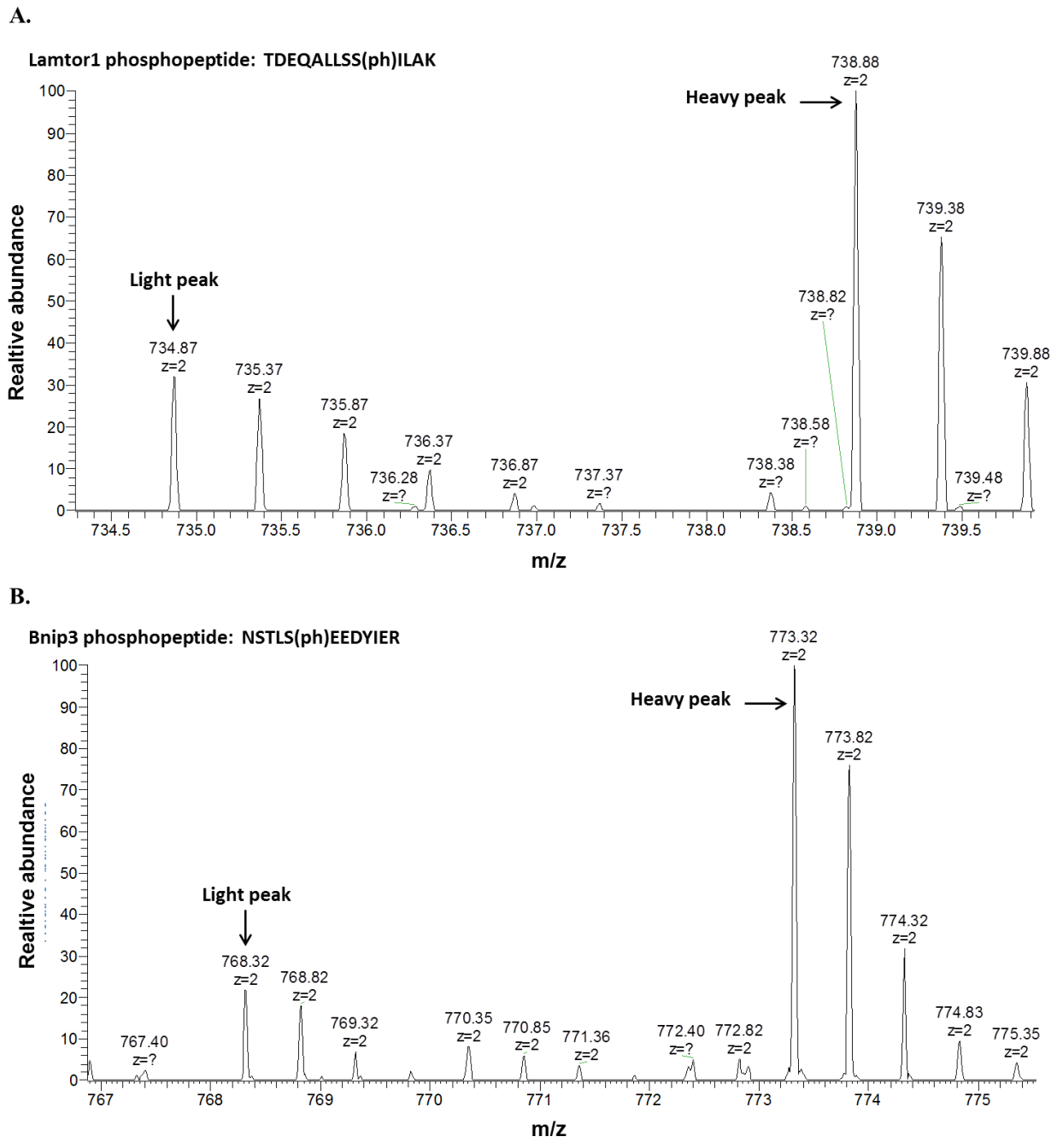

Figure 6.15 Manual validation of SILAC ratios using LC-MS survey scans.
LC-MS/MS raw data were analyzed manually using Xcalibur software (https://www.thermofisher.com/order/catalog/product/OPTON-30487) to corroborate the results obtained from the Maxquant software. Light and heavy spectra correspondent to the candidate phosphopeptides were detected, and their intensities were compared by dividing relative abundance of the heavy peak to the light peak. As examples LAMTOR1 (**A**) and BNIP3 (**B**), light and heavy peaks are shown here.

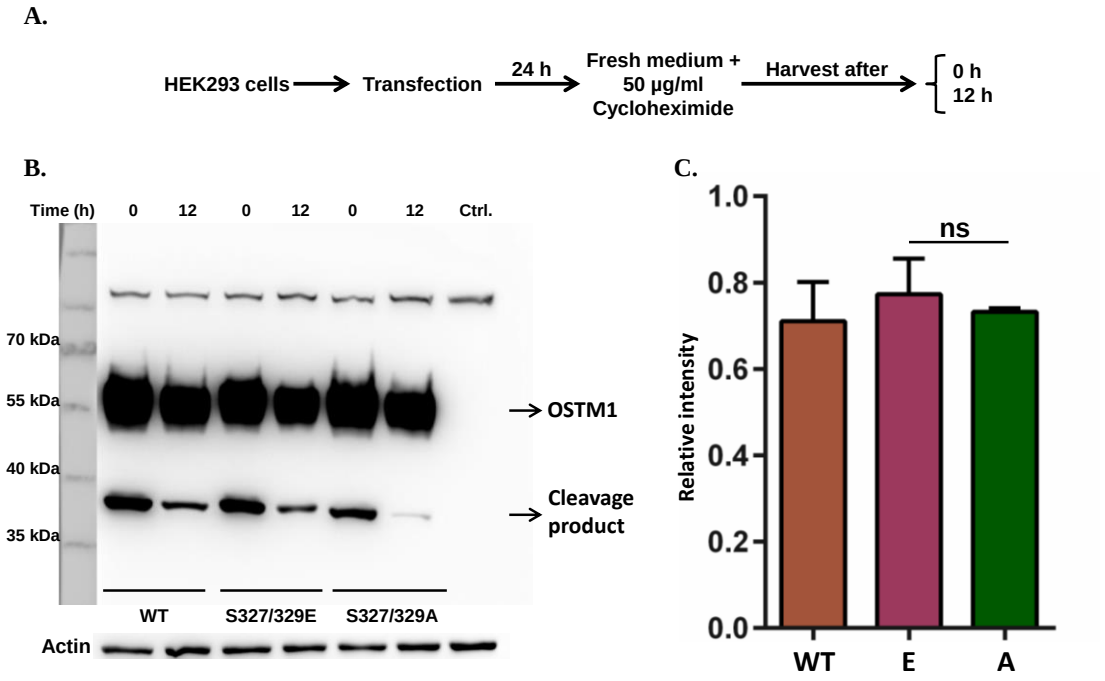

Figure 6.16 Effect of phosphorylation on the stability of Ostm1.
A. HEK293 cells were transfected with Ostm1 WT, S327/329E and S327/329A constructs and after 24 h fresh medium containing 50 µg/ml cycloheximide (eukaryotic protein synthesis inhibitor) was added to the cells and samples were harvested after 12 h incubation time. **B.** Harvested samples were lysed, and 20 µg of each protein lysate was size-separated by 10% SDS-PAGE gel. Subsequently, the gel was semi-dry blotted and blocked using 5% (wt/vol) non-fat milk in Tris-buffered saline containing 0.1% Tween 20. Next, the blot was incubated with either anti-Myc (ab9106 (Abcam)) or β-Actin (A5316 (Sigma-Aldrich)) antibodies following with incubation with proper secondary antibodies. Blots were visualized using Fusion imaging system. **C.** The Fusion software was employed to quantify the relative amount of protein signal. The level of Myc in each sample was normalized against the level of β-Actin. Relative intensity was calculated by dividing the normalized value of time 12 h to time 0 h. Statistical analysis was conducted using the GraphPad Prism 6 software. Shown are mean values + SEM; n=3; paired T-test (P-value: 0.6655); ns: not significant.

site-directed mutagenesis. Wild-type (WT) and mutated genes were expressed in HEK293 cells, and later the protein synthesis was terminated using cycloheximide. Western blot assays were employed to compare the degradation rate of the proteins of interest. In the following, the results of the follow-up experiments for different candidate phosphoproteins are presented.

6.2.4.1.Phosphorylation affects OSTM1 cleavage

Myc-tag was placed at the C-terminus of OSTM1 and the protein expression was driven by the CMV promoter (Appendix 2) to investigate the Ser 327/329 phosphorylation effects. HEK293 cells were transiently transfected with phosphomimetic or phospho-resistant forms of the OSTM1

protein. Cells were treated with cycloheximide for 24 h and subsequently

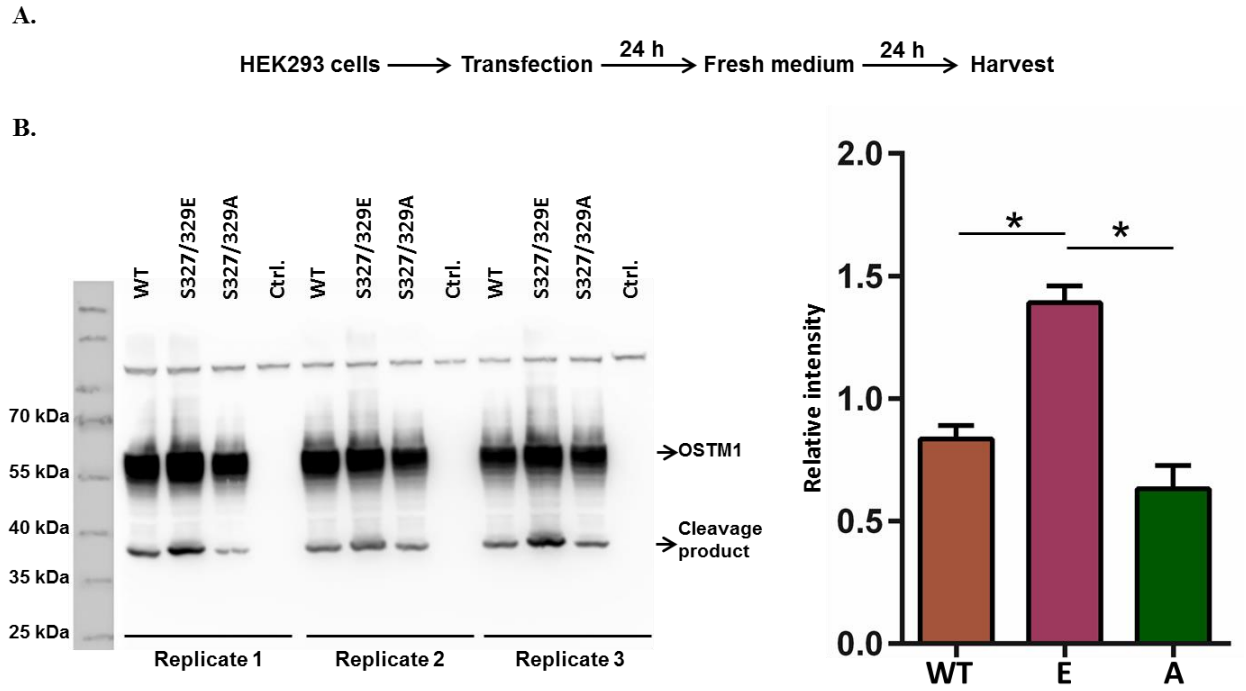

Figure 6.17 Effect of phosphorylation on Ostm1 cleavage.
A. HEK293 cells were transfected with Ostm1 WT, S327/329E and S327/329A constructs and after 24 h fresh medium was added to the cells and samples were harvested after 24 h. **B.** Harvested samples were lysed, and 20 µg of each protein lysate was size-separated by 10% SDS-PAGE gel. Subsequently, the gel was semi-dry blotted and blocked using 5% (wt/vol) non-fat milk in Tris-buffered saline containing 0.1% Tween 20. Next, the blot was incubated with either anti-Myc (ab9106 (Abcam)) antibody following with incubation with proper secondary antibody. Blots were visualized using Fusion imaging system. The Fusion software was employed to quantify the relative amount of protein signal. The relative intensity of the cleavage product was calculated by dividing the amount of cleavage product in each sample to the amount of total Ostm1 in the same sample. Statistical analysis was conducted using the GraphPad Prism 6 software. Shown are mean values + SEM; n=3; *, $p < 0.05$-paired T-test.

harvested and analyzed by Western blot. As it is shown in figure 6.16, phosphorylation of Ser 327/329 did not alter OSTM1 degradation rate. However, a direct relationship between OSTM1 phosphorylation and the intra-lysosomal formation/stability of its proteolytically processed form was observed (Figure 6.16 (B)). Therefore, another experiment was carried out to confirm that phosphorylation affects OSTM1 proteolysis. HEK293 cells were transfected with WT and mutated constructs, and after 24 h the fresh medium was added to the samples and 24 h later samples were harvested. The relative intensity of the cleavage products was assessed by dividing the intensity of the cleavage product to the intensity of the full length protein. It is shown in

figure 6.17, that S327/329E mutant generates significantly more C-terminal cleavage product

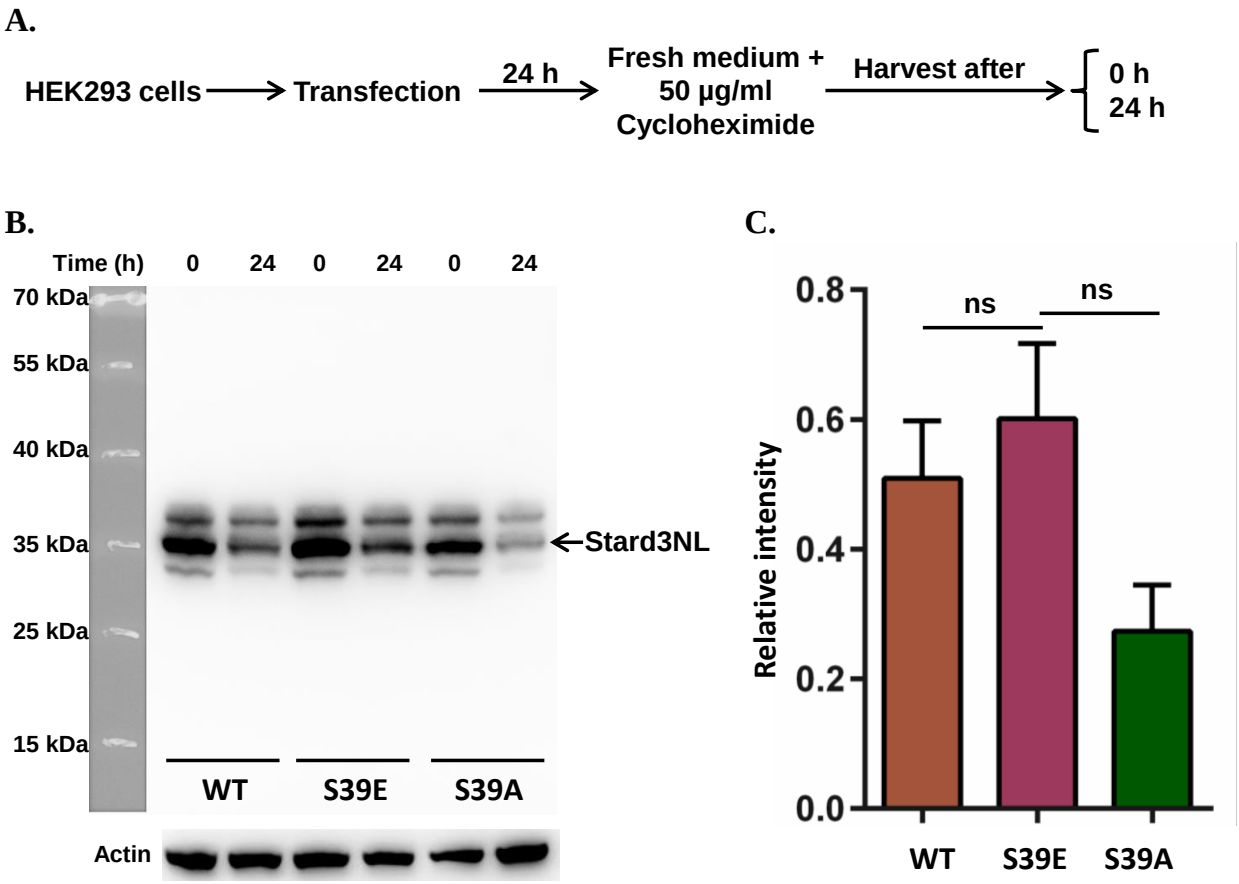

Figure 6.18 Effect of phosphorylation on the stability of Stard3nl.
A. HEK293 cells were transfected with Stard3nl WT, E-mutated, and A-mutated constructs and after 24 h fresh medium containing 50 µg/ml cycloheximide (eukaryotic protein synthesis inhibitor) was added to the cells and samples were harvested after 24 h incubation time. **B.** Harvested samples were lysed, and 20 µg of each protein lysate was size-separated by 10% SDS-PAGE gel. Subsequently, the gel was semi-dry blotted and blocked using 5% (wt/vol) non-fat milk in Tris-buffered saline containing 0.1% Tween 20. Next, the blot was incubated with either anti-Myc (ab9106 (Abcam)) or β-Actin (A5316 (Sigma-Aldrich)) antibodies following with incubation with proper secondary antibodies. Blots were visualized using Fusion imaging system. **C.** The Fusion software was employed to quantify the relative amount of protein signal. The level of Myc in each sample was normalized against the level of β-Actin. Relative intensity was calculated by dividing the normalized value of time 24 h to time 0 h. Statistical analysis was conducted using the GraphPad Prism 6 software. Shown are mean values + SEM; n=3; paired T-test ; P-value WT vs. E: 0.1857, P-value E vs A: 0.1771; ns: not significant.

compared to S327/329A and WT. These results suggest that phosphorylation at Ser 327/329 promotes OSTM1 cleavage.

6.2.4.2.Phosphorylation does not affect STARD3NL, BNIP3, and VAMP8 degradation rate

The STARD3NL and VAMP8 genes were expressed using the CMV promoter (Appendix 2), and Myc-tag was placed at the C-terminus of these genes. In the case of BNIP3, the Myc-tag was added at the N-terminus, and it was cloned under RSV promoter (Appendix 3). HEK293 cells were transfected with the WT and mutated forms of STARD3NL and 24 h later time "0 h" samples were harvested and fresh medium containing 50 µg/ml cycloheximide was added. Samples "24 h" were harvested after 24 h incubation time with cycloheximide (Figure 6.18 (A)). Although it is shown in figure 6.18 (B) that S39E mutated form of the STARD3NL is slightly more stable than S39A, however, this difference is not statistically significant (Figure 6.18 (C)).

The same cycloheximide experiment was conducted for phosphoresistant/-mimetic versions of Vamp8 and BNIP3. Figure 6.19 (A and B) shows the Western blots results of these experiments. These results indicate that phosphorylation at T54 VAMP8 and S88 BNIP3 does not affect the stability of these proteins, therefore this experiment was performed in just one replicate (Figure 6.19 (C and D)).

6.2.4.3.Phosphorylation affects LAMTOR1 but not RagC stability

LAMTOR1 and RagC cDNAs were cloned downstream of the RSV promoter (Appendix 3), and Myc-tag was fused at the N-terminus of the proteins. Ser to Glu phosphomimetic and Ser to Ala phospho-resistant constructs for S56 of LAMTOR1 and S381 of RagC were generated. LAMTOR1 WT and S56 to A/E were transiently expressed in HEK293 cells for 24 h and thereafter cycloheximide was added and lysates were prepared at the indicated time points (0, 0.5, 1, 2, 4, 8, and 12 h) (Figure 6.20 (A)). Subsequently, the amount of remaining protein after the pulse was determined by Western blot. Figure 6.20 (B) shows a representative result for LAMTOR1 and its S56A and S56E mutants after cycloheximide treatment and figure 6.20 (C) shows the densitometric quantification of the Western blot bands for the four independent biological replicates. The phospho-resistant S56A LAMTOR1 showed significantly increased stability compared to WT LAMTOR1 and the phosphomimetic S56E LAMTOR1.

Cycloheximide experiments were also performed with the phosphoresistant/-mimetic versions of

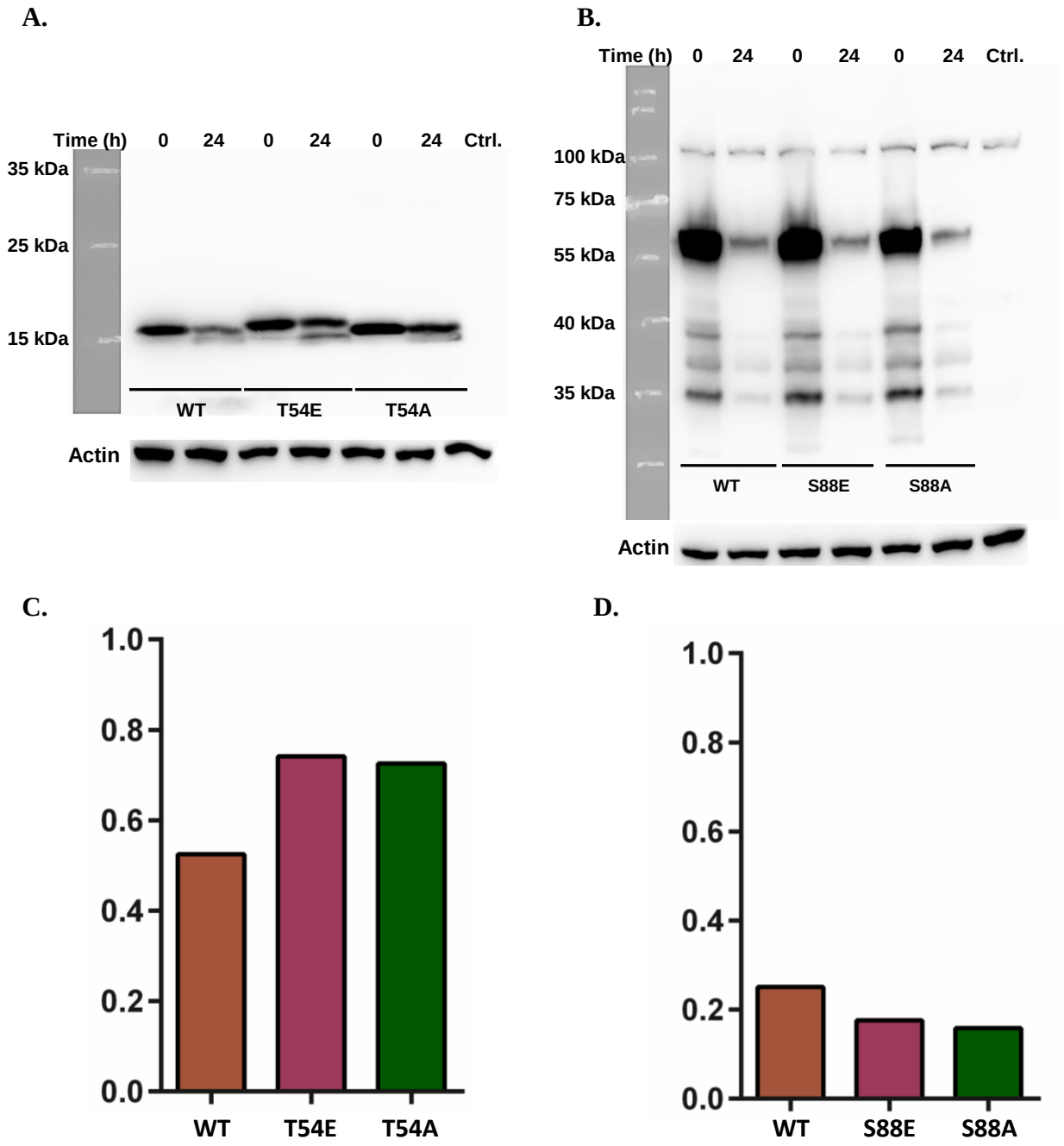

Figure 6.19 Effect of phosphorylation on the stability of Vamp8 and Bnip3.
HEK293 cells were transfected with either Vamp8 or Bnip3 WT, E-mutated, and A-mutated constructs and after 24 h fresh medium containing 50 µg/ml cycloheximide (eukaryotic protein synthesis inhibitor) was added to the cells and samples were harvested after 24 h incubation time. Harvested samples were lysed, and 20 µg of each protein lysate was size-separated by 10% SDS-PAGE gel. Subsequently, the gel was semi-dry blotted and blocked using 5% (wt/vol) non-fat milk in Tris-buffered saline containing 0.1% Tween 20. Next, the blot was incubated with either anti-Myc (ab9106 (Abcam)) or β-Actin (A5316 (Sigma-Aldrich)) antibodies following with incubation with proper secondary antibodies. Vamp8

(**A**) and Bnip3 (**B**) Blots were visualized using Fusion imaging system. **C** and **D**. The Fusion software was employed to quantify the relative amount of protein signal. The level of Myc in each sample was normalized against the level of β-Actin. Relative intensity was calculated by dividing the normalized value of time 24 h to time 0 h for Vamp8 (**C**) and Bnip3 (**D**). n=1

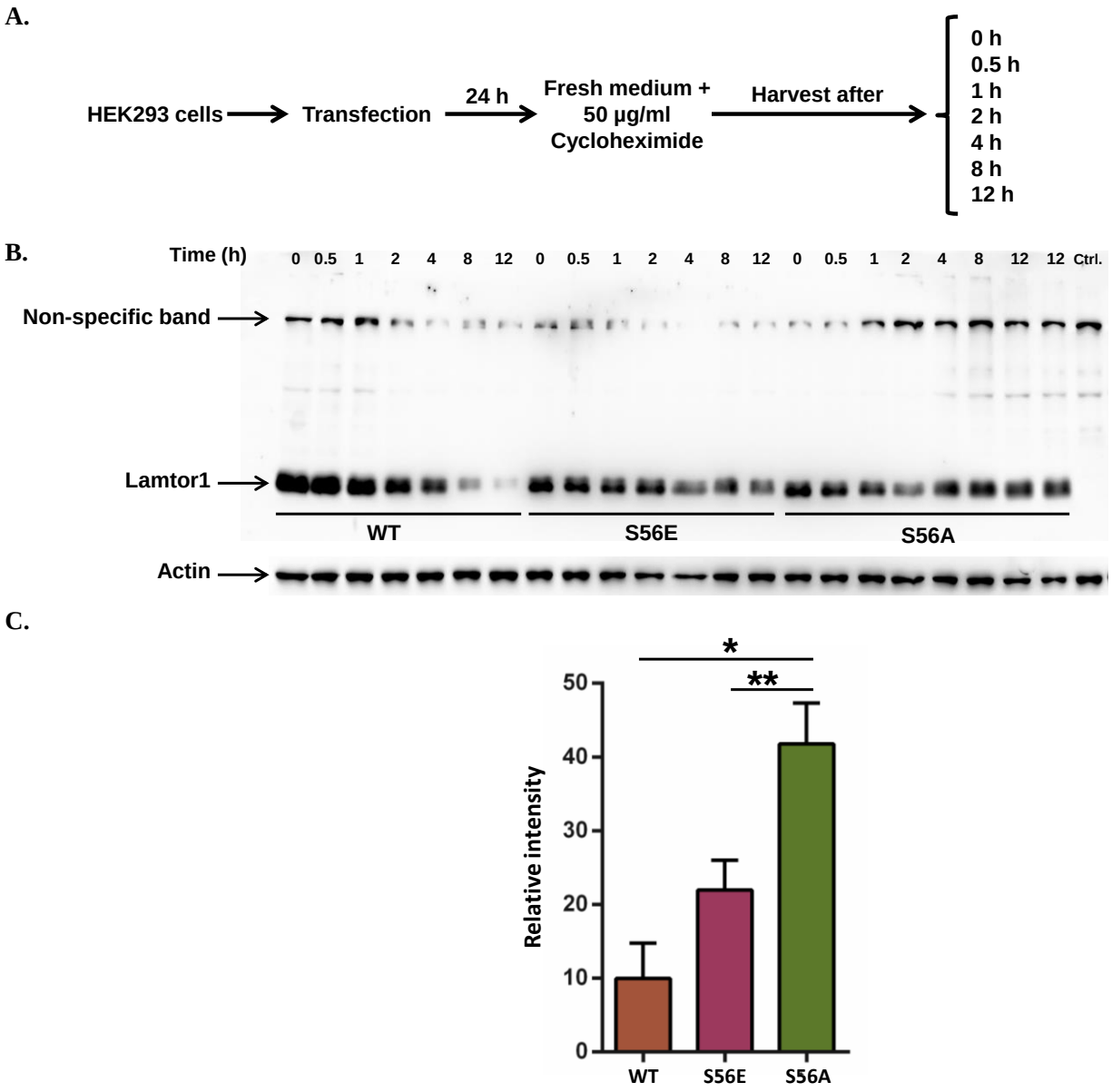

Figure 6.20 Effect of phosphorylation on the LAMTOR1 stability.
A. HEK293 cells were transfected with LAMTOR1 WT, S56E, and S56A constructs. After 24 h fresh medium containing 50 µg/ml cycloheximide (eukaryotic protein synthesis inhibitor) was added to the cells and samples were harvested in different time points. **B.** Harvested samples were lysed, and 20 µg of each protein lysate was size-separated by 10% SDS-PAGE gel. Subsequently, the gel was semi-dry blotted and blocked using 5% (wt/vol) non-fat milk in Tris-buffered saline containing 0.1% Tween 20. Next, the blot was incubated with either anti-Myc (ab9106 (Abcam)) or β-Actin (A5316 (Sigma-Aldrich)) antibodies following with incubation with proper secondary antibodies. Blots were

visualized using Fusion imaging system. **C.** The Fusion software was employed to quantify the relative amount of each protein. The level of Myc in each sample was normalized against the level of β-Actin. Relative intensity was calculated by dividing the normalized value of time 12 h to time 0 h. Statistical analysis was conducted using the GraphPad Prism 6 software. Shown are mean values + SEM; n=4; **, p < 0.01-paired T-test (P-value S56A vs S56E: 0.0044, P-value S56A vs WT: 0.0317).

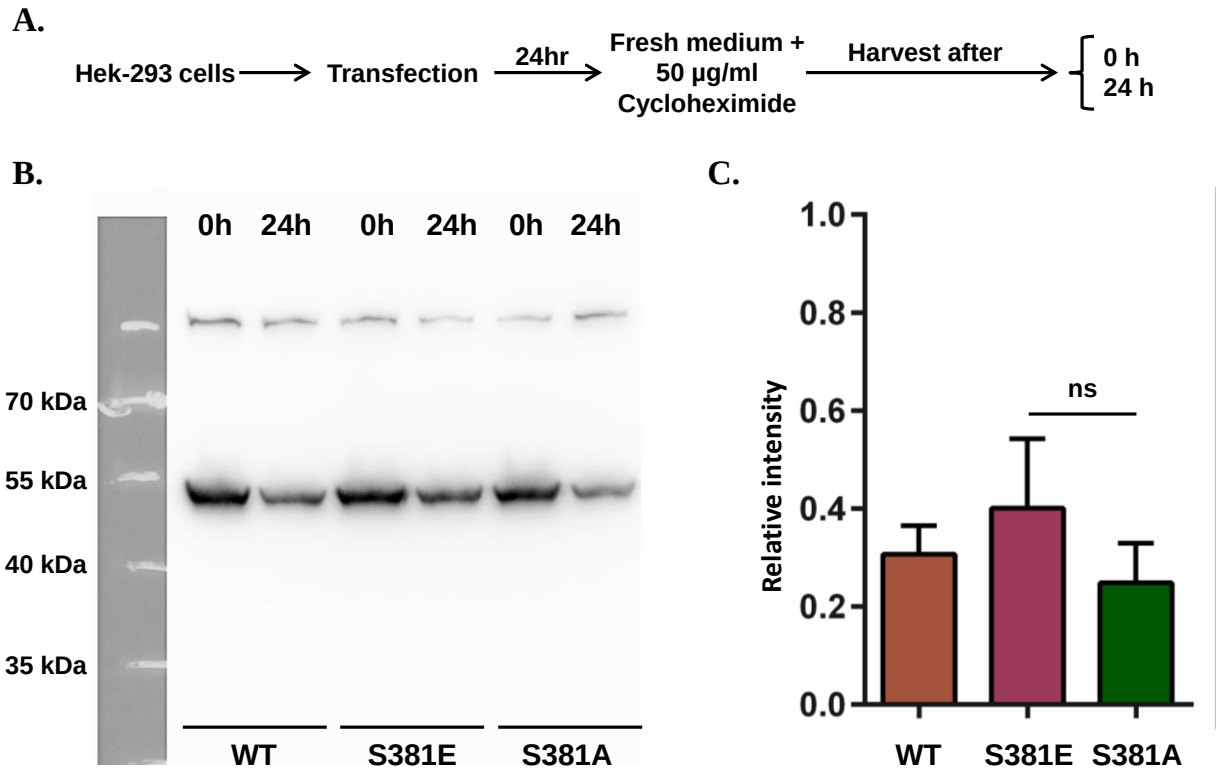

Figure 6.21 Effect of phosphorylation on the stability of RagC.
A. HEK293 cells were transfected with RagC WT, S381E, and S381A constructs. After 24 h fresh medium containing 50 µg/ml cycloheximide (eukaryotic protein synthesis inhibitor) was added to the cells and samples were harvested after 24 h. **B.** Harvested samples were lysed, and 20 µg of each protein lysate was size-separated by 10% SDS-PAGE gel. Subsequently, the gel was semi-dry blotted and blocked using 5% (wt/vol) non-fat milk in Tris-buffered saline containing 0.1% Tween 20. Next, the blot was incubated with either anti-Myc (ab9106 (Abcam)) or β-Actin (A5316 (Sigma-Aldrich)) antibodies followed by incubation with proper secondary antibodies. Blots were visualized using Fusion imaging system. **C.** The Fusion software was employed to quantify the relative amount of each protein. The level of Myc in each sample was normalized against the level of β-Actin. Relative intensity was calculated by dividing the normalized value of time 24 h to time 0 h. Statistical analysis was conducted using the GraphPad Prism 6 software. Shown are mean values + SEM; n=3; paired T-test (P-value: 0.1670); ns: not significant

RagC S381. No statistically significant alteration was observed between the HEK293 cells transfected with the WT protein and mutants regarding protein stability (Figure 6.21).

6.2.4.4.Phosphorylaton affects LAMTOR1 interaction with Rag complex members and SLC38A9

Knowing that phosphorylation alters LAMTOR1 stability, next, it was investigated whether phosphorylation influences LAMTOR1 interaction with other proteins such as members of the Ragulator and Rag complexes. To that end, HEK293 cells were transfected with LAMTOR1 WT and S56E, and S56A mutants and after 40 h transfected cells were harvested and lysed. Myc-Trap agarose beads were employed to isolate transiently expressed LAMTOR1 along with its interaction partners from the lysate. Captured proteins were eluted by boiling for 10 min at 95°C and thereafter were resolved using 10% SDS-PAGE. As it is shown in figure 6.22 (A), the efficiency of the Myc-Trap beads in isolating Myc-tagged LAMTOR1 from the lysate is relatively high, and almost 50% of the Myc-tagged LAMTOR1 proteins are captured using the beads. It is shown in figure 6.22 (B) that the difference in expression level of the endogenous and exogenous LAMTOR1 is not pronounced. Proteins that were co-IP with LAMTOR1 were investigated using antibodies against Ragulator and Rag complex members as well as SLC38A9 in three biological replicates. Figures 6.22 (C) and (D) show that LAMTOR1 phosphorylation did not affect its interaction with LAMTOR2, 3, and 5. Western-blot analysis did not detect LAMTOR4 protein using the mentioned protocol in the methods section (Figure 6.22 (E)). However, results presented in figure 6.23 (A) and (B) show that LAMTOR1 phosphorylation significantly reduces its interaction with Rag complex members such as RagA, B, and C. RagD protein was detected in just one replicate and the intensity of the band was faint compared to that seen for other Rags (Figure 6.23 (C)).

Next, it was investigated whether LAMTOR1 phosphorylation influences its interaction with SLC38A9. SLC38A9 is a lysosomal membrane protein, and it has been shown recently in several independent studies that this protein has a key role in the regulation of mTORC1 complex in the presence of amino acids and cholesterol by interaction with LAMTOR members (Wang et al. 2015a; Castellano et al. 2017). As it was mentioned before, SLC38A9 is a lysosomal membrane protein with several glycosylation sites; therefore the Western blot protocol was modified accordingly for this protein. Samples were incubated for 30 min in 40ºC before running on SDS-PAGE instead of boiling for 10 min, and more eluate was needed for SLC38A9 Western blot. Two double bands were observed at about 60 kDa and 100 kDa corresponding to non-glycosylated and glycosylated SLC38A9, respectively (Figure 6.24 (A)). Rebsamen et al. also reported the same molecular weights for nonglycosylated and glycosylated forms of the

SLC38A9 (Rebsamen et al. 2015). In the eluates, only the glycosylated form of

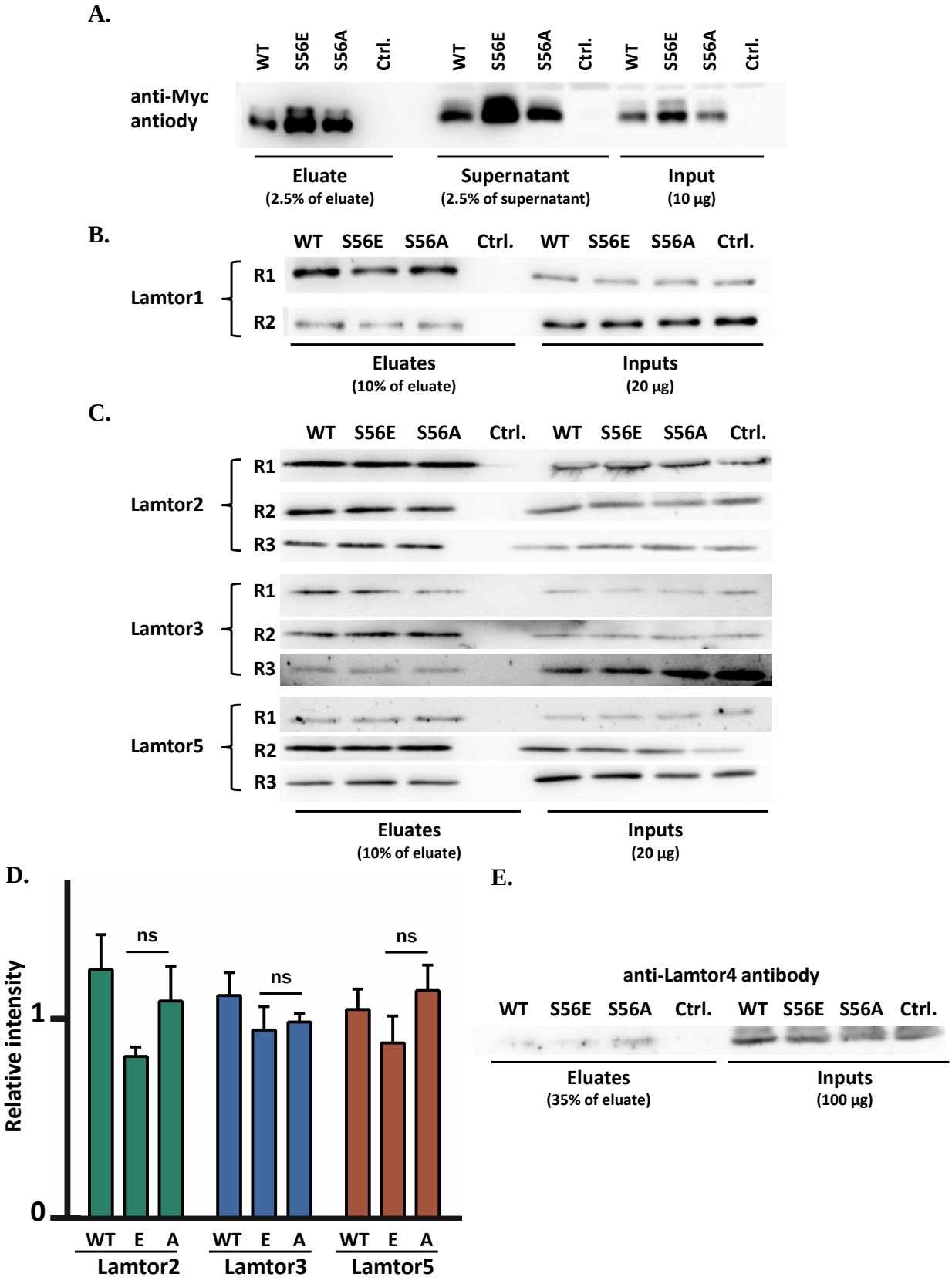

Figure 6.22 Co-IP experiment for the cells transfected with LAMTOR1 constructs.
HEK293 cells were transfected with LAMTOR1 WT, E-mutated and A-mutated constructs and after 40 h cells were harvested and lysed. Co-IP was performed using Myc-Trap agarose beads to isolate exogenous LAMTOR1. After several washes captured proteins were eluted by incubating for 10 min at 95°C in 2 x Laemmli sample buffer. Next, eluates, supernatants, and inputs were resolved using 10% SDS-PAGE gel. The gel was semi-dry blotted and blocked using 5% (wt/vol) non-fat milk in Tris-buffered saline containing 0.1% Tween 20. Subsequently, blots were incubated with primary and secondary antibodies and finally were visualized using Fusion imaging system. **A.** The same percentage of the eluates and supernatants (2.5%) and 10 µg of each input were resolved using 10% SDS-PAGE gel. The blot was incubated with anti-Myc (ab9106 (Abcam)) primary antibody. **B** and **C.** The same amount of eluates and inputs were applied to SDS-PAGE, and the blots were incubated with the following primary antibodies: LAMTOR1 (HPA002997 (Sigma-Aldrich)), Lamtor2 (#8145 (Cell Signaling Technology)), Lamtor3 (ab32134 (Abcam)), Lamtor5 (#14633 (Cell Signaling Technology)). **D.** The Fusion software was employed to quantify the relative amount of each protein. The level of protein of interest in each sample was normalized against the level of Myc expression level, representing transfection efficiency. Statistical analysis was conducted using the GraphPad Prism 6 software. Shown are mean values + SEM; n=3; ns: not significant. **E.** The same amount of eluates and inputs were applied to SDS-PAGE, and the blot was incubated with Lamtor4 (HPA020998 (Sigma-Aldrich)) primary antibody.

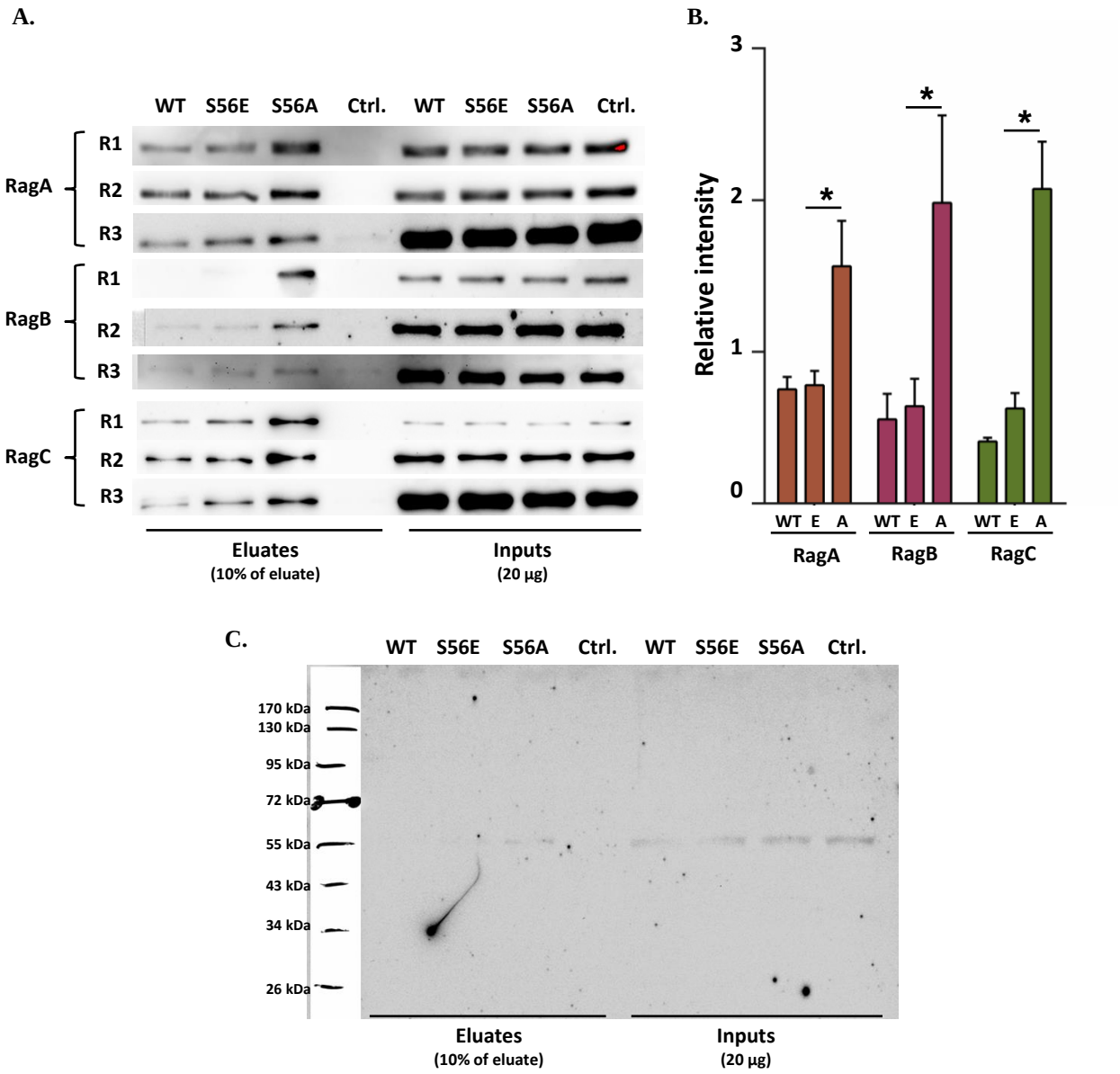

Figure 6.23 Co-IP experiment for the cells transfected with LAMTOR1 constructs.
HEK293 cells were transfected with LAMTOR1 WT, E-mutated, and A-mutated constructs and after 40 h cells were harvested and lysed. Co-IP was performed using Myc-Trap agarose beads to isolate exogenous LAMTOR1. After several washes captured proteins were eluted by boiling for 10 min at 95°C in 2X Laemmli sample buffer. Next, eluates, and inputs were resolved using 10% SDS-PAGE gel. The gel was semi-dry blotted and blocked using 5% (wt/vol) non-fat milk in Tris-buffered saline containing 0.1% Tween 20. Subsequently, blots were incubated with primary and secondary antibodies and finally were visualized using Fusion imaging system. **A.** The same amount of eluates and inputs were applied to SDS-PAGE, and the blots were incubated with the following primary antibodies: RagA (#4357 (Cell Signaling Technology)), RagB (#8150 (Cell Signaling Technology)), RagC (#5466 (Cell Signaling Technology)). **B.** The Fusion software was employed to quantify the relative amount of each protein. The level of protein of interest in each sample was normalized against the level of Myc expression level, representing transfection efficiency. Statistical analysis was conducted using the GraphPad Prism 6

software. Shown are mean values + SEM; n=3; *,p < 0.05-paired T-test **C.** The same amount of eluates and inputs were applied to SDS-PAGE, and the blot was incubated with RagD (#4470 (Cell Signaling Technology)) primary antibody.

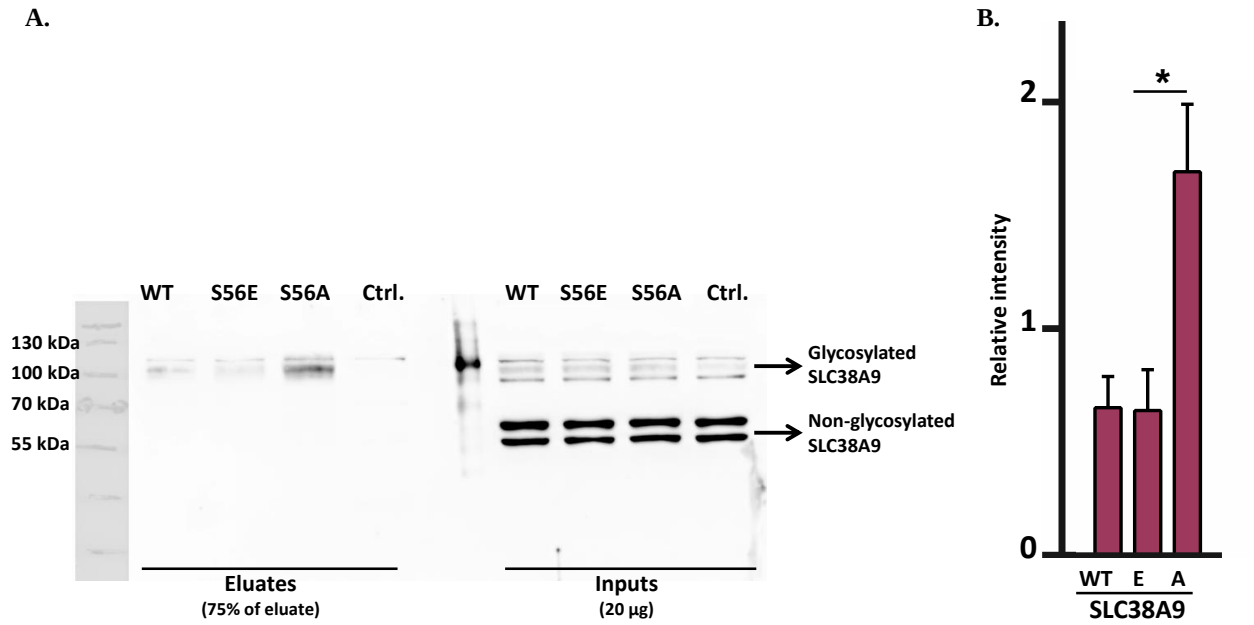

Figure 6.24 SLC38A9 interaction with LAMTOR1 constructs.
A. HEK293 cells were transfected with LAMTOR1 WT, E-mutated, and A-mutated constructs and after 40 h cells were harvested and lysed. Co-IP was performed using Myc-Trap agarose beads to isolate exogenous LAMTOR1. After several washes captured proteins were eluted by incubating for 30 min at 40°C in 2X Laemmli sample buffer. Next, eluates, and inputs were resolved using 10% SDS-PAGE. The gel was semi-dry blotted and blocked using 5% (wt/vol) non-fat milk in Tris-buffered saline containing 0.1% Tween 20. Subsequently, blots were incubated with SLC38A9 (HPA043785) primary antibody and proper secondary antibody and visualized using Fusion imaging system. **B.** The Fusion software was employed to quantify the relative amount of each protein. The level of protein of interest in each sample was normalized against the level of Myc expression level, representing transfection efficiency. Statistical analysis was conducted using the GraphPad Prism 6 software. Shown are mean values + SEM; n=3; *,p < 0.05-paired T-test.

SLC38A9 was observed (Figure 6.24 (A)). These results showed that SLC38A9 has a stronger interaction with LAMTOR1 S56A mutant than with the S56E mutant (Figure 6.24 (B)).

The same co-IP experiment was also conducted for the HEK293 cells transfected with Myc-tagged RagC WT, S381E, and S381A mutants. Regarding RagC interaction with RagA and B, no reproducible pattern was observed among the replicates (Figure 6.25 (A)). These results suggest that S381 phosphorylation does not affect RagC interaction with other Rag complex members.

Surprisingly, Ragulator complex members (LAMTOR1 and LAMTOR5) did not co-

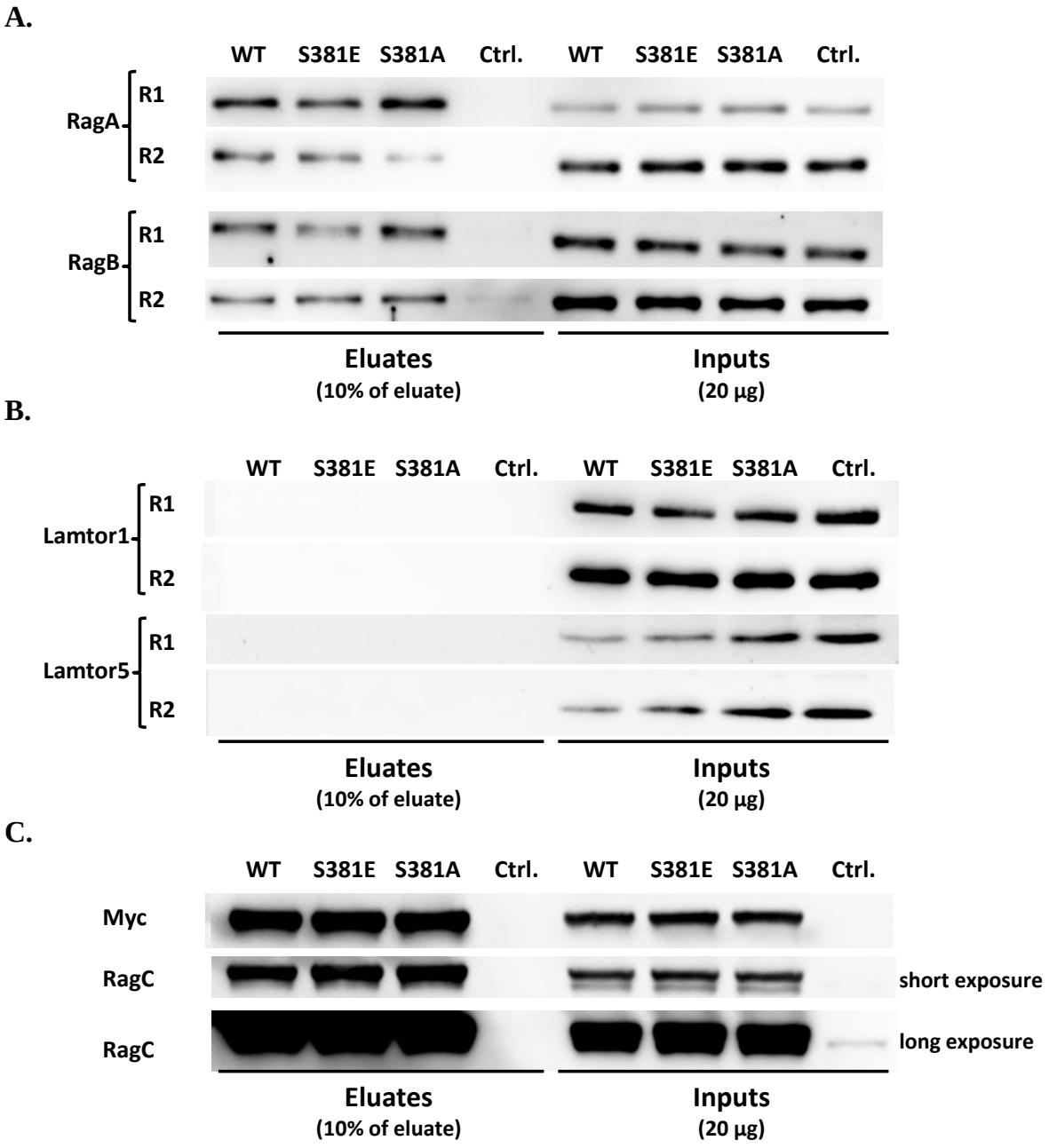

Figure 6.25 Co-IP experiment for the cells transfected with RagC constructs.
HEK293 cells were transfected with RagC WT, E-mutated and A-mutated constructs and after 40 h cells were harvested and lysed. Co-IP was performed using Myc-Trap agarose beads to isolate Myc-fused RagC. After several washes captured proteins were eluted by boiling for 10 min at 95°C in 2X Laemmli sample buffer. Next, eluates, supernatants, and inputs were resolved using 10% SDS-PAGE gel. The gel was semi-dry blotted and blocked using 5% (wt/vol) non-fat milk in Tris-buffered saline containing 0.1% Tween 20. Subsequently, blots were incubated with primary and secondary antibodies and finally were visualized using Fusion imaging system. **A.** The same amount of eluates and inputs were applied to SDS-PAGE, and the blots were incubated with the following primary

antibodies: RagA (#4357 (Cell Signaling Technology)), RagB (#8150 (Cell Signaling Technology)). **B.** The same amount of eluates and inputs were applied to SDS-PAGE, and the blots were incubated with the following primary antibodies: LAMTOR1 (HPA002997 (Sigma-Aldrich)), and Lamtor5 (#14633 (Cell Signaling Technology)). **C.** The same amount of eluates and inputs were applied to SDS-PAGE, and the blots were incubated with anti-Myc (ab9106 (Abcam)) and RagC (#5466 (Cell Signaling Technology)) primary antibodies. The RagC blot was exposed for a longer time also to detect endogenous RagC in the negative control.

immunoprecipitate with RagC (Figure 6.25 (B)). Unlike LAMTOR1, a significant difference in expression level between endogenous and exogenous RagC was observed (Figure 6.25 (C)).

6.2.5. Deactivation of mTORC1 upon treatment with U18666A

LAMTOR1 is a vital part of the amino acid sensing machinery that activates mTORC1. According to the results of this study, upon U18666A stimulation, LAMTOR1 gets phosphorylated at S56 residue and this leads to its degradation and alters its interaction with other proteins. Therefore, it was examined whether U18666A treatment of the cells also affects mTORC1 activity and localization. Since Ribosomal protein S6 kinase 1 (S6K1) is one of the mTORC1 substrates (Isotani et al. 1999), Western blot assay was performed using phospho-p70 S6 kinase (Thr389) antibody as a readout for mTORC1 activity. As shown in figure 6.26, incubation of MEFs for 24 h with U18666A inhibitor leads to mTORC1 deactivation. Next, the effects of U18666A treatment on the mTORC1 localization was investigated using immunofluorescence (IF) microscopy. Lysosomes were stained using an antibody against the lysosomal membrane protein LAMP-2, and a monoclonal antibody against mTOR was employed for mTORC1 detection. MEF cells were cultured on glass coverslips and incubated for 24 h with either U18666A or DMSO. Afterwards, cells were fixed and stained using the mentioned antibodies, and DAPI was used for nuclear staining. Figure 6.27 shows that in control cells (DMSO-treated), mTORC1 and LAMP2 are colocalized however, after treating cells with U18666A, mTORC1 dissociates from the lysosomal membrane. The IF findings confirm the Western blot results and show that after U18666A treatment, mTORC1 is deactivated and dissociated from the lysosomal membrane. Moreover, it was observed that U18666A stimulation alters lysosomal positioning. In control cells, lysosomes are dispersed into the cytoplasm, however, after stimulation lysosomes move toward the nucleus and show perinuclear localization (Figure 6.27).

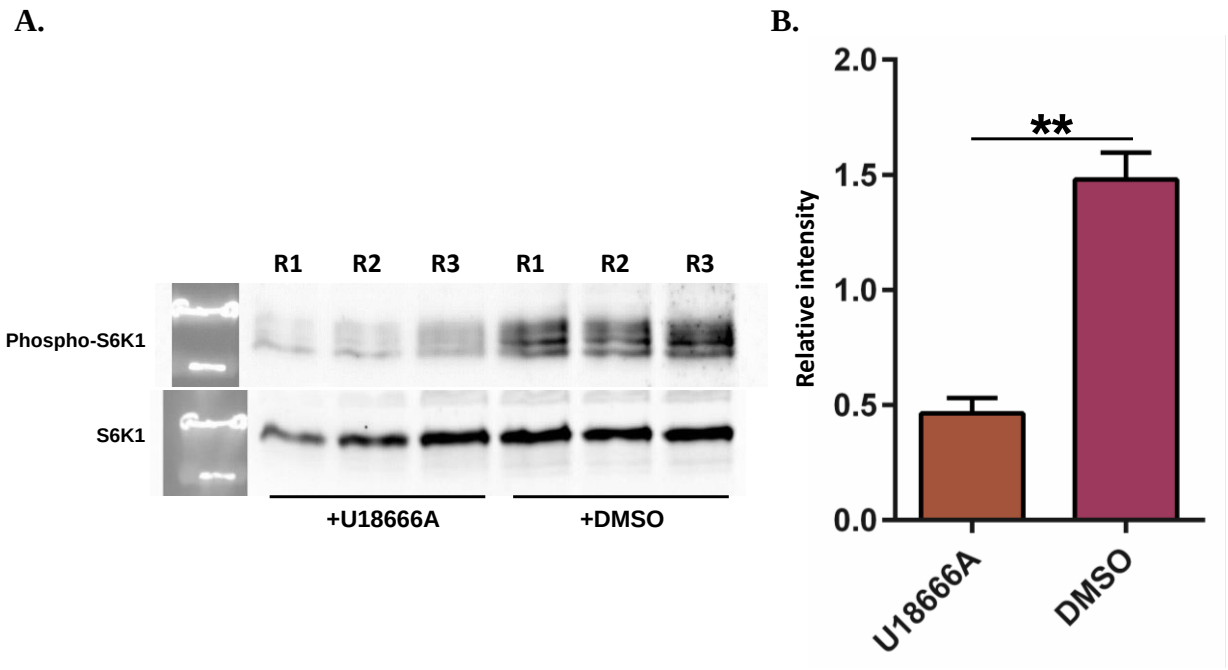

Figure 6.26 Evaluation of mTORC1 activity in MEF cells treated with U18666A.
A. Mouse embryonic fibroblast (MEF) cells were treated with either U18666A (3 µg/ml) or DMSO and after 24 h harvested and lysed. 20 µg of protein lysate was applied to each lane of an SDS-PAGE gel. Subsequently, the gel was semi-dry blotted, and the blots were blocked using 5% BSA (wt/vol) in Tris-buffered saline containing 0.1% Tween 20. Next, blots were incubated with either Phospho-p70 S6 Kinase (Thr389) (#9205 Cell Signaling Technology) as a readout for mTORC1 activity or total p70 S6 Kinase (#9202 Cell Signaling Technology) primary antibodies. After incubation with proper secondary antibodies, protein signals were visualized using FUSION system. The figure shows the results of 3 independent biological experiments. **B.** The Fusion software was employed for quantification of protein signals. Phospho-p70 S6 Kinase intensity in each condition was normalized against total p70 S6 Kinase. Statistical analysis was conducted using the GraphPad Prism 6 software. Shown are mean values + SEM; n=3; **,$p < 0.01$-paired T-test (P-value: 0.0025).

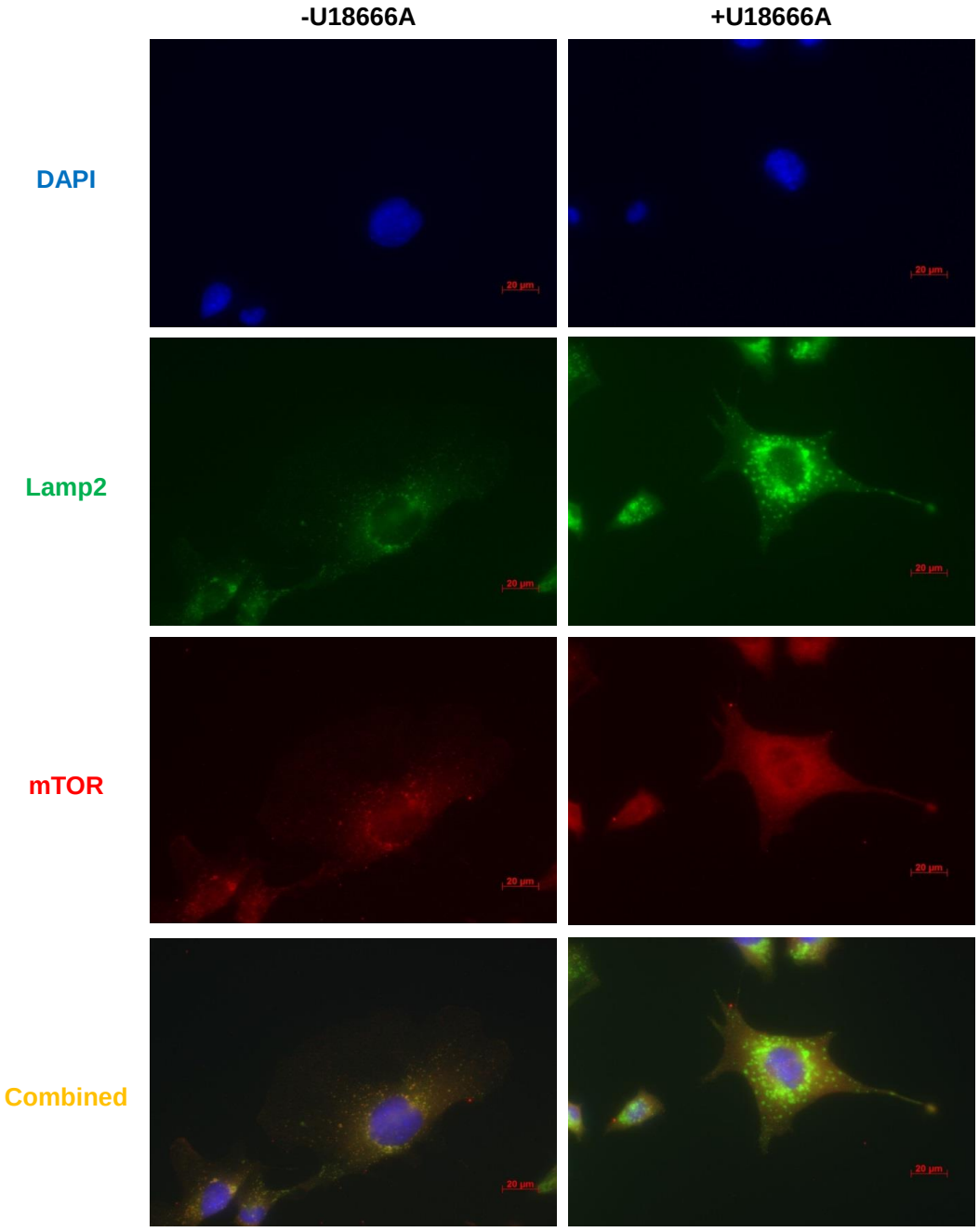

Figure 6.27 mTORC1 localization alteration in MEFs treated with U18666A.
MEF cells were seeded on 12 mm coverslips and incubated for 24 h with either U18666A (3 µg/ml) or DMSO. After 24 h incubation time, cells were permeabilized with 0.1% Triton X-100 and blocked using 10% FCS. Anti-Lamp2 (ABL-93, DSHB) and anti-mTOR (#2983, Cell Signaling Technology) primary antibodies were employed to identify lysosomes and mTORC1, respectively. After 4 h incubation with primary antibodies, cells were washed and incubated with proper secondary antibodies for 1 h. Afterward, the coverslips were washed and mounted using DAPI-fluoromount-G™. Immunocytochemistry images were acquired using Axiovert 200M equipped with an AxioCamMR3 (60x objective). Filter sets 38, 43 and 49 were used for detecting Alexa 488 (green fluorescence), Cy3 (red fluorescence), and DAPI, respectively.

6.3. Discussion and conclusion

6.3.1. U18666A treatment of the MEF cells

In this study, lysosomal cholesterol storage was chemically induced by treating cells with U18666A. This compound is an inhibitor of the lysosomal membrane protein NPC1 which is vital for cholesterol transport from lysosomes to the endoplasmic reticulum (ER) and cytoplasm (Cenedella 2009; Lange et al. 2002; Sztolsztener et al. 2012). From the analytical point of view this is an ideal model, since except for treatment with U18666A, there is no, e.g., genetic interference, which helps to minimize the number of observed artifacts and allows for tight control of experimental conditions. However, one of the potential drawbacks of U18666A is its unknown effects on cells and signaling pathways. Considering U18666A benefits and drawbacks, it has been widely used in cholesterol and lipid studies through the years (Cenedella 2009). The fluorescence microscopy results of filipin-stained cells showed an increase in fluorescence emission in U18666A-treated cells in comparison to the control cells. In a similar experiment, Shen et al. incubated CHO cells with U18666A, and they observed significant increases in cholesterol levels in treated cells (Shen et al. 2012). In another study, Kulinski and Vence compared the cholesterol content of NPC1 knockout hepatocytes with WT cells and reported that in knock-out cells cholesterol amount is 5-fold higher (Kulinski and Vance 2007). Although the total free cholesterol amount increases upon adding U18666A, cholesterol accumulates mainly in the lysosomes and cell compartments undergo cholesterol deficiency (Lange et al. 1999). Given the vast functions of cholesterol in cells and its importance for the cell maintenance, treating cells with U18666A trigger a broad spectrum of alterations in proteins and their modifications.

6.3.2. Proteomics analysis of U18666A-treated MEF cells

In recent years mass spectrometry has been established as a powerful tool for quantitative and qualitative characterization of the macromolecules in large-scale studies (Aebersold and Mann 2016). In this study, the bottom-up proteomics approach was employed to investigate the alterations of proteins in U18666A-treated cells at both the proteome and phosphoproteome level. To that end, the stable-isotope labeling by amino acids in cell culture (SILAC) method was used as a simple and quantitative method for labeling the proteins in MEF cells (Blagoev et al. 2003). SILAC method is based on the metabolic incorporation of labeled amino acids (usually 13C/15N arginine and/or lysine) with stable isotopes into proteins of cultured cells (or animals). This

results in a mass difference between the acquired samples from different culture conditions. This method was first introduced by Mann and co-workers at 2003 (Blagoev et al. 2003), and since then thousands of studies have exploited the capacities of this approach in different fields of biology.

In total, 5502 proteins in all replicates were detected, and more than 83% of them were common between all three replicates, indicating high reproducibility within replicates. Out of these 5502 proteins, only 90 of them (less than 2%) were significantly regulated (66 up- and 8 down-regulated). Yates and co-workers also performed a large-scale proteomic study for NPC1-mutated human fibroblast cells using quantitative mass spectrometry. In total, in two replicates they found 4308 distinct proteins, 281 of them differentially expressed (Rauniyar et al. 2015). In their study, they compared mutated cells with WTs and identified 61 proteins which were upregulated in both replicates. These 61 proteins were compared to the 66 upregulated proteins in this study and only the following three proteins, Carboxypeptidase D (cpd), Mitochondrial 10-formyltetrahydrofolate dehydrogenase (aldh1l2), and Pyrroline-5-carboxylate reductase 1, mitochondrial (pycr1) proteins were in common between the two studies. The discrepancy between these two studies could be due to the different model systems used in these two studies. While in this study U18666A was used for mimicking NPC1 disease, Yates and co-workers employed human NPC1-mutant fibroblasts with the I1061T missense mutation. Although this mutation is the most common mutation in NPC disease however it has been shown that NPC1(I1061T) is functional and the mutated proteins which escape from degradation can properly localize to the lysosomal membrane and transfer cholesterol from lysosome to the cytoplasm and ER (Gelsthorpe et al. 2008). Therefore, applying U18666A can be considered as a more convenient method for proteome alterations investigation rather than using NPC1 (I1061T) mutant cells.

6.3.3. Gene ontology (GO) analysis of the regulated proteins in the proteomics dataset

To evaluate the biological significance of the differentially expressed proteins and understand their functions in the pathophysiological mechanism of NPC disease, GO analysis was performed to determine whether the regulated proteins are enriched for specific GO categories. Upregulated proteins were applied to GO analysis using Gorilla and PANTHER, two online GO tools. GO analysis results of both tools indicated that most of the upregulated proteins were involved in cholesterol biosynthesis process, as e.g., one of the top GO categories in the dataset was found to

be "Regulation of cholesterol biosynthesis by SREBP (SREBF)". These results are consistent with the findings of other studies that have shown, upon reaching ER, LDL cholesterol inhibits sterol regulatory element-binding (SREBP) pathway (Goldstein et al. 2006). The SREBP-2 downstream target genes are mainly the enzymes involved in the cholesterol synthesis pathway (Engelking et al. 2018). Moreover, several studies have indicated that the amount of mature form of SREBP-2 increases in the NPC1 deficient cells or the cells treated with U18666A (Lu et al. 2015; Colgan et al. 2007). Therefore, it is not surprising that most of the upregulated proteins in the proteomics dataset, are involved in the cholesterol synthesis.

6.3.4. Differentially expressed proteins in the proteomics dataset are related to cholesterol metabolism

As it was mentioned before, LDL cholesterol in the ER inhibits cholesterol synthesis. The inhibition takes place by promoting the proteasomal degradation of the enzymes involved in cholesterol de novo synthesis including squalene monooxygenase (SQLE) (Gill et al. 2011) and 3-hydroxy-3-methylglutaryl-CoA (HMG-CoA) reductase (HMGCR) (DeBose-Boyd 2008). In U18666A-treated cells, ER undergoes cholesterol deficiency (Lange et al. 1999), and therefore degradation of cholesterol synthesis enzymes is inhibited. Moreover, U18666A induces the expression of the SREBP2 downstream genes (Lu et al. 2015; Colgan et al. 2007). Because of these reasons, it was expected that proteins involved in cholesterol synthesis such as SQLE and HMGCR are among the top upregulated proteins. SQLE is the most differentially expressed protein in the proteomics dataset with more than nine folds increase. HMGCR shows 3.71 folds upregulation in U18666A-treated cells in comparison to the controls. HMGCR is a rate-controlling enzyme of the mevalonate pathway, the primary metabolic pathway responsible for cholesterol synthesis (DeBose-Boyd 2008). 16 of the top 20 upregulated proteins are involved in cholesterol synthesis, and only for four proteins no direct linkage to cholesterol biosynthesis was found in the literature. These four proteins are Tapasin (Tapbp), Retinol dehydrogenase 11 (Rdh11), Complement C1s-A subcomponent (C1sa), and Fructose-bisphosphate aldolase C (Aldoc) which can be considered as promising candidates to investigate their possible relation with the cholesterol biosynthesis pathway. Next, the alteration of NPC1 and NPC2 proteins was examined. The NPC2 protein showed slight upregulation with the 2.05 fold increase upon U18666A treatment; however, the intensity of the NPC1 gene remained almost constant (1.45 fold increase).

6.3.5. Regulated kinases and phosphatases in the proteomics dataset

In total 266 kinases were found in the proteomics dataset, which represents 4.95% of all detected proteins. Considering the fact that ~2.5% of the total genes encode kinases (Olsen et al. 2010), this group of low-abundant enzymes is not underrepresented in this study. In total, four kinases were found to be upregulated in the dataset. 2 of these kinases are part of the mevalonate pathway: phosphomevalonate kinase (PMVK) and mevalonate kinase (MVK) (Thurnher et al. 2012). The other two upregulated kinases are pyruvate dehydrogenase kinase isozyme 1(PDK1) and Adenylate kinase 4, mitochondrial (AK4). PDK1 showed 2.26 folds elevated expression in the cells treated with U18666A. PDK1 is a mitochondrial enzyme that plays a pivotal role in the regulation of fatty acid and glucose metabolism by phosphorylating and inhibiting pyruvate dehydrogenase from converting pyruvate into acetyl-coenzyme A (Papandreou et al. 2006). Acetyl-CoA is a precursor for the mevalonate pathway that leads to cholesterol synthesis (Thurnher et al. 2012). Upregulation of PDK1 is in contrary with the earlier results, since all enzymes involved in the mevalonate pathway are upregulated and promote cholesterol de novo synthesis; however, upregulation of the PDK1 hinders this pathway by inhibiting acetyl-CoA synthesis (Papandreou et al. 2006). Different reasons could have caused this discrepancy. It has to be considered that pyruvate dehydrogenase complex (PDC) is not the only source of the acetyl-CoA for the mevalonate pathway. Moreover, various modifications such as phosphorylation could restore the activity of PDK1 as it was shown before (Riojas et al. 2006) and attenuate its upregulation effect.

6.3.6. Phosphoproteomics analysis of U18666A-treated MEF cells

It has been shown that aberrant protein phosphorylation plays an essential role in the model systems with NPC phenotype (Xu et al. 2010; Sawamura et al. 2003); however, there hasn't been any large-scale phosphoproteomic study to investigate the protein phosphorylation alterations in this disease or cholesterol metabolism defects in general. Therefore, this study is the first large-scale phosphoproteomic study that investigates NPC disease. The phosphopeptide enrichment was carried out using double TiO_2 method and in total 12881 phosphosites were detected that 9695 of them were localized with more than 75% certainty of phosphosite localization (class I phosphosites). Class I phosphosites were investigated using Perseus (from MaxQuant software package), and 288 phosphosites were found regulated. 55.4% of the phosphosites were detected in all three replicates which implies a good reproducibility for a phosphoproteomic study. In the

method development project which was explained in chapter one, almost the same reproducibility was achieved using HeLa lysates (53.8% common phosphosites between three replicates).

6.3.7. Gene ontology analysis of the differentially expressed phosphorylation sites

Proteins represented by regulated phosphosites were subjected to Gene Ontology (GO) analysis for biological processes. GO study identified enrichment for genes involved in the regulation of proteins localization and organization of cellular components and organelles. Therefore, the GO study results suggest that treatment of the cells with U18666A and consequently perturbation in cholesterol trafficking leads to the mislocalization of different proteins and organelles, and thereafter cells try to cope with new conditions using phosphorylation of various proteins. These results are in line with those of many previous studies that reported alterations in the localization of various proteins such as amyloid-beta A4 protein (Ehehalt et al. 2003), beta-secretase 1 (Simons et al. 1998) and presenilin-1 (Wahrle et al. 2002) in the cholesterol-depleted and NPC cells. It also has been shown that cholesterol regulates the localizations, trafficking, and clustering of various SNARE (soluble NSF (N-ethylmaleimide-sensitive fusion protein) attachment protein receptor membrane) proteins such as synaptosomal-associated protein 23, syntaxin-4, and syntaxin-6 (Reverter et al. 2014).

6.3.8. Candidate phosphorylation sites

LAMTOR1, RagC, OSTM1, STARD3NL, BNIP3, and VAMP8 were chosen as candidate phosphoproteins for further investigation. A major criterion for the selection of the candidate phosphoproteins was that all proteins are lysosomal or lysosomal-associated proteins. LAMTOR1 and RagC are part of the amino acid sensing machinery that activates mTORC1 in the presence of amino acids (Shimobayashi and Hall 2016). Both OSTM1 (Lange et al. 2006) and STARD3NL (Alpy et al. 2013) are lysosomal transmembrane proteins, and both BNIP3 (Ma et al. 2012) and VAMP8 (Itakura et al. 2012) are involved in autophagy and required for autophagosome-lysosome fusion.

6.3.8.1.Phosphorylation affects OSTM1 cleavage

OSTM1 is mainly known as the β subunit of the Cl-/H+ exchanger CLCN7. The OSTM1/CLCN7 heterodimer is essential for lysosomal function, as a disruption in either gene results in osteopetrosis as well as severe lysosomal storage disease in neurons and renal proximal tubular cells (Lange et al. 2006; Kasper et al. 2005). Clinically, Osteopetrosis due to the lack of OSTM1 is more severe compared to Osteopetrosis due to the lack of CLCN7, possibly indicating

additional functions for OSTM1 beyond acting as the β subunit for CLCN7 (Pandruvada et al. 2016). In cells, the highly glycosylated OSTM1 is found in the ER and lysosomes. Most likely within the lysosomal lumen, it undergoes proteolysis, yielding two parts of the protein connected by a disulfide bridge (Lange et al. 2006). The phosphomimetic and phosphoresistant results indicated no effect of Ser 327/329 phosphorylation on OSTM1 stability. However, a direct relationship between the phosphorylation of OSTM1 within its cytoplasmic domain and the intra-lysosomal formation/stability of its proteolytically processed form was observed. In case of the Ser 327/329 to Ala OSTM1 mutant, the amount of the cleaved protein compared to WT OSTM1 was reduced while for the Ser 327/329 to Glu version, more cleavage product was observed. This strongly suggests a regulatory role of the cytoplasmic phosphorylation sites for the intra-lysosomal formation of the proteolytically processed form and/or the stability of the protein.

The cytoplasmic C-terminal domain of OSTM1, in which the regulated phosphorylation sites are located, is neither required for the interaction with CLCN7, nor for the ability of CLCN7 to act as a Cl-/H+ exchanger, since replacement of this domain with a non-functional surrogate even increased CLCN7 ion exchange activity (Leisle et al. 2011). The transmembrane domain of OSTM1 is essential and sufficient for interaction of both proteins (Leisle et al. 2011) while the domain present in the lysosomal lumen seems to be crucial for the function of CLCN7, as its replacement results in strongly reduced ion exchange activity of CLCN7. This may be due to the lack of N-linked glycosylation sites on CLCN7 which implies a protective role for the heavily glycosylated luminal domain of OSTM1 for CLCN7 (Lange et al. 2006). Interestingly, almost exclusively proteolytically processed OSTM1 was co-immunoprecipitated with CLCN7 from WT cells (Lange et al. 2006). Furthermore, OSTM1 proteolysis is impaired in $CLCN7^{-/-}$ mice. This is in agreement with the fact that CLCN7 is required for transport of OSTM1 to lysosomes where the proteolytic processing is most likely taking place (Lange et al. 2006). Lange et al. observed only the cleaved form OSTM1 in the lysosomal fractions (Lange et al. 2006); therefore, phosphorylation effect on the OSTM1 cleavage is likely a transport phenotype.

In cells transiently expressing OSTM1, proteolytic processing is impaired, most likely due to the altered stoichiometry of OSTM1/CLCN7 due to OSTM1 overexpression, resulting in retention of the majority of OSTM1 in the ER. Accordingly, co-overexpression of CLCN7 can compensate this effect (Lange et al. 2006). In this study's experiments, the cleavage product relative to the total amount of OSTM1 also only presents a fraction of the total OSTM1 amount, indicating that

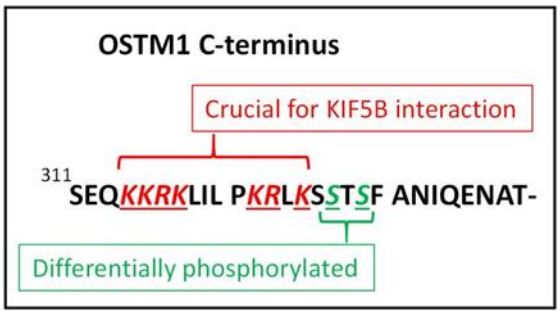

Figure 6.28 OSTM1 differentially expressed phosphorylation sites and their adjacent residues.

the majority of OSTM1 still resides in the ER, where it is not proteolytically processed. Therefore the observed formation of the cleavage product will be far more pronounced if the CLCN7 and OSTM1 plasmids were co-transfected or OSTM1 was expressed at the endogenous levels, and consequently, the substitution effect (S327/329 E) also might be more significant. Beside the function of OSTM1 as CLCN7 β-subunit, it was shown recently that it interacts with KIF5B (Pandruvada et al. 2016). KIF5B is the kinesin-1 heavy chain and impacts the distribution of lysosomes being involved in their transport to the periphery of the cells. Accordingly, in KIF5B depleted cells, lysosomes show perinuclear localization. Interestingly, KIF5B interacts with the C-terminal region of OSTM1, for which the 7 Arg/Lys residues depicted in figure 6.28 are essential, while these are not involved in the interaction with CLCN7 (Pandruvada et al. 2016). The two upregulated phosphorylation sites observed in this study are located directly adjacent to these positively charged amino acids (Figure 6.28) thereby shifting the charge of this region towards a more negative value. Therefore it could be speculated that this phosphorylation event disrupts the interaction between OSTM1 and KIF5B allowing for reversible regulation of this interaction.

Based on these data, the following hypothesis was developed: The dephosphorylated version of OSTM1 stabilizes the complex between KIF5B and OSTM1 and prevents OSTM1 proteolytic processing, and therefore acts as CLCN7 β-subunit, for which its proteolytic processing is needed. In the phosphorylated (or phosphomimetic Ser to Glu) version of the protein, interaction between KIF5B and OSTM1 is weakened leading to increased interaction with CLCN7 and in turn proteolytic processing. However, these results have to be viewed cautiously, since the cleavage effect that was observed in the phosphomimetic study could be an artifact of Ostm1 overexpression. It also has to be considered that S327/329E mutation does not mimic the phosphorylation effects completely. Therefore, more investigation such as co-overexpression of CLCN7 and OSTM1 is needed to confirm these preliminary results.

6.3.8.2.Phosphorylation does not affect STARD3NL stability

STARD3NL (MENTHO) is a transmembrane protein that localizes at late endosomes (LEs)/lysosomes (LSs) and serves as a tethering protein between ER and LEs/LSs. N-terminus of

the STARD3NL is similar to the STARD3/ MLN64 N-terminus, however, lacks the C-terminus START domain. Both of these proteins contain a FFAT motif which enables them to interact with VAP family proteins from ER (Alpy et al. 2013). Although STARD3 and STARD3NL have the cholesterol-sensing ability, however, their role in transporting cholesterols from LEs to ERs has not been clarified. It has been postulated that these proteins make contacts between LSs and ERs prior to cholesterol transfer through other proteins such as NPC1/NPC2 (Raiborg et al. 2015). STARD3NL contains a N-terminal cytoplasmic domain, four transmembrane domains, and a C-terminus cytoplasmic domain (Alpy et al. 2005). The regulated phosphosite (S39) resides at the cytoplasmic N-terminus of the STARD3NL. Cycloheximide experiment was performed in 3 replicates and in all three replicates the E-mutated STARD3NL was found to be more stable than A-mutated; however this difference was not statistically significant. Although phosphorylation does not alter the STARD3NL stability, it could affect the interaction of this protein with other proteins and therefore, LE-ER connection could also be affected.

6.3.8.3.Phosphorylation does not affect BNIP3 and VAMP8 degradation rate

The next two investigated proteins in this study are BNIP3 and VAMP8. VAMP8 is a lysosomal SNARE protein (soluble N-ethylmaleimide-sensitive factor-attachment protein receptors) which directly controls lysosome-autophagosome membrane fusion through its interaction with STX17 and SNAP-29 proteins (Itakura et al. 2012). It has been shown that BNIP3 also plays a vital role in autophagosome-lysosome fusion (Ma et al. 2012). Recently Fu et al. showed that BNIP3 overexpression in MCF-7 cells hinders autophagosome-lysosome fusion via inhibition of the interaction between VAMP8 and SNAP29. They concluded that BNIP3 could interact with SNAP29 and therefore inhibits this protein to interact with VAMP8 and STX17 and consequently abrogates autophagosome-lysosome fusion (Fu et al. 2018). BNIP3 regulated phosphosite (S88) was found to be in the N-terminal PEST domain (proline (P), glutamic acid (E), serine (S), and threonine (T) rich domain) (Vasagiri and Kutala 2014). Proteins containing this domain have a short intracellular half-life, and it has been shown that the PEST sequence targets proteins for degradation (Rogers et al. 1986). Moreover, it has been found that phosphorylation in the PEST domain affects the protein's stability (Lin et al. 1996). Therefore it was hypothesized that phosphorylation in the PEST domain of BNIP3 leads to the same effect. The detected VAMP8 phosphosite is T54 resides in the cytoplasmic domain of this protein; therefore, phosphorylation can affect in VAMP8 interaction with other proteins such as STX17 and SNAP-29. Malmersjö et al. showed that protein kinase C (PKCB) phosphorylates multiple residues in the SNARE domain

of VAMP8 including T54. They suggested that VAMP8 phosphorylation attenuates vesicle fusion in vitro and suppresses secretion in living cells (Malmersjö et al. 2016). The phosphomimetic studies showed that phosphorylation in the mentioned regulated phosphosites does not affect the stability of these two proteins and therefore VAMP8 and BNIP3 were excluded from further analysis.

6.3.8.4. Phosphorylation affects LAMTOR1 interaction with Rag GTPases complex members and SLC38A9

Ragulator complex protein LAMTOR1 is localized at late endosomes/lysosomes exclusively and is part of a heteropentameric protein complex which is involved in activation of mTORC1 (Bar-Peled et al. 2012). LAMTOR1 is directly responsible for anchoring the Ragulator complex to the lysosomal membrane via myristoylated and palmitoylated residues at its N-terminus (Bar-Peled et al. 2012). The crystal structure of the Ragulator complex in combination with the Ras-related GTP-binding proteins (Rag GTPases) (Figure 6.29) revealed that LAMTOR1 surrounds the other members of Ragulator complex and interacts with all of them (Araujo et al. 2017). The detected regulated phosphorylated serine (S56) is located in the first α-helical domain (residues 50 to 64) of the protein which interacts with the C-terminal region of RagC as well as LAMTOR3 (Figure 6.29). Mutation of amino acids in this region abolished the interaction with RagA/C and SLC38A9 while interaction with the other LAMTOR proteins was not affected (Araujo et al. 2017). Yonehara et al. showed that Gln51–Lys60 residues of the LAMTOR1 N-terminal α1 helix are crucial for stabilizing the Ragulator-Rag complex interaction and consequently amino-acid-dependent activation of mTORC1 (Yonehara et al.). This implies a regulatory function for this region of LAMTOR1 as changes in the formation of the Ragulator-RagA/B/C/D-SLC38A9 complex influence the recruitment of mTORC1 to the lysosome. Ragulator complex acts as a guanine nucleotide exchange factor (GEF) for the Rag A/B/C/D complex which locates mTORC1 onto the lysosomal surface (Shimobayashi and Hall 2016). In the Rag A/B/C/D complex, another regulated phosphorylation site, S381 of RagC, was found in this study. Intriguingly, S381 is located at the C-terminal region of RagC which has been shown to interact with the LAMTOR1 region harboring the regulated S56 phosphosite (Figure 6.29) (Araujo et al. 2017).

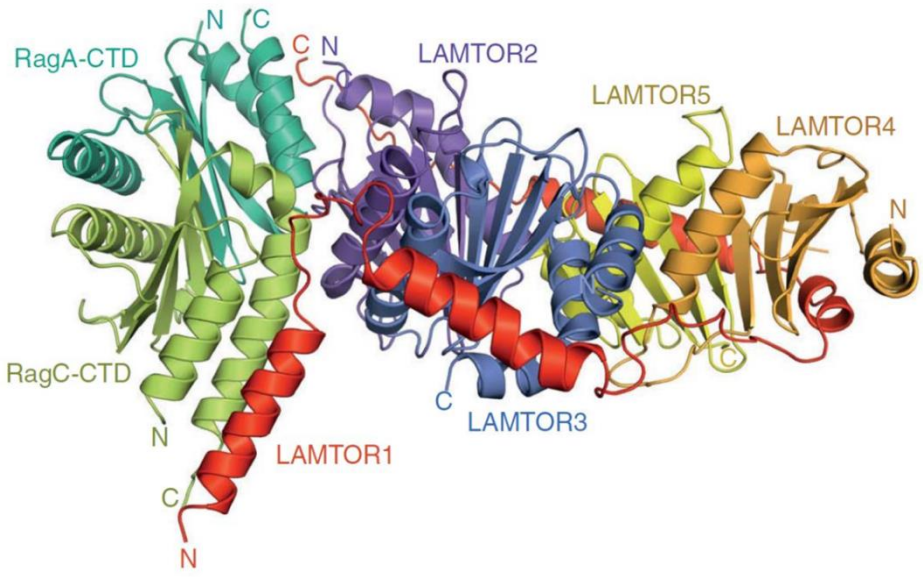

Figure 6.29 Crystal structure of the Rag GTPases interaction with the LAMTOR complex. Red, LAMTOR1; purple, LAMTOR2; blue, LAMTOR3; orange, LAMTOR4; yellow, LAMTOR5; dark green, RagA CTD; light green, RagC CTD; N and C termini are labeled. CTD: C-terminal domain. Adopted from de Araujo et al. (Araujo et al. 2017).

Therefore, it was hypothesized that phosphorylation in this region of the LAMTOR1 (S56) could affect the interaction of the Rag and Ragulator complexes. To that end, HEK293 cells were transfected with LAMTOR1 Myc-tagged constructs (WT, S56E, and S56A), and protein complex immunoprecipitation (co-IP) was performed using Myc-Trap agarose beads. The results indicate that S56A LAMTOR1 has a significantly stronger interaction with the Rag complex members including RagA, B, and C in comparison to the S56E and WT. However, mutation has no effect on LAMTOR1 interaction with other Ragulator complex members such as LAMTOR2, 3, and 5. The same results for WT and S56E mutant was obtained, this suggests two possibilities: either under the experimental settings all LAMTOR1 WT proteins are phosphorylated, and therefore the results are the same as S56E, or S56E mutation does not fully mimic the phosphorylated Ser56. The first possibility can be tested by various techniques such as targeted quantification of Lamtor1 S56 phosphorylation by mass spectrometry (Hahn et al. 2011). Regarding the second possibility aspartic acid (D) can be used instead of glutamic acid that in some cases is a better choice for phosphomimetic studies.

Knowing that upon LAMTOR1 phosphorylation, the Ragulator complex dissociates from the Rag GTPases, it was investigated whether U18666A treatment deactivates mTORC1. Using Western blot and IF microscopy, it was shown that upon treating cells with U18666A, mTORC1

dissociates from the lysosomal membrane and consequently gets deactivated. It was also observed in the microscopy results that U18666A treatment of the cells causes juxtanuclear positioning of the lysosomes. Xu et al. also obtained the same results using human umbilical vein endothelial cells (HUVECs). They showed that treating HUVECs with 10 µm of U18666A for 24 h completely deactivates mTORC1 (Xu et al. 2010). It has been shown that Ragulator complex can interact with either mTORC1 complex or with BLOC-1-related complex (BORC) (Filipek et al. 2017). In amino acid-repleted conditions, Ragulator complex interacts with SLC38A9 and Rag GTPases and the whole complex recruits mTORC1 to the lysosomal membrane. Under this condition, BORC and Arl8 interact with kinesin and facilitate anterograde transport of lysosomes. However, in amino acid-depleted conditions, weakening the interaction of Ragulator complex and SLC38A9 leads to dissociating of Ragulator complex from mTORC1 and therefore its inactivation. At the same time, Ragulator complex starts interacting with BORC and Arl8 and interferes with recruitment of kinesins to lysosomes and causes lysosomes juxtanuclear positioning (Figure 6.30) (Pu et al. 2017; Filipek et al. 2017).

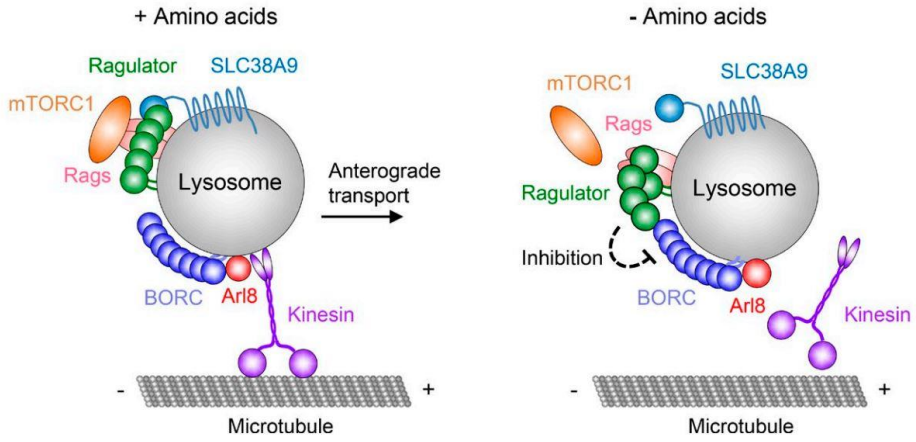

Figure 6.30 Proposed hypothetical model by Pu et al. for the regulation of lysosome positioning by BORC and Ragulator interaction.
Adopted from Pu et al. (Pu et al. 2017)

Based on the obtained results in this study, SLC38A9 has a stronger interaction with LAMTOR1 S56A rather than WT and E-mutated. It implies that phosphorylation results in dissociation of Ragulator from the SLC38A9/v-ATPase complex at the lysosomal membrane. LAMTOR1 phosphorylation at Ser56 could therefore possibly act as a binding switch to allow the Ragulator complex to bind either to mTORC1 (through SLC38A9/vATPase) or BORC complex and therefore leads to either mTORC1 activation or deactivation and lysosomal perinuclear localization, respectively (Figure 6.31).

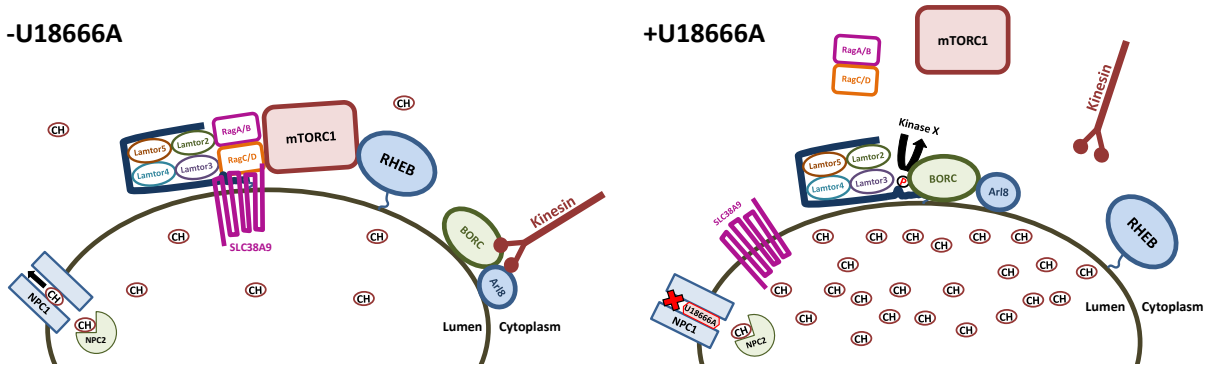

Figure 6.31 Hypothetical model for the effects of LAMTOR1 phosphorylation on mTORC1 activation and lysosomal positioning.
After U18666A treatment of the cells, an unknown kinase (kinase X) phosphorylates LAMTOR1 at Ser56. Phosphorylation affects LAMTOR1 interaction with RagA/B/C/D-SLC38A9 complex and leads to mTORC1 deactivation and dissociation from the lysosomal membrane. mTORC1 dissociation facilitates Ragulator complex interaction with BORC and Arl8. BORC complex interaction with Ragulator complex interferes with recruitment of kinesins to lysosomes and leads to lysosomes perinuclear positioning. (CH: cholesterol)

Unfortunately, it was not possible to assess the effect of LAMTOR1 phosphorylation on mTORC1 activity. Because such an experiment has to be carried out using LAMTOR1 knock-out cell line, otherwise interference of endogenous LAMTOR1 makes it impossible to obtain reliable results. Despite efforts to generate LAMTOR1-KO cell line using CRISPR/CAS systems, it was not successful. LAMTOR1 depletion induces p53-dependent apoptosis through perturbation of lysosomal function (Malek et al. 2012). Moreover, there are reports that showed that LAMTOR1 is as an essential gene for the cells (Wang et al. 2015b; Blomen et al. 2015). Therefore, it was postulated that the reason for the failure in generating LAMTOR1-null cells is the high lethality rate of the full knock-out cells.

The effect of phosphorylation on LAMTOR1 degradation rate and stability also was investigated. The phospho-resistant S56A LAMTOR1 version reproducibly showed significantly increased stability when compared to WT LAMTOR1 and the phosphomimetic S56E LAMTOR1. However, the latter is still more stable than the wild-type which might be due to the non-physiologic protein levels due to overexpression or substitution of glutamate for serine at S56 does not mimic phosphorylation of this residue. Based on these data, it was hypothesized that phosphorylation at S56 destabilizes LAMTOR1. As it has been shown previously, the stabilities of the Ragulator subunits are dependent on each other and degradation of one of the LAMTOR proteins causes degradation of other LAMTORs and results in deactivation of mTORC1 (Araújo

et al. 2013). In summary, it was concluded that LAMTOR1 phosphorylation has regulatory effects on the mTORC1 complex by both affecting LAMTOR1 interaction with other proteins and its degradation rate.

6.3.8.5.Phosphorylation does not affect RagC stability

Cycloheximide experiments were performed with the phosphoresistant/-mimetic versions of RagC S381. A statistically significant difference in the protein stability of the RagC WT and mutated versions was not observed. Since RagC is directly involved in the lysosomal association of mTORC1 and TFEB, its phosphorylation may influence its ability to locate these proteins to the lysosomal surface. There are several basic amino acids present in the vicinity of S381 (2 histidines, 1 lysine, and 1 arginine) and dephosphorylation could lead to a change from a neutral to a more basic charge state. This could directly influence Rag complex interaction with the Ragulator complex or with mTORC1 (Bar-Peled et al. 2012).

RagC S381 is the only downregulated phosphorylation site among the candidate phosphosites. This alteration in RagC phosphorylation may either be due to reduced activity of mTORC1 itself (or another kinase) or to the activity of a phosphatase which is recruited or activated due to impairment of lysosomal function.

Knowing that phosphorylation does not affect RagC stability, it was examined whether phosphorylation at S381 alters RagC interaction with other Ragulator-RagA/B/C/D members. To that end, co-IP experiment was carried out for the transfected HEK293 cells with the RagC Myc-tagged constructs (WT, S381A, and S381E). The results of the first replicate indicated that S381A has a stronger interaction with other Rag family members such as RagA and RagB; however, the results of the second replicate did not corroborate the earlier observation.

Although there are reports that show LAMTROs co-immunoprecipitate with RagC and other Rags (Filipek et al. 2017; Schweitzer et al. 2015; Tsun et al. 2013), however, Ragulator complex did not co-IP with the RagC protein in this study. This can be due to different reasons such as the experimental condition, the amount of the material (lysate) and the co-IP protocol that was used for this experiment. The co-IP protocol has a significant effect on the results. This protocol can be optimized by changing different parameters such as lysis buffer or elution condition to enable co-elution of all possible interaction partners of LAMTOR1 and RagC with them. Therefore,

these results are inconclusive and more investigation is needed to determine whether RagC Ser381 phosphorylation affects its interaction with other Ragulator/Rag complex proteins.

7. List of abbreviations

°C	Degree celsius
A	Alanine
Å	Ångström
ACN	Acetonitrile
AcOH	Acetic acid
ADP	Adenosine diphosphate
Ala	Alanine
APS	Ammonium persulfate
Asp	Aspartic acid
ATP	Adenosine triphosphate
Basic-RP	High ph reversed-phase
bp	Base pair
BRP	Basic reversed-phase
BSA	Bovine serum albumin
cDNA	Complementary DNA
CID	Collision-induced dissociation
Co-IP	Co-immunoprecipitation
CSCX	Column chromatography SCX
Ctrl.	Control
D	Aspartic acid
DAPI	4’,6-diamidin-2-phenylindol
DDA	Data-dependent acquisition
ddH2O	Double destilled water
DMEM	Dulbecco’s modified eagle medium
DMSO	Dimethyl sulfoxide
DNA	Deoxyribonucleic acid
DPBS	Dulbecco’s phosphate buffered saline
DTT	Dithiothreitol
E	Glutamic acid
ECL	Enhanced chemiluminescence
EDTA	Ethylenediaminetetraacetic acid
ER	Endoplasmatic reticulum
ERLIC	Electrostatic repulsion-hydrophilic interaction chromatography
ESI	Electrospray ionization
EtOH	Ethanol
FA	Formic acid
FCS	Fetal calf serum
FDR	False discovery rate
FT-ICR	Fourier transform – ion cyclotron resonance
g	Gram
GEF	Guanine nucleotide exchange factor
Glu	Glutamic acid
GO	Gene ontology
h	Hour
HBSS	Hank’s balanced salt solution
HEK293	Human embryonic kidney cells
HeLa	Henrietta Lacks cells (immortal cell line)
HEPES	4-(2-hydroxyethyl)-1-piperazineethanesulfonic acid
HILIC	Hydrophilic interaction liquid chromatography
HPLC	High pressure liquid chromatography

List of abbreviations

HRP	Horseradish peroxidase
ICC	Immunocytochemistry
IF	Immunofluorescence
IP	Immunoprecipitation
iTRAQ	Isobaric tags for relative and absolute quantitation
K	Lysine
KD	Knockdown
kDa	Kilodalton
KO	Knockout
LB	Lysogeny broth
LC-MS/MS	Liquid chromatography – tandem mass spectrometry
LE	Late endosome
LSDs	Lysosomal storage diseases
LTQ	Linear trap quadrupole
Lys	Lysosome
M	Molar
m/z	Mass-to-charge ratio
MALDI	Matrix-assisted laser desorption/ionization
MEFs	Mouse embryonic fibroblast cells
MeOH	Methanol
mg	Milligram
min	Minute
ml	Milliliter
MLD	Metachromatic leukodystrophy
mM	Millimolar
mm	Millimeter
MOAC	Metal oxide affinity chromatography
mRNA	Messenger RNA
MS	Mass spectrometry
MS	Multiple sclerosis
MSA	Multi-stage activation
NA	Not applicable
NaCl	Sodium chloride
Nano-LC	Nanoscale liquid chromatography
Neg. ctrl.	Negative control
nl	Nanoliter
nM	Nanomolar
ns	Not significant
PAGE	Polyacrylamide gel electrophoresis
PBS	Phosphate buffered saline
PCR	Polymerase chain reaction
PEST (SP-rich)	Proline (P), glutamic acid (E), serine (S), and threonine (T) risch domain
PFA	Paraformaldehyde
PMF	Peptide-mass fingerprinting
PTM	Post-translational modification
Puck’s BSS	Puck’s balanced salt solution
R	Arginine
rb	Rabbit
RNA	Ribonucleic acid
RP	Reversed-phase
RPLC	Reversed-phase liquid chromatography
RT	Room temperature

List of abbreviations

RT-PCR	Reverse transcriptase PCR
S	Serine
SAX	Strong anion exchange
SCX	Strong cation exchange
SDM	Site directed mutagenesis
SDS	Sodium dodecyl sulfate
Ser	Serine
SILAC	Stable Isotope Labeling by Amino Acids in Cell Culture
SIMAC	Sequential Elution from IMAC
SPE	Solid phase extraction
StageTips	Stop-and-go-extraction tips
TBS	Tris-buffered saline
TEAB	Triethylammonium bicarbonate
TEMED	Tetramethylethylenediamine
TFA	Trifluoroacetic acid
TiO_2	Titanium dioxide
TiSH	TiO_2-SIMAC-HILIC
Tm	Melting temperature
TMT	Tandem mass tag
TOF	Time-of-Flight
Tris	2-Amino-2-hydroxymethyl-propane-1,3-diol
Tris-HCl	Tris(hydroxymethyl)-aminomethan hydrochloride
UPLC	Ultra-performance liquid chromatography
WB	Western blot
WT	Wild type
x g	Earth's gravitational acceleration
β-ME	2-Sulfanylethan-1-ol
µg	Microgram
µl	Microliter
µM	Micromolar

8. List of figures

List of figures

9. List of tables

10. List of supplementary tables

Supplementary table 5.1: Phosphorylation sites acquired from all experiments and all biological replicates.

Supplementary table 5.2: Peptides identified in each biological replicate from SAX, SCX, and BRP tip-based, as well as column chromatography SCX (CSCX), fractionated samples.

Supplementary table 5.3: Gene ontology (GO) analysis results for the individual datasets obtained from PANTHER

Supplementary table 6.1: Chapter 2 proteomic study results

Supplementary table 6.2: Chapter 2 phosphoproteomic study results

11. Publication bibliography

Adachi, Jun; Hashiguchi, Kazunari; Nagano, Maiko; Sato, Misako; Sato, Ayako; Fukamizu, Kazuna et al. (2016): Improved Proteome and Phosphoproteome Analysis on a Cation Exchanger by a Combined Acid and Salt Gradient. In *Analytical chemistry* 88 (16), pp. 7899–7903. DOI: 10.1021/acs.analchem.6b01232.

Aebersold, Ruedi; Mann, Matthias (2003): Mass spectrometry-based proteomics. In *Nature* 422 (6928), pp. 198–207. DOI: 10.1038/nature01511.

Aebersold, Ruedi; Mann, Matthias (2016): Mass-spectrometric exploration of proteome structure and function. In *Nature* 537 (7620), pp. 347–355. DOI: 10.1038/nature19949.

Alonso, Andres; Sasin, Joanna; Bottini, Nunzio; Friedberg, Ilan; Friedberg, Iddo; Osterman, Andrei et al. (2004): Protein tyrosine phosphatases in the human genome. In *Cell* 117 (6), pp. 699–711. DOI: 10.1016/j.cell.2004.05.018.

Alpert, Andrew J. (2008): Electrostatic repulsion hydrophilic interaction chromatography for isocratic separation of charged solutes and selective isolation of phosphopeptides. In *Analytical chemistry* 80 (1), pp. 62–76. DOI: 10.1021/ac070997p.

Alpy, Fabien; Latchumanan, Vinoth K.; Kedinger, Valérie; Janoshazi, Agnes; Thiele, Christoph; Wendling, Corinne et al. (2005): Functional characterization of the MENTAL domain. In *The Journal of biological chemistry* 280 (18), pp. 17945–17952. DOI: 10.1074/jbc.M500723200.

Alpy, Fabien; Rousseau, Adrien; Schwab, Yannick; Legueux, François; Stoll, Isabelle; Wendling, Corinne et al. (2013): STARD3 or STARD3NL and VAP form a novel molecular tether between late endosomes and the ER. In *Journal of cell science* 126 (Pt 23), pp. 5500–5512. DOI: 10.1242/jcs.139295.

Araujo, Mariana E. G. de; Naschberger, Andreas; Fürnrohr, Barbara G.; Stasyk, Taras; Dunzendorfer-Matt, Theresia; Lechner, Stefan et al. (2017): Crystal structure of the human lysosomal mTORC1 scaffold complex and its impact on signaling. In *Science (New York, N.Y.)* 358 (6361), pp. 377–381. DOI: 10.1126/science.aao1583.

Araújo, Mariana E. G. de; Stasyk, Taras; Taub, Nicole; Ebner, Hannes L.; Fürst, Beatrix; Filipek, Przemyslaw et al. (2013): Stability of the endosomal scaffold protein LAMTOR3 depends on heterodimer assembly and proteasomal degradation. In *The Journal of biological chemistry* 288 (25), pp. 18228–18242. DOI: 10.1074/jbc.M112.349480.

Arthur, Julian R.; Heinecke, Karie A.; Seyfried, Thomas N. (2011): Filipin recognizes both GM1 and cholesterol in GM1 gangliosidosis mouse brain. In *Journal of lipid research* 52 (7), pp. 1345–1351. DOI: 10.1194/jlr.M012633.

Ashburner, M.; Ball, C. A.; Blake, J. A.; Botstein, D.; Butler, H.; Cherry, J. M. et al. (2000): Gene ontology: tool for the unification of biology. The Gene Ontology Consortium. In *Nature genetics* 25 (1), pp. 25–29. DOI: 10.1038/75556.

List of supplementary tables

Awad, Hanan; Khamis, Mona M.; El-Aneed, Anas (2015): Mass Spectrometry, Review of the Basics: Ionization. In *Applied Spectroscopy Reviews* 50 (2), pp. 158–175. DOI: 10.1080/05704928.2014.954046.

Ballabio, Andrea; Gieselmann, Volkmar (2009): Lysosomal disorders: from storage to cellular damage. In *Biochimica et biophysica acta* 1793 (4), pp. 684–696. DOI: 10.1016/j.bbamcr.2008.12.001.

Barillot, Emmanuel (2013): Computational systems biology of cancer [electronic resource]. Boca Raton, FL: CRC Press (Chapman & Hall/CRC mathematical and computational biology series).

Bar-Peled, Liron; Schweitzer, Lawrence D.; Zoncu, Roberto; Sabatini, David M. (2012): Ragulator is a GEF for the rag GTPases that signal amino acid levels to mTORC1. In *Cell* 150 (6), pp. 1196–1208. DOI: 10.1016/j.cell.2012.07.032.

Batth, Tanveer S.; Francavilla, Chiara; Olsen, Jesper V. (2014): Off-line high-pH reversed-phase fractionation for in-depth phosphoproteomics. In *Journal of proteome research* 13 (12), pp. 6176–6186. DOI: 10.1021/pr500893m.

Beausoleil, Sean A.; Jedrychowski, Mark; Schwartz, Daniel; Elias, Joshua E.; Villén, Judit; Li, Jiaxu et al. (2004): Large-scale characterization of HeLa cell nuclear phosphoproteins. In *Proceedings of the National Academy of Sciences of the United States of America* 101 (33), pp. 12130–12135. DOI: 10.1073/pnas.0404720101.

Blagoev, Blagoy; Kratchmarova, Irina; Ong, Shao-En; Nielsen, Mogens; Foster, Leonard J.; Mann, Matthias (2003): A proteomics strategy to elucidate functional protein-protein interactions applied to EGF signaling. In *Nature biotechnology* 21 (3), pp. 315–318. DOI: 10.1038/nbt790.

Blomen, Vincent A.; Májek, Peter; Jae, Lucas T.; Bigenzahn, Johannes W.; Nieuwenhuis, Joppe; Staring, Jacqueline et al. (2015): Gene essentiality and synthetic lethality in haploid human cells. In *Science (New York, N.Y.)* 350 (6264), pp. 1092–1096. DOI: 10.1126/science.aac7557.

Boersema, Paul J.; Raijmakers, Reinout; Lemeer, Simone; Mohammed, Shabaz; Heck, Albert J. R. (2009): Multiplex peptide stable isotope dimethyl labeling for quantitative proteomics. In *Nature protocols* 4 (4), pp. 484–494. DOI: 10.1038/nprot.2009.21.

Byun, Kyunghee; Kim, Jaewoo; Cho, Sang-Yun; Hutchinson, Brian; Yang, Se-Ran; Kang, Kyung-Sun et al. (2006): Alteration of the glutamate and GABA transporters in the hippocampus of the Niemann-Pick disease, type C mouse using proteomic analysis. In *Proteomics* 6 (4), pp. 1230–1236. DOI: 10.1002/pmic.200500412.

Cadigan, K. M.; Spillane, D. M.; Chang, T. Y. (1990): Isolation and characterization of Chinese hamster ovary cell mutants defective in intracellular low density lipoprotein-cholesterol trafficking. In *The Journal of cell biology* 110 (2), pp. 295–308.

Castellano, Brian M.; Thelen, Ashley M.; Moldavski, Ofer; Feltes, McKenna; van der Welle, Reini E. N.; Mydock-McGrane, Laurel et al. (2017): Lysosomal cholesterol activates mTORC1 via an SLC38A9-Niemann-Pick C1 signaling complex. In *Science (New York, N.Y.)* 355 (6331), pp. 1306–1311. DOI: 10.1126/science.aag1417.

Cenedella, Richard J. (2009): Cholesterol synthesis inhibitor U18666A and the role of sterol metabolism and trafficking in numerous pathophysiological processes. In *Lipids* 44 (6), pp. 477–487. DOI: 10.1007/s11745-009-3305-7.

Colgan, Stephen M.; Tang, Damu; Werstuck, Geoff H.; Austin, Richard C. (2007): Endoplasmic reticulum stress causes the activation of sterol regulatory element binding protein-2. In *The international journal of biochemistry & cell biology* 39 (10), pp. 1843–1851. DOI: 10.1016/j.biocel.2007.05.002.

Cologna, Stephanie M.; Jiang, Xiao-Sheng; Backlund, Peter S.; Cluzeau, Celine V. M.; Dail, Michelle K.; Yanjanin, Nicole M. et al. (2012): Quantitative proteomic analysis of Niemann-Pick disease, type C1 cerebellum identifies protein biomarkers and provides pathological insight. In *PloS one* 7 (10), e47845. DOI: 10.1371/journal.pone.0047845.

Cox, Jürgen; Hein, Marco Y.; Luber, Christian A.; Paron, Igor; Nagaraj, Nagarjuna; Mann, Matthias (2014): Accurate proteome-wide label-free quantification by delayed normalization and maximal peptide ratio extraction, termed MaxLFQ. In *Molecular & cellular proteomics : MCP* 13 (9), pp. 2513–2526. DOI: 10.1074/mcp.M113.031591.

Cox, Jürgen; Mann, Matthias (2008): MaxQuant enables high peptide identification rates, individualized p.p.b.-range mass accuracies and proteome-wide protein quantification. In *Nature biotechnology* 26 (12), pp. 1367–1372. DOI: 10.1038/nbt.1511.

Dai, Jie; Wang, Lian-Shui; Wu, Yi-Bo; Sheng, Quan-Hu; Wu, Jia-Rui; Shieh, Chia-Hui; Zeng, Rong (2009): Fully automatic separation and identification of phosphopeptides by continuous pH-gradient anion exchange online coupled with reversed-phase liquid chromatography mass spectrometry. In *Journal of proteome research* 8 (1), pp. 133–141. DOI: 10.1021/pr800381w.

Dalby, K. N.; Morrice, N.; Caudwell, F. B.; Avruch, J.; Cohen, P. (1998): Identification of regulatory phosphorylation sites in mitogen-activated protein kinase (MAPK)-activated protein kinase-1a/p90rsk that are inducible by MAPK. In *The Journal of biological chemistry* 273 (3), pp. 1496–1505.

DeBose-Boyd, Russell A. (2008): Feedback regulation of cholesterol synthesis: sterol-accelerated ubiquitination and degradation of HMG CoA reductase. In *Cell research* 18 (6), pp. 609–621. DOI: 10.1038/cr.2008.61.

Dehghani, Alireza; Gödderz, Markus; Winter, Dominic (2018): Tip-Based Fractionation of Batch-Enriched Phosphopeptides Facilitates Easy and Robust Phosphoproteome Analysis. In *Journal of proteome research* 17 (1), pp. 46–54. DOI: 10.1021/acs.jproteome.7b00256.

Dibble, Christian C.; Elis, Winfried; Menon, Suchithra; Qin, Wei; Klekota, Justin; Asara, John M. et al. (2012): TBC1D7 is a third subunit of the TSC1-TSC2 complex upstream of mTORC1. In *Molecular cell* 47 (4), pp. 535–546. DOI: 10.1016/j.molcel.2012.06.009.

Eden, Eran; Navon, Roy; Steinfeld, Israel; Lipson, Doron; Yakhini, Zohar (2009): GOrilla: a tool for discovery and visualization of enriched GO terms in ranked gene lists. In *BMC bioinformatics* 10, p. 48. DOI: 10.1186/1471-2105-10-48.

Ehehalt, Robert; Keller, Patrick; Haass, Christian; Thiele, Christoph; Simons, Kai (2003): Amyloidogenic processing of the Alzheimer beta-amyloid precursor protein depends on lipid rafts. In *The Journal of cell biology* 160 (1), pp. 113–123. DOI: 10.1083/jcb.200207113.

Engelking, Luke J.; Cantoria, Mary Jo; Xu, Yanchao; Liang, Guosheng (2018): Developmental and extrahepatic physiological functions of SREBP pathway genes in mice. In *Seminars in cell & developmental biology* 81, pp. 98–109. DOI: 10.1016/j.semcdb.2017.07.011.

Engholm-Keller, Kasper; Birck, Pernille; Størling, Joachim; Pociot, Flemming; Mandrup-Poulsen, Thomas; Larsen, Martin R. (2012): TiSH--a robust and sensitive global phosphoproteomics strategy employing a combination of TiO2, SIMAC, and HILIC. In *Journal of proteomics* 75 (18), pp. 5749–5761. DOI: 10.1016/j.jprot.2012.08.007.

Engholm-Keller, Kasper; Larsen, Martin R. (2013): Technologies and challenges in large-scale phosphoproteomics. In *Proteomics* 13 (6), pp. 910–931. DOI: 10.1002/pmic.201200484.

Erickson, Brian K.; Jedrychowski, Mark P.; McAlister, Graeme C.; Everley, Robert A.; Kunz, Ryan; Gygi, Steven P. (2015): Evaluating multiplexed quantitative phosphopeptide analysis on a hybrid quadrupole mass filter/linear ion trap/orbitrap mass spectrometer. In *Analytical chemistry* 87 (2), pp. 1241–1249. DOI: 10.1021/ac503934f.

Filipek, Przemyslaw A.; Araujo, Mariana E. G. de; Vogel, Georg F.; Smet, Cedric H. de; Eberharter, Daniela; Rebsamen, Manuele et al. (2017): LAMTOR/Ragulator is a negative regulator of Arl8b- and BORC-dependent late endosomal positioning. In *The Journal of cell biology* 216 (12), pp. 4199–4215. DOI: 10.1083/jcb.201703061.

Fu, Ruoqiu; Deng, Qin; Zhang, Hongwei; Hu, Xiaoye; Li, Yunong; Liu, Yanxia et al. (2018): A novel autophagy inhibitor berbamine blocks SNARE-mediated autophagosome-lysosome fusion through upregulation of BNIP3. In *Cell death & disease* 9 (2), p. 243. DOI: 10.1038/s41419-018-0276-8.

Futerman, Anthony H.; van Meer, Gerrit (2004): The cell biology of lysosomal storage disorders. In *Nature reviews. Molecular cell biology* 5 (7), pp. 554–565. DOI: 10.1038/nrm1423.

Garver, W. S.; Hossain, G. S.; Winscott, M. M.; Heidenreich, R. A. (1999): The Npc1 mutation causes an altered expression of caveolin-1, annexin II and protein kinases and phosphorylation of caveolin-1 and annexin II in murine livers. In *Biochimica et biophysica acta* 1453 (2), pp. 193–206.

Gelsthorpe, Mark E.; Baumann, Nikola; Millard, Elizabeth; Gale, Sarah E.; Langmade, S. Joshua; Schaffer, Jean E.; Ory, Daniel S. (2008): Niemann-Pick type C1 I1061T mutant encodes a functional protein that is selected for endoplasmic reticulum-associated degradation due to protein misfolding. In *The Journal of biological chemistry* 283 (13), pp. 8229–8236. DOI: 10.1074/jbc.M708735200.

Gerber, Scott A.; Rush, John; Stemman, Olaf; Kirschner, Marc W.; Gygi, Steven P. (2003): Absolute quantification of proteins and phosphoproteins from cell lysates by tandem MS. In *Proceedings of the National Academy of Sciences of the United States of America* 100 (12), pp. 6940–6945. DOI: 10.1073/pnas.0832254100.

Gill, Saloni; Stevenson, Julian; Kristiana, Ika; Brown, Andrew J. (2011): Cholesterol-dependent degradation of squalene monooxygenase, a control point in cholesterol synthesis beyond HMG-CoA reductase. In *Cell metabolism* 13 (3), pp. 260–273. DOI: 10.1016/j.cmet.2011.01.015.

Goldstein, Joseph L.; DeBose-Boyd, Russell A.; Brown, Michael S. (2006): Protein sensors for membrane sterols. In *Cell* 124 (1), pp. 35–46. DOI: 10.1016/j.cell.2005.12.022.

Hahn, Bettina; Böhm, Martin; Raia, Valentina; Zinn, Nico; Möller, Peter; Klingmüller, Ursula; Lehmann, Wolf-Dieter (2011): One-source peptide/phosphopeptide standards for accurate phosphorylation degree determination. In *Proteomics* 11 (3), pp. 490–494. DOI: 10.1002/pmic.201000569.

Hahne, Hannes; Pachl, Fiona; Ruprecht, Benjamin; Maier, Stefan K.; Klaeger, Susan; Helm, Dominic et al. (2013): DMSO enhances electrospray response, boosting sensitivity of proteomic experiments. In *Nature methods* 10 (10), pp. 989–991. DOI: 10.1038/nmeth.2610.

Han, Dohyun; Jin, Jonghwa; Woo, Jongmin; Min, Hophil; Kim, Youngsoo (2014): Proteomic analysis of mouse astrocytes and their secretome by a combination of FASP and StageTip-based, high pH, reversed-phase fractionation. In *Proteomics* 14 (13-14), pp. 1604–1609. DOI: 10.1002/pmic.201300495.

Han, Guanghui; Ye, Mingliang; Zhou, Houjiang; Jiang, Xinning; Feng, Shun; Jiang, Xiaogang et al. (2008): Large-scale phosphoproteome analysis of human liver tissue by enrichment and fractionation of phosphopeptides with strong anion exchange chromatography. In *Proteomics* 8 (7), pp. 1346–1361. DOI: 10.1002/pmic.200700884.

Hornbeck, Peter V.; Zhang, Bin; Murray, Beth; Kornhauser, Jon M.; Latham, Vaughan; Skrzypek, Elzbieta (2015): PhosphoSitePlus, 2014: mutations, PTMs and recalibrations. In *Nucleic acids research* 43 (Database issue), D512-20. DOI: 10.1093/nar/gku1267.

Hsu, Jue-Liang; Chen, Shu-Hui (2016): Stable isotope dimethyl labelling for quantitative proteomics and beyond. In *Philosophical transactions. Series A, Mathematical, physical, and engineering sciences* 374 (2079). DOI: 10.1098/rsta.2015.0364.

Huang, Xun; Suyama, Kaye; Buchanan, Joann; Zhu, Alan J.; Scott, Matthew P. (2005): A Drosophila model of the Niemann-Pick type C lysosome storage disease: dnpc1a is required for molting and sterol homeostasis. In *Development (Cambridge, England)* 132 (22), pp. 5115–5124. DOI: 10.1242/dev.02079.

Huttlin, Edward L.; Jedrychowski, Mark P.; Elias, Joshua E.; Goswami, Tapasree; Rad, Ramin; Beausoleil, Sean A. et al. (2010): A tissue-specific atlas of mouse protein phosphorylation and expression. In *Cell* 143 (7), pp. 1174–1189. DOI: 10.1016/j.cell.2010.12.001.

Iesmantavicius, Vytautas; Weinert, Brian T.; Choudhary, Chunaram (2014): Convergence of ubiquitylation and phosphorylation signaling in rapamycin-treated yeast cells. In *Molecular & cellular proteomics : MCP* 13 (8), pp. 1979–1992. DOI: 10.1074/mcp.O113.035683.

Isotani, S.; Hara, K.; Tokunaga, C.; Inoue, H.; Avruch, J.; Yonezawa, K. (1999): Immunopurified mammalian target of rapamycin phosphorylates and activates p70 S6 kinase alpha in vitro. In *The Journal of biological chemistry* 274 (48), pp. 34493–34498.

List of supplementary tables

Itakura, Eisuke; Kishi-Itakura, Chieko; Mizushima, Noboru (2012): The hairpin-type tail-anchored SNARE syntaxin 17 targets to autophagosomes for fusion with endosomes/lysosomes. In *Cell* 151 (6), pp. 1256–1269. DOI: 10.1016/j.cell.2012.11.001.

Jin, Jing; Pawson, Tony (2012): Modular evolution of phosphorylation-based signalling systems. In *Philosophical transactions of the Royal Society of London. Series B, Biological sciences* 367 (1602), pp. 2540–2555. DOI: 10.1098/rstb.2012.0106.

Juan Carlos Oliveros: VENNY. Version 2.1. Available online at http://bioinfogp.cnb.csic.es/tools/venny/index.html.

Käll, Lukas; Vitek, Olga (2011): Computational mass spectrometry-based proteomics. In *PLoS computational biology* 7 (12), e1002277. DOI: 10.1371/journal.pcbi.1002277.

Kanshin, Evgeny; Michnick, Stephen; Thibault, Pierre (2012): Sample preparation and analytical strategies for large-scale phosphoproteomics experiments. In *Seminars in cell & developmental biology* 23 (8), pp. 843–853. DOI: 10.1016/j.semcdb.2012.05.005.

Kasper, Dagmar; Planells-Cases, Rosa; Fuhrmann, Jens C.; Scheel, Olaf; Zeitz, Oliver; Ruether, Klaus et al. (2005): Loss of the chloride channel ClC-7 leads to lysosomal storage disease and neurodegeneration. In *The EMBO journal* 24 (5), pp. 1079–1091. DOI: 10.1038/sj.emboj.7600576.

Krüger, Marcus; Moser, Markus; Ussar, Siegfried; Thievessen, Ingo; Luber, Christian A.; Forner, Francesca et al. (2008): SILAC mouse for quantitative proteomics uncovers kindlin-3 as an essential factor for red blood cell function. In *Cell* 134 (2), pp. 353–364. DOI: 10.1016/j.cell.2008.05.033.

Kulinski, Agnes; Vance, Jean E. (2007): Lipid homeostasis and lipoprotein secretion in Niemann-Pick C1-deficient hepatocytes. In *The Journal of biological chemistry* 282 (3), pp. 1627–1637. DOI: 10.1074/jbc.M610001200.

Kundra, R.; Kornfeld, S. (1999): Asparagine-linked oligosaccharides protect Lamp-1 and Lamp-2 from intracellular proteolysis. In *The Journal of biological chemistry* 274 (43), pp. 31039–31046.

Kwon, Hyock Joo; Abi-Mosleh, Lina; Wang, Michael L.; Deisenhofer, Johann; Goldstein, Joseph L.; Brown, Michael S.; Infante, Rodney E. (2009): Structure of N-terminal domain of NPC1 reveals distinct subdomains for binding and transfer of cholesterol. In *Cell* 137 (7), pp. 1213–1224. DOI: 10.1016/j.cell.2009.03.049.

Lange, Philipp F.; Wartosch, Lena; Jentsch, Thomas J.; Fuhrmann, Jens C. (2006): ClC-7 requires Ostm1 as a beta-subunit to support bone resorption and lysosomal function. In *Nature* 440 (7081), pp. 220–223. DOI: 10.1038/nature04535.

Lange, Y.; Ye, J.; Rigney, M.; Steck, T. L. (1999): Regulation of endoplasmic reticulum cholesterol by plasma membrane cholesterol. In *Journal of lipid research* 40 (12), pp. 2264–2270.

Lange, Yvonne; Ye, Jin; Rigney, Mike; Steck, Theodore L. (2002): Dynamics of lysosomal cholesterol in Niemann-Pick type C and normal human fibroblasts. In *Journal of lipid research* 43 (2), pp. 198–204.

List of supplementary tables

Leisle, Lilia; Ludwig, Carmen F.; Wagner, Florian A.; Jentsch, Thomas J.; Stauber, Tobias (2011): ClC-7 is a slowly voltage-gated 2Cl(-)/1H(+)-exchanger and requires Ostm1 for transport activity. In *The EMBO journal* 30 (11), pp. 2140–2152. DOI: 10.1038/emboj.2011.137.

Lin, R.; Beauparlant, P.; Makris, C.; Meloche, S.; Hiscott, J. (1996): Phosphorylation of IkappaBalpha in the C-terminal PEST domain by casein kinase II affects intrinsic protein stability. In *Molecular and Cellular Biology* 16 (4), pp. 1401–1409.

Liscum, L. (1989): The intracellular transport of low density lipoprotein-derived cholesterol is defective in Niemann-Pick type C fibroblasts. In *The Journal of cell biology* 108 (5), pp. 1625–1636. DOI: 10.1083/jcb.108.5.1625.

Loftus, S. K.; Morris, J. A.; Carstea, E. D.; Gu, J. Z.; Cummings, C.; Brown, A. et al. (1997): Murine model of Niemann-Pick C disease: mutation in a cholesterol homeostasis gene. In *Science (New York, N.Y.)* 277 (5323), pp. 232–235.

Long, Xiaomeng; Lin, Yenshou; Ortiz-Vega, Sara; Yonezawa, Kazuyoshi; Avruch, Joseph (2005): Rheb binds and regulates the mTOR kinase. In *Current biology : CB* 15 (8), pp. 702–713. DOI: 10.1016/j.cub.2005.02.053.

LOWRY, O. H.; ROSEBROUGH, N. J.; FARR, A. L.; RANDALL, R. J. (1951): Protein measurement with the Folin phenol reagent. In *The Journal of biological chemistry* 193 (1), pp. 265–275.

Lu, Feiran; Liang, Qiren; Abi-Mosleh, Lina; Das, Akash; Brabander, Jef K. de; Goldstein, Joseph L.; Brown, Michael S. (2015): Identification of NPC1 as the target of U18666A, an inhibitor of lysosomal cholesterol export and Ebola infection. In *eLife* 4. DOI: 10.7554/eLife.12177.

Luzio, J. Paul; Pryor, Paul R.; Bright, Nicholas A. (2007): Lysosomes: fusion and function. In *Nature reviews. Molecular cell biology* 8 (8), pp. 622–632. DOI: 10.1038/nrm2217.

Ma, Xiucui; Godar, Rebecca J.; Liu, Haiyan; Diwan, Abhinav (2012): Enhancing lysosome biogenesis attenuates BNIP3-induced cardiomyocyte death. In *Autophagy* 8 (3), pp. 297–309. DOI: 10.4161/auto.18658.

Macías-Vidal, Judit; Guerrero-Hernández, Martina; Estanyol, Josep Maria; Aguado, Carmen; Knecht, Erwin; Coll, Maria Josep; Bachs, Oriol (2016): Identification of lysosomal Npc1-binding proteins: Cathepsin D activity is regulated by NPC1. In *Proteomics* 16 (1), pp. 150–158. DOI: 10.1002/pmic.201500110.

Malathi, Krishnamurthy; Higaki, Katsumi; Tinkelenberg, Arthur H.; Balderes, Dina A.; Almanzar-Paramio, Dorca; Wilcox, Lisa J. et al. (2004): Mutagenesis of the putative sterol-sensing domain of yeast Niemann Pick C-related protein reveals a primordial role in subcellular sphingolipid distribution. In *The Journal of cell biology* 164 (4), pp. 547–556. DOI: 10.1083/jcb.200310046.

Malek, M.; Guillaumot, P.; Huber, A-L; Lebeau, J.; Pétrilli, V.; Kfoury, A. et al. (2012): LAMTOR1 depletion induces p53-dependent apoptosis via aberrant lysosomal activation. In *Cell death & disease* 3, e300. DOI: 10.1038/cddis.2012.39.

Malmersjö, Seth; Di Palma, Serena; Diao, Jiajie; Lai, Ying; Pfuetzner, Richard A.; Wang, Austin L. et al. (2016): Phosphorylation of residues inside the SNARE complex suppresses secretory vesicle fusion. In *The EMBO journal* 35 (16), pp. 1810–1821. DOI: 10.15252/embj.201694071.

Manning, G.; Whyte, D. B.; Martinez, R.; Hunter, T.; Sudarsanam, S. (2002): The protein kinase complement of the human genome. In *Science (New York, N.Y.)* 298 (5600), pp. 1912–1934. DOI: 10.1126/science.1075762.

McNulty, Dean E.; Annan, Roland S. (2008): Hydrophilic interaction chromatography reduces the complexity of the phosphoproteome and improves global phosphopeptide isolation and detection. In *Molecular & cellular proteomics : MCP* 7 (5), pp. 971–980. DOI: 10.1074/mcp.M700543-MCP200.

Mi, Huaiyu; Huang, Xiaosong; Muruganujan, Anushya; Tang, Haiming; Mills, Caitlin; Kang, Diane; Thomas, Paul D. (2017): PANTHER version 11: expanded annotation data from Gene Ontology and Reactome pathways, and data analysis tool enhancements. In *Nucleic acids research* 45 (D1), D183-D189. DOI: 10.1093/nar/gkw1138.

Mi, Huaiyu; Muruganujan, Anushya; Casagrande, John T.; Thomas, Paul D. (2013): Large-scale gene function analysis with the PANTHER classification system. In *Nature protocols* 8 (8), pp. 1551–1566. DOI: 10.1038/nprot.2013.092.

Miyawaki, S.; Yoshida, H.; Mitsuoka, S.; Enomoto, H.; Ikehara, S. (1986): A mouse model for Niemann-Pick disease. Influence of genetic background on disease expression in spm/spm mice. In *The Journal of heredity* 77 (6), pp. 379–384.

Mohammed, Shabaz; Heck, Albert (2011): Strong cation exchange (SCX) based analytical methods for the targeted analysis of protein post-translational modifications. In *Current opinion in biotechnology* 22 (1), pp. 9–16. DOI: 10.1016/j.copbio.2010.09.005.

Nielsen, Gitte Krogh; Dagnaes-Hansen, Frederik; Holm, Ida Elisabeth; Meaney, Steve; Symula, Derek; Andersen, Niels Trolle; Heegaard, Christian Würtz (2011): Protein replacement therapy partially corrects the cholesterol-storage phenotype in a mouse model of Niemann-Pick type C2 disease. In *PloS one* 6 (11), e27287. DOI: 10.1371/journal.pone.0027287.

Ohkuma, S.; Moriyama, Y.; Takano, T. (1982): Identification and characterization of a proton pump on lysosomes by fluorescein-isothiocyanate-dextran fluorescence. In *Proceedings of the National Academy of Sciences of the United States of America* 79 (9), pp. 2758–2762.

Olsen, Jesper V.; Mann, Matthias (2013): Status of Large-scale Analysis of Post-translational Modifications by Mass Spectrometry*. In *Molecular & cellular proteomics : MCP* 12 (12), pp. 3444–3452. DOI: 10.1074/mcp.O113.034181.

Olsen, Jesper V.; Vermeulen, Michiel; Santamaria, Anna; Kumar, Chanchal; Miller, Martin L.; Jensen, Lars J. et al. (2010): Quantitative phosphoproteomics reveals widespread full phosphorylation site occupancy during mitosis. In *Science signaling* 3 (104), ra3. DOI: 10.1126/scisignal.2000475.

Ong, Shao-En; Blagoev, Blagoy; Kratchmarova, Irina; Kristensen, Dan Bach; Steen, Hanno; Pandey, Akhilesh; Mann, Matthias (2002): Stable isotope labeling by amino acids in cell culture, SILAC, as a

simple and accurate approach to expression proteomics. In *Molecular & cellular proteomics : MCP* 1 (5), pp. 376–386.

Ong, Shao-En; Mann, Matthias (2005): Mass spectrometry-based proteomics turns quantitative. In *Nature chemical biology* 1 (5), pp. 252–262. DOI: 10.1038/nchembio736.

Pandruvada, Subramanya N. M.; Beauregard, Janie; Benjannet, Suzanne; Pata, Monica; Lazure, Claude; Seidah, Nabil G.; Vacher, Jean (2016): Role of Ostm1 Cytosolic Complex with Kinesin 5B in Intracellular Dispersion and Trafficking. In *Molecular and Cellular Biology* 36 (3), pp. 507–521. DOI: 10.1128/MCB.00656-15.

Papandreou, Ioanna; Cairns, Rob A.; Fontana, Lucrezia; Lim, Ai Lin; Denko, Nicholas C. (2006): HIF-1 mediates adaptation to hypoxia by actively downregulating mitochondrial oxygen consumption. In *Cell metabolism* 3 (3), pp. 187–197. DOI: 10.1016/j.cmet.2006.01.012.

Paradela, Alberto; Albar, Juan Pablo (2008): Advances in the analysis of protein phosphorylation. In *Journal of proteome research* 7 (5), pp. 1809–1818. DOI: 10.1021/pr7006544.

Pawson, Tony (2004): Specificity in signal transduction: from phosphotyrosine-SH2 domain interactions to complex cellular systems. In *Cell* 116 (2), pp. 191–203.

Piraud, Monique; Pettazzoni, Magali; Lavoie, Pamela; Ruet, Séverine; Pagan, Cécile; Cheillan, David et al. (2018): Contribution of tandem mass spectrometry to the diagnosis of lysosomal storage disorders. In *Journal of inherited metabolic disease* 41 (3), pp. 457–477. DOI: 10.1007/s10545-017-0126-3.

Platt, Frances M.; Boland, Barry; van der Spoel, Aarnoud C. (2012): The cell biology of disease: lysosomal storage disorders: the cellular impact of lysosomal dysfunction. In *The Journal of cell biology* 199 (5), pp. 723–734. DOI: 10.1083/jcb.201208152.

Possemato, Anthony P.; Paulo, Joao A.; Mulhern, Daniel; Guo, Ailan; Gygi, Steven P.; Beausoleil, Sean A. (2017): Multiplexed Phosphoproteomic Profiling Using Titanium Dioxide and Immunoaffinity Enrichments Reveals Complementary Phosphorylation Events. In *Journal of proteome research* 16 (4), pp. 1506–1514. DOI: 10.1021/acs.jproteome.6b00905.

Pu, Jing; Keren-Kaplan, Tal; Bonifacino, Juan S. (2017): A Ragulator-BORC interaction controls lysosome positioning in response to amino acid availability. In *The Journal of cell biology* 216 (12), pp. 4183–4197. DOI: 10.1083/jcb.201703094.

Puth, Marie-Therese; Neuhäuser, Markus; Ruxton, Graeme D. (2014): Effective use of Pearson's product–moment correlation coefficient. In *Animal Behaviour* 93, pp. 183–189. DOI: 10.1016/j.anbehav.2014.05.003.

Raiborg, Camilla; Wenzel, Eva M.; Stenmark, Harald (2015): ER-endosome contact sites: molecular compositions and functions. In *The EMBO journal* 34 (14), pp. 1848–1858. DOI: 10.15252/embj.201591481.

Rappsilber, Juri; Ishihama, Yasushi; Mann, Matthias (2003): Stop and go extraction tips for matrix-assisted laser desorption/ionization, nanoelectrospray, and LC/MS sample pretreatment in proteomics. In *Analytical chemistry* 75 (3), pp. 663–670.

Rappsilber, Juri; Mann, Matthias; Ishihama, Yasushi (2007): Protocol for micro-purification, enrichment, pre-fractionation and storage of peptides for proteomics using StageTips. In *Nature protocols* 2 (8), pp. 1896–1906. DOI: 10.1038/nprot.2007.261.

Rauniyar, Navin; Subramanian, Kanagaraj; Lavallée-Adam, Mathieu; Martínez-Bartolomé, Salvador; Balch, William E.; Yates, John R. (2015): Quantitative Proteomics of Human Fibroblasts with I1061T Mutation in Niemann-Pick C1 (NPC1) Protein Provides Insights into the Disease Pathogenesis. In *Molecular & cellular proteomics : MCP* 14 (7), pp. 1734–1749. DOI: 10.1074/mcp.M114.045609.

Rebsamen, Manuele; Pochini, Lorena; Stasyk, Taras; Araújo, Mariana E. G. de; Galluccio, Michele; Kandasamy, Richard K. et al. (2015): SLC38A9 is a component of the lysosomal amino acid sensing machinery that controls mTORC1. In *Nature* 519 (7544), pp. 477–481. DOI: 10.1038/nature14107.

Reverter, Meritxell; Rentero, Carles; Garcia-Melero, Ana; Hoque, Monira; Vilà de Muga, Sandra; Alvarez-Guaita, Anna et al. (2014): Cholesterol regulates Syntaxin 6 trafficking at trans-Golgi network endosomal boundaries. In *Cell reports* 7 (3), pp. 883–897. DOI: 10.1016/j.celrep.2014.03.043.

Rikova, Klarisa; Guo, Ailan; Zeng, Qingfu; Possemato, Anthony; Yu, Jian; Haack, Herbert et al. (2007): Global survey of phosphotyrosine signaling identifies oncogenic kinases in lung cancer. In *Cell* 131 (6), pp. 1190–1203. DOI: 10.1016/j.cell.2007.11.025.

Riojas, Ramon A.; Kikani, Chintan K.; Wang, Changhua; Mao, Xuming; Zhou, Lijun; Langlais, Paul R. et al. (2006): Fine tuning PDK1 activity by phosphorylation at Ser163. In *The Journal of biological chemistry* 281 (31), pp. 21588–21593. DOI: 10.1074/jbc.M600393200.

Rodriguez-Lafrasse, C.; Rousson, R.; Bonnet, J.; Pentchev, P. G.; Louisot, P.; Vanier, M. T. (1990): Abnormal cholesterol metabolism in imipramine-treated fibroblast cultures. Similarities with Niemann-Pick type C disease. In *Biochimica et biophysica acta* 1043 (2), pp. 123–128.

Rogers, S.; Wells, R.; Rechsteiner, M. (1986): Amino acid sequences common to rapidly degraded proteins: the PEST hypothesis. In *Science (New York, N.Y.)* 234 (4774), pp. 364–368.

Ross, Philip L.; Huang, Yulin N.; Marchese, Jason N.; Williamson, Brian; Parker, Kenneth; Hattan, Stephen et al. (2004): Multiplexed protein quantitation in Saccharomyces cerevisiae using amine-reactive isobaric tagging reagents. In *Molecular & cellular proteomics : MCP* 3 (12), pp. 1154–1169. DOI: 10.1074/mcp.M400129-MCP200.

Rush, John; Moritz, Albrecht; Lee, Kimberly A.; Guo, Ailan; Goss, Valerie L.; Spek, Erik J. et al. (2005): Immunoaffinity profiling of tyrosine phosphorylation in cancer cells. In *Nature biotechnology* 23 (1), pp. 94–101. DOI: 10.1038/nbt1046.

Saito, Yuko; Suzuki, Kinuko; Hulette, Christine M.; Murayama, Shigeo (2004): Aberrant phosphorylation of alpha-synuclein in human Niemann-Pick type C1 disease. In *Journal of neuropathology and experimental neurology* 63 (4), pp. 323–328.

Sancak, Yasemin; Bar-Peled, Liron; Zoncu, Roberto; Markhard, Andrew L.; Nada, Shigeyuki; Sabatini, David M. (2010): Ragulator-Rag complex targets mTORC1 to the lysosomal surface and is necessary for its activation by amino acids. In *Cell* 141 (2), pp. 290–303. DOI: 10.1016/j.cell.2010.02.024.

Sarkar, Sovan; Carroll, Bernadette; Buganim, Yosef; Maetzel, Dorothea; Ng, Alex H. M.; Cassady, John P. et al. (2013): Impaired autophagy in the lipid-storage disorder Niemann-Pick type C1 disease. In *Cell reports* 5 (5), pp. 1302–1315. DOI: 10.1016/j.celrep.2013.10.042.

Sawamura, Naoya; Gong, Jian-Sheng; Chang, Ta-Yuan; Yanagisawa, Katsuhiko; Michikawa, Makoto (2003): Promotion of tau phosphorylation by MAP kinase Erk1/2 is accompanied by reduced cholesterol level in detergent-insoluble membrane fraction in Niemann-Pick C1-deficient cells. In *Journal of neurochemistry* 84 (5), pp. 1086–1096.

Schmidt, Andreas; Forne, Ignasi; Imhof, Axel (2014): Bioinformatic analysis of proteomics data. In *BMC systems biology* 8 Suppl 2, S3. DOI: 10.1186/1752-0509-8-S2-S3.

Schroeder, Melanie J.; Shabanowitz, Jeffrey; Schwartz, Jae C.; Hunt, Donald F.; Coon, Joshua J. (2004): A neutral loss activation method for improved phosphopeptide sequence analysis by quadrupole ion trap mass spectrometry. In *Analytical chemistry* 76 (13), pp. 3590–3598. DOI: 10.1021/ac0497104.

Schweitzer, Lawrence D.; Comb, William C.; Bar-Peled, Liron; Sabatini, David M. (2015): Disruption of the Rag-Ragulator Complex by c17orf59 Inhibits mTORC1. In *Cell reports* 12 (9), pp. 1445–1455. DOI: 10.1016/j.celrep.2015.07.052.

Seidler, Joerg; Zinn, Nico; Haaf, Erik; Boehm, Martin E.; Winter, Dominic; Schlosser, Andreas; Lehmann, Wolf D. (2011): Metal ion-mobilizing additives for comprehensive detection of femtomole amounts of phosphopeptides by reversed phase LC-MS. In *Amino acids* 41 (2), pp. 311–320. DOI: 10.1007/s00726-010-0647-7.

Settembre, Carmine; Fraldi, Alessandro; Medina, Diego L.; Ballabio, Andrea (2013): Signals for the lysosome: a control center for cellular clearance and energy metabolism. In *Nature reviews. Molecular cell biology* 14 (5), pp. 283–296. DOI: 10.1038/nrm3565.

Shen, Dongbiao; Wang, Xiang; Li, Xinran; Zhang, Xiaoli; Yao, Zepeng; Dibble, Shannon et al. (2012): Lipid storage disorders block lysosomal trafficking by inhibiting a TRP channel and lysosomal calcium release. In *Nature communications* 3, p. 731. DOI: 10.1038/ncomms1735.

Shimobayashi, Mitsugu; Hall, Michael N. (2016): Multiple amino acid sensing inputs to mTORC1. In *Cell research* 26 (1), pp. 7–20. DOI: 10.1038/cr.2015.146.

Simons, Mikael; Keller, Patrick; Strooper, Bart de; Beyreuther, Konrad; Dotti, Carlos G.; Simons, Kai (1998): Cholesterol depletion inhibits the generation of β-amyloid in hippocampal neurons. In *Proceedings of the National Academy of Sciences of the United States of America* 95 (11), pp. 6460–6464.

Sokol, J.; Blanchette-Mackie, J.; Kruth, H. S.; Dwyer, N. K.; Amende, L. M.; Butler, J. D. et al. (1988): Type C Niemann-Pick disease. Lysosomal accumulation and defective intracellular mobilization of low density lipoprotein cholesterol. In *The Journal of biological chemistry* 263 (7), pp. 3411–3417.

Sztolsztener, Malgorzata E.; Dobrzyn, Agnieszka; Pikula, Slawomir; Tylki-Szymanska, Anna; Bandorowicz-Pikula, Joanna (2012): Impaired dynamics of the late endosome/lysosome compartment in human Niemann-Pick type C skin fibroblasts carrying mutation in NPC1 gene. In *Molecular bioSystems* 8 (4), pp. 1197–1205. DOI: 10.1039/c2mb05447g.

Tharkeshwar, Arun Kumar; Trekker, Jesse; Vermeire, Wendy; Pauwels, Jarne; Sannerud, Ragna; Priestman, David A. et al. (2017): A novel approach to analyze lysosomal dysfunctions through subcellular proteomics and lipidomics: the case of NPC1 deficiency. In *Scientific reports* 7, p. 41408. DOI: 10.1038/srep41408.

Thingholm, Tine E.; Jensen, Ole N.; Robinson, Phillip J.; Larsen, Martin R. (2008): SIMAC (sequential elution from IMAC), a phosphoproteomics strategy for the rapid separation of monophosphorylated from multiply phosphorylated peptides. In *Molecular & cellular proteomics : MCP* 7 (4), pp. 661–671. DOI: 10.1074/mcp.M700362-MCP200.

Thompson, Andrew; Schäfer, Jürgen; Kuhn, Karsten; Kienle, Stefan; Schwarz, Josef; Schmidt, Günter et al. (2003): Tandem mass tags: a novel quantification strategy for comparative analysis of complex protein mixtures by MS/MS. In *Analytical chemistry* 75 (8), pp. 1895–1904.

Thurnher, Martin; Nussbaumer, Oliver; Gruenbacher, Georg (2012): Novel aspects of mevalonate pathway inhibitors as antitumor agents. In *Clinical cancer research : an official journal of the American Association for Cancer Research* 18 (13), pp. 3524–3531. DOI: 10.1158/1078-0432.CCR-12-0489.

Tsun, Zhi-Yang; Bar-Peled, Liron; Chantranupong, Lynne; Zoncu, Roberto; Wang, Tim; Kim, Choah et al. (2013): The folliculin tumor suppressor is a GAP for the RagC/D GTPases that signal amino acid levels to mTORC1. In *Molecular cell* 52 (4), pp. 495–505. DOI: 10.1016/j.molcel.2013.09.016.

Valm, Alex M.; Cohen, Sarah; Legant, Wesley R.; Melunis, Justin; Hershberg, Uri; Wait, Eric et al. (2017): Applying systems-level spectral imaging and analysis to reveal the organelle interactome. In *Nature* 546 (7656), pp. 162–167. DOI: 10.1038/nature22369.

Vance, Jean E.; Karten, Barbara (2014): Niemann-Pick C disease and mobilization of lysosomal cholesterol by cyclodextrin. In *Journal of lipid research* 55 (8), pp. 1609–1621. DOI: 10.1194/jlr.R047837.

Vanier, Marie T. (2010): Niemann-Pick disease type C. In *Orphanet Journal of Rare Diseases* 5, p. 16. DOI: 10.1186/1750-1172-5-16.

Vanier, Marie T. (2015): Complex lipid trafficking in Niemann-Pick disease type C. In *Journal of inherited metabolic disease* 38 (1), pp. 187–199. DOI: 10.1007/s10545-014-9794-4.

Vasagiri, Nagarjuna; Kutala, Vijay Kumar (2014): Structure, function, and epigenetic regulation of BNIP3: a pathophysiological relevance. In *Molecular biology reports* 41 (11), pp. 7705–7714. DOI: 10.1007/s11033-014-3664-x.

Villén, Judit; Gygi, Steven P. (2008): The SCX/IMAC enrichment approach for global phosphorylation analysis by mass spectrometry. In *Nature protocols* 3 (10), pp. 1630–1638. DOI: 10.1038/nprot.2008.150.

Vitner, Einat B.; Platt, Frances M.; Futerman, Anthony H. (2010): Common and uncommon pathogenic cascades in lysosomal storage diseases. In *The Journal of biological chemistry* 285 (27), pp. 20423–20427. DOI: 10.1074/jbc.R110.134452.

Wahrle, Suzanne; Das, Pritam; Nyborg, Andrew C.; McLendon, Chris; Shoji, Mikio; Kawarabayashi, Takeshi et al. (2002): Cholesterol-dependent gamma-secretase activity in buoyant cholesterol-rich membrane microdomains. In *Neurobiology of disease* 9 (1), pp. 11–23. DOI: 10.1006/nbdi.2001.0470.

Wang, Shuyu; Tsun, Zhi-Yang; Wolfson, Rachel L.; Shen, Kuang; Wyant, Gregory A.; Plovanich, Molly E. et al. (2015a): Metabolism. Lysosomal amino acid transporter SLC38A9 signals arginine sufficiency to mTORC1. In *Science (New York, N.Y.)* 347 (6218), pp. 188–194. DOI: 10.1126/science.1257132.

Wang, Tim; Birsoy, Kıvanç; Hughes, Nicholas W.; Krupczak, Kevin M.; Post, Yorick; Wei, Jenny J. et al. (2015b): Identification and characterization of essential genes in the human genome. In *Science (New York, N.Y.)* 350 (6264), pp. 1096–1101. DOI: 10.1126/science.aac7041.

Weinert, Brian T.; Schölz, Christian; Wagner, Sebastian A.; Iesmantavicius, Vytautas; Su, Dan; Daniel, Jeremy A.; Choudhary, Chunaram (2013): Lysine succinylation is a frequently occurring modification in prokaryotes and eukaryotes and extensively overlaps with acetylation. In *Cell reports* 4 (4), pp. 842–851. DOI: 10.1016/j.celrep.2013.07.024.

Winter, Dominic; Hung, Chien-Wen; Jaskolla, Thorsten W.; Karas, Michael; Lehmann, Wolf D. (2012): Enzyme-cleavable tandem peptides for quantitative studies in MS-based proteomics. In *Proteomics* 12 (23-24), pp. 3470–3474. DOI: 10.1002/pmic.201200290.

Winter, Dominic; Kugelstadt, Dominik; Seidler, Joerg; Kappes, Barbara; Lehmann, Wolf D. (2009a): Protein phosphorylation influences proteolytic cleavage and kinase substrate properties exemplified by analysis of in vitro phosphorylated Plasmodium falciparum glideosome-associated protein 45 by nano-ultra performance liquid chromatography-tandem mass spectrometry. In *Analytical biochemistry* 393 (1), pp. 41–47. DOI: 10.1016/j.ab.2009.06.022.

Winter, Dominic; Seidler, Joerg; Ziv, Yael; Shiloh, Yosef; Lehmann, Wolf D. (2009b): Citrate boosts the performance of phosphopeptide analysis by UPLC-ESI-MS/MS. In *Journal of proteome research* 8 (1), pp. 418–424. DOI: 10.1021/pr800304n.

Wiśniewski, Jacek R.; Nagaraj, Nagarjuna; Zougman, Alexandre; Gnad, Florian; Mann, Matthias (2010): Brain phosphoproteome obtained by a FASP-based method reveals plasma membrane protein topology. In *Journal of proteome research* 9 (6), pp. 3280–3289. DOI: 10.1021/pr1002214.

Wiśniewski, Jacek R.; Zougman, Alexandre; Mann, Matthias (2009): Combination of FASP and StageTip-based fractionation allows in-depth analysis of the hippocampal membrane proteome. In *Journal of proteome research* 8 (12), pp. 5674–5678. DOI: 10.1021/pr900748n.

Witze, Eric S.; Old, William M.; Resing, Katheryn A.; Ahn, Natalie G. (2007): Mapping protein post-translational modifications with mass spectrometry. In *Nature methods* 4 (10), pp. 798–806. DOI: 10.1038/nmeth1100.

Xu, Jing; Dang, Yongjun; Ren, Yunzhao R.; Liu, Jun O. (2010): Cholesterol trafficking is required for mTOR activation in endothelial cells. In *Proceedings of the National Academy of Sciences of the United States of America* 107 (10), pp. 4764–4769. DOI: 10.1073/pnas.0910872107.

List of supplementary tables

Yonehara, Ryo; Nada, Shigeyuki; Nakai, Tomokazu; Nakai, Masahiro; Kitamura, Ayaka; Ogawa, Akira et al.: Structural basis for the assembly of the Ragulator-Rag GTPase complex. In *Nature communications* 8 (1), p. 1625. DOI: 10.1038/s41467-017-01762-3.

Yue, Xiao-Shan; Hummon, Amanda B. (2013): Combination of multistep IMAC enrichment with high-pH reverse phase separation for in-depth phosphoproteomic profiling. In *Journal of proteome research* 12 (9), pp. 4176–4186. DOI: 10.1021/pr4005234.

Zarei, Mostafa; Sprenger, Adrian; Rackiewicz, Michal; Dengjel, Joern (2016): Fast and easy phosphopeptide fractionation by combinatorial ERLIC-SCX solid-phase extraction for in-depth phosphoproteome analysis. In *Nature protocols* 11 (1), pp. 37–45. DOI: 10.1038/nprot.2015.134.

Zhang, Yaoyang; Fonslow, Bryan R.; Shan, Bing; Baek, Moon-Chang; Yates, John R. (2013): Protein analysis by shotgun/bottom-up proteomics. In *Chemical reviews* 113 (4), pp. 2343–2394. DOI: 10.1021/cr3003533.

12. Appendix

Appendix1. Letter of consent

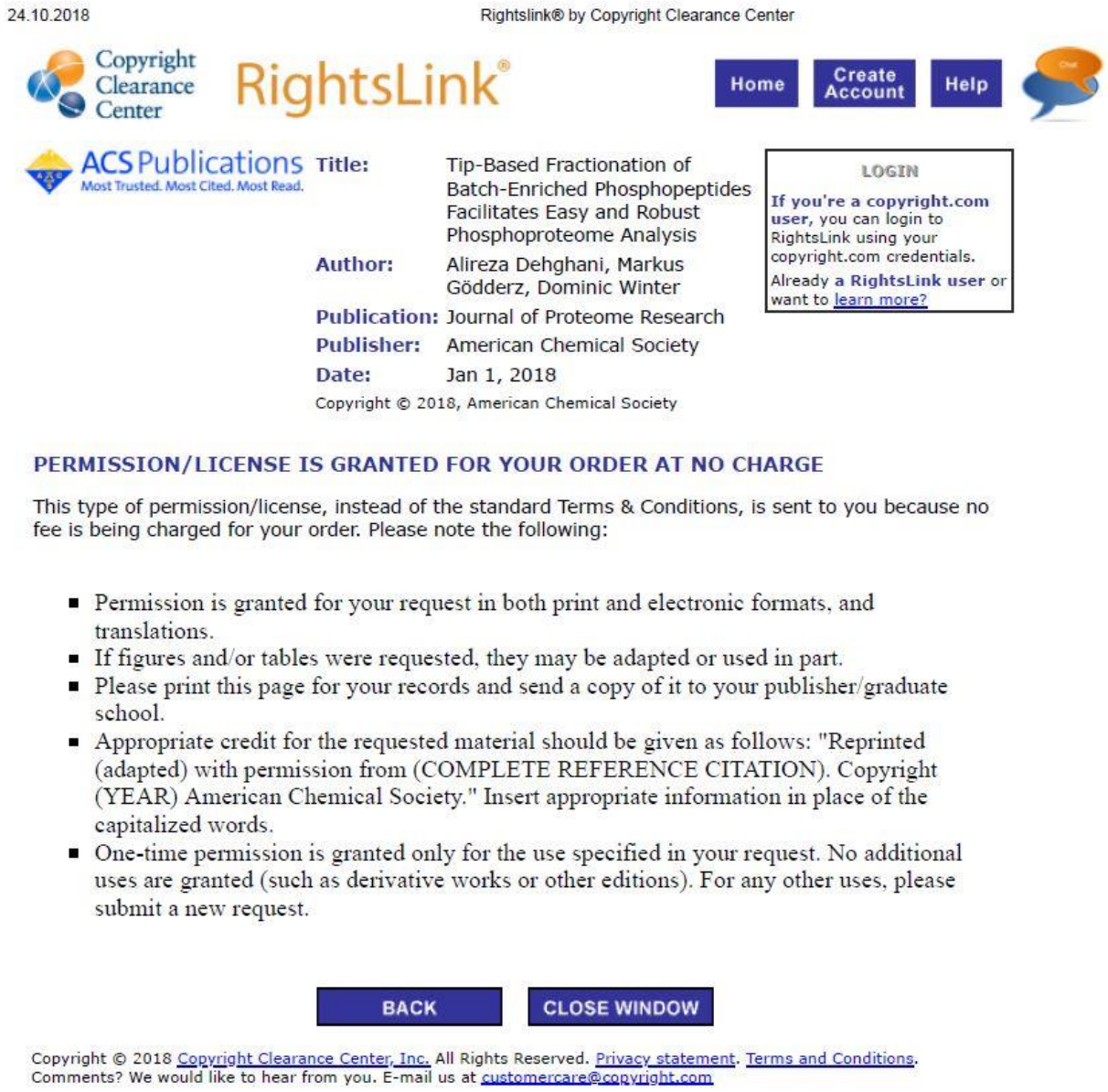

24.10.2018 Rightslink® by Copyright Clearance Center

Copyright Clearance Center RightsLink®

Home | Create Account | Help

ACS Publications
Most Trusted. Most Cited. Most Read.

Title: Tip-Based Fractionation of Batch-Enriched Phosphopeptides Facilitates Easy and Robust Phosphoproteome Analysis

Author: Alireza Dehghani, Markus Gödderz, Dominic Winter

Publication: Journal of Proteome Research

Publisher: American Chemical Society

Date: Jan 1, 2018

Copyright © 2018, American Chemical Society

LOGIN

If you're a copyright.com user, you can login to RightsLink using your copyright.com credentials.

Already **a RightsLink user** or want to learn more?

PERMISSION/LICENSE IS GRANTED FOR YOUR ORDER AT NO CHARGE

This type of permission/license, instead of the standard Terms & Conditions, is sent to you because no fee is being charged for your order. Please note the following:

- Permission is granted for your request in both print and electronic formats, and translations.
- If figures and/or tables were requested, they may be adapted or used in part.
- Please print this page for your records and send a copy of it to your publisher/graduate school.
- Appropriate credit for the requested material should be given as follows: "Reprinted (adapted) with permission from (COMPLETE REFERENCE CITATION). Copyright (YEAR) American Chemical Society." Insert appropriate information in place of the capitalized words.
- One-time permission is granted only for the use specified in your request. No additional uses are granted (such as derivative works or other editions). For any other uses, please submit a new request.

BACK | CLOSE WINDOW

Copyright © 2018 Copyright Clearance Center, Inc. All Rights Reserved. Privacy statement. Terms and Conditions.
Comments? We would like to hear from you. E-mail us at customercare@copyright.com

Appendix 2. Plasmid map of pCMV6-Entry vector (retrieved from OriGene)

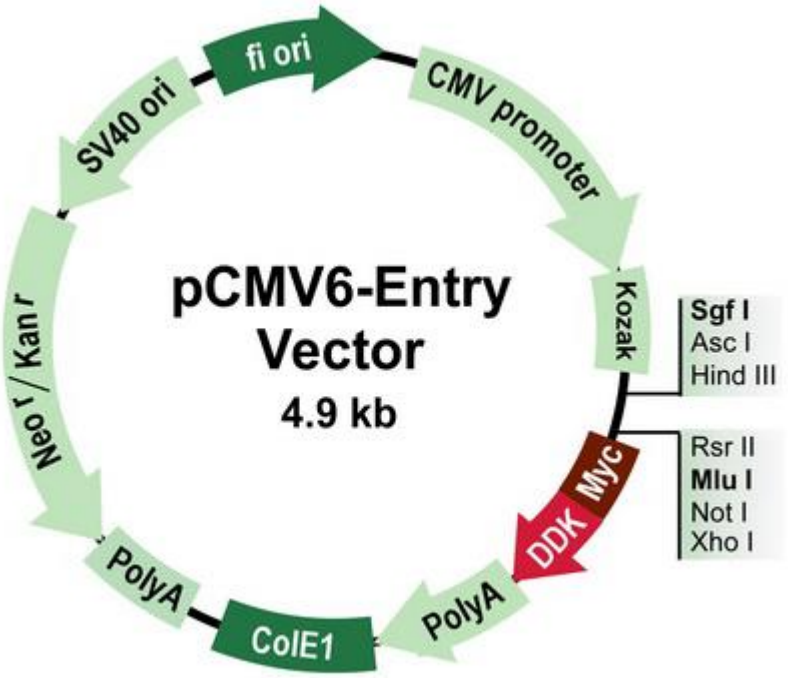

Appendix 3. Plasmid map of G0656 pFIV3.2RSVmcs vector (retrieved from University of Iowa)

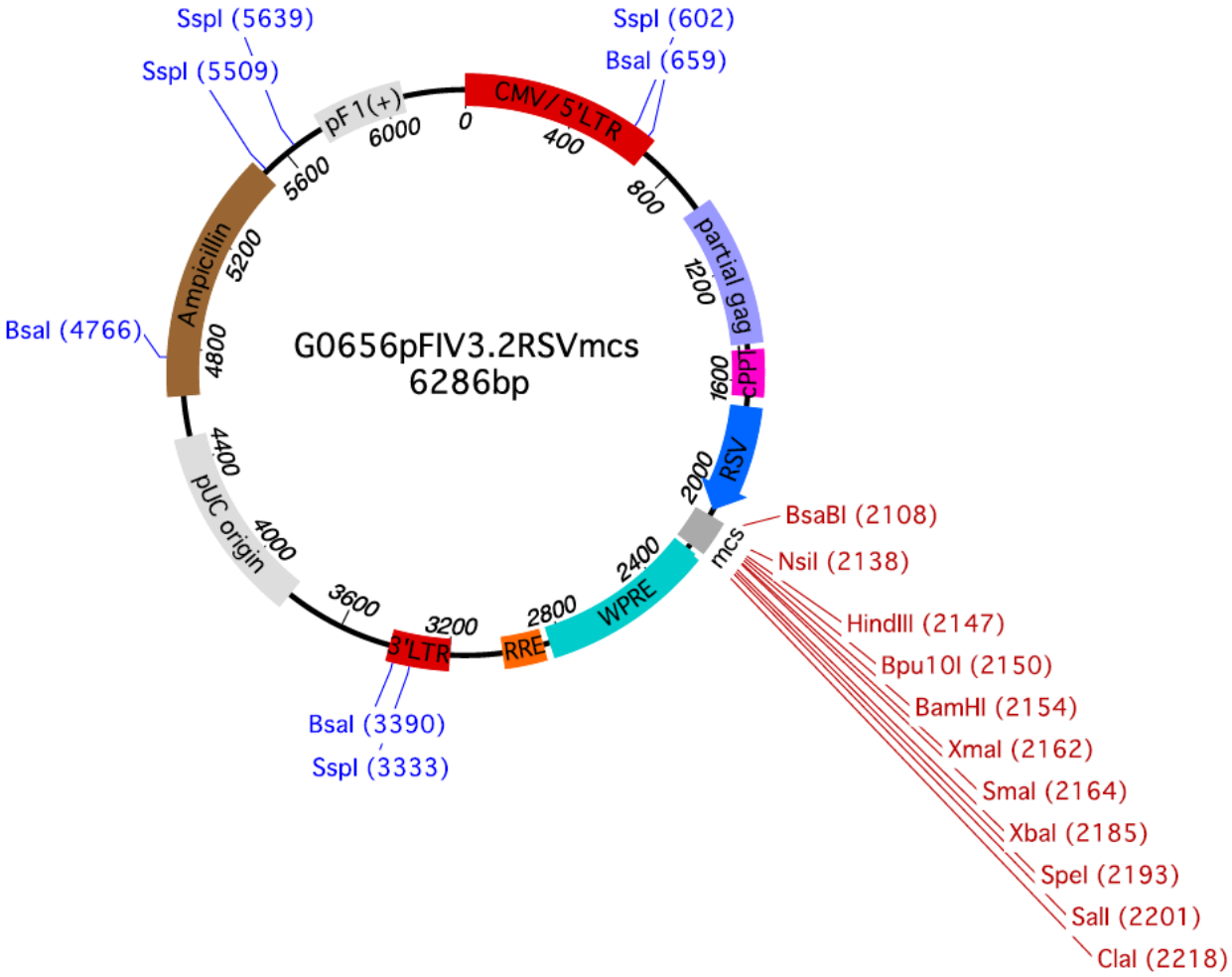

13. Acknowledgement

I would like to first thank my direct supervisor Dr. Dominic Winter for his steady support and his suggestions and ideas. The door to Dr. Winter's office was always open whenever I ran into a trouble spot or had a question about my research.

I also would like to formally thank Prof. Gieselmann for giving me the opportunity to work in his group and for accepting to be the first reference for this work. Furthermore, I especially thank him for his support and advice regarding my project. Moreover, I would like to thank Prof. Witke for accepting to be the second reference, as well as Prof. Odermatt and Prof. Kroupa who readily agreed to be 'fachnahe' and 'fachfremde' members on short notice.

I also would like to thank all my colleagues in the AG Winter group, Shiva Ahmadi, Dr. Carmen Schoor, Fatema Akter, Srigayatri Ponnaiyan, Elham Pourbarkhordari, Peter Mosen, Jasjot Singh, Markus Goedderz, Thea van den Bosch, Asisa Muchamedin, Edgar Kaade, Nur Cengiz, Deniz Pinar Savcigil, and especially our technical assistant Norbert Rösel for his support and availability. My gratitude also goes to Claudia Yaghootfam, Heidi Simonis and Karola Ragout for their technical and administrative support. In this regard, I feel grateful to all my other colleagues of the AG Sylvester, AG Thelen, AG Eckhardt, and AG Matzner for the pleasant time we spent together and their help.

I enjoyed my last couple of years in the 'IBMB' thanks to the friendly atmosphere in the AG Winter and the institute. I will miss the times we spent together in the office, laboratory and wherever we were together.

Finally, I must express my very profound gratitude to my family, my mother, father, brothers, and sisters-in-law, for providing me unfailing support and continuous encouragement throughout my years of study and through the process of research and writing this thesis. This accomplishment would not have been possible without them. Thank you.

14. Declaration

Hiermit versichere ich, dass ich die hier vorliegende Arbeit selbständig angefertigt und keine anderen, als die angegebenen Hilfsmittel und Quellen benutzt habe. Ferner erkläre ich, die vorliegende Arbeit an keiner anderen Hochschule als Dissertation eingereicht zu haben.

Bonn, Januar 2019
Alireza Dehghani